

## **INFORMATION TO USERS**

**This manuscript has been reproduced from the microfilm master. UMI films the text directly from the original or copy submitted. Thus, some thesis and dissertation copies are in typewriter face, while others may be from any type of computer printer.**

**The quality of this reproduction is dependent upon the quality of the copy submitted. Broken or indistinct print, colored or poor quality illustrations and photographs, print bleedthrough, substandard margins, and improper alignment can adversely affect reproduction.**

**In the unlikely event that the author did not send UMI a complete manuscript and there are missing pages, these will be noted. Also, if unauthorized copyright material had to be removed, a note will indicate the deletion.**

**Oversize materials (e.g., maps, drawings, charts) are reproduced by sectioning the original, beginning at the upper left-hand corner and continuing from left to right in equal sections with small overlaps. Each original is also photographed in one exposure and is included in reduced form at the back of the book.**

**Photographs included in the original manuscript have been reproduced xerographically in this copy. Higher quality 6" x 9" black and white photographic prints are available for any photographs or illustrations appearing in this copy for an additional charge. Contact UMI directly to order.**

# **UMI**

A Bell & Howell Information Company  
300 North Zeeb Road, Ann Arbor, MI 48106-1346 USA  
313:761-4700 800:521-0600



MEASUREMENT OF DYNAMIC PROPERTIES OF TORSIONAL ELASTIC  
COUPLING AND SIMULATION OF MARINE PROPULSION  
SYSTEM TORSIONAL VIBRATIONS

By  
Anying Shen

A Dissertation  
Submitted to the Faculty of  
Mississippi State University  
in Partial Fulfillment of the Requirements  
for the Degree of Doctor of Philosophy  
in Mechanical Engineering  
in the Department of Mechanical Engineering

Mississippi State, Mississippi

August 1995

**UMI Number: 9604874**

---

**UMI Microform 9604874**  
**Copyright 1995, by UMI Company. All rights reserved.**

**This microform edition is protected against unauthorized  
copying under Title 17, United States Code.**

---

**UMI**

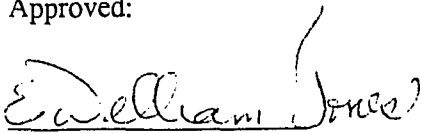
**300 North Zeeb Road  
Ann Arbor, MI 48103**

MEASUREMENT OF DYNAMIC PROPERTIES OF TORSIONAL ELASTIC  
COUPLING AND SIMULATION OF MARINE PROPULSION  
SYSTEM TORSIONAL VIBRATIONS

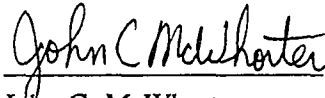
By

Anying Shen

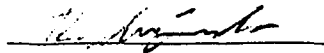
Approved:



E. William Jones  
Professor of Mechanical Engineering  
Major Professor and Director of  
Dissertation



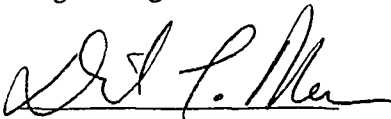
John C. McWhorter  
Professor and Head of Aerospace  
Engineering  
Minor Professor



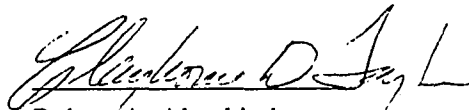
Rogelio Luck  
Assistant Professor of Mechanical  
Engineering



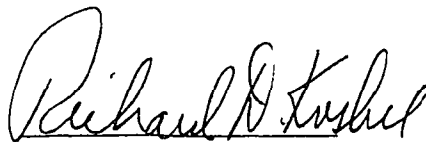
Emmanuel I. Agba  
Assistant Professor of Mechanical  
Engineering



David L. Marcum  
Associate Professor and Graduate  
Coordinator of the Department of  
Mechanical Engineering



Robert A. Altenkirch  
Dean of the College of Engineering



Richard D. Koshel  
Dean of the Graduate School

Name: Anying Shen

Date of Degree: August 4, 1995

Institution: Mississippi State University

Major Field: Mechanical Engineering

Major Professor: Dr. E. William Jones

Title of Study: MEASUREMENT OF DYNAMIC PROPERTIES OF  
TORSIONAL ELASTIC COUPLING AND SIMULATION OF  
MARINE PROPULSION SYSTEM TORSIONAL VIBRATIONS

Pages in Study: 115

Candidate for Degree of Doctor of Philosophy

A time domain simulation model for torsional vibrations of a work boat propulsion system was developed. It is suitable for both linear and nonlinear cases. The model is a combination of the Bond graph method and SIMULINK™ software. A typical work boat propulsion system is used as an example to illustrate the simulation procedure. Although the program is mainly designed for work boat torsional vibration simulation, it has application for a general dynamic system.

A dynamic test stand for testing elastic couplings was designed and fabricated. The dynamic properties of the coupling were measured. The test data were analyzed. The results show both stiffness and damping are strong functions of mean torque, vibratory velocity and temperature. The test results are presented in two different ways for the convenience of the user. One form is suitable for traditional frequency domain analysis. The other form is for time domain simulation.

## ACKNOWLEDGMENTS

Sincere appreciation is extended to Dr. E. William Jones for serving as major advisor during my graduate studies and for providing guidance, facilities, and support for the research described in this dissertation. As director of this dissertation, he has provided many professional and logical suggestions. His expert advice in the art of engineering applications has always been motivating.

The author is grateful also for the encouragement and assistance provided by Drs. Rogelio Luck, Robert Taylor, Emmanuel Agba, and Richard Patton. I also wish to convey my sincere thanks to Dr. John McWhorter who agreed to be my minor advisor.

Appreciation is expressed to Mr. Ray Haley and Marine Gears, Inc., for furnishing the test apparatus and financial support. I would also like to thank Mr. Victor Latham, Mr. Dean Green, Mr. Feng Li for their assistance during the measurement of the elastic coupling.

I thank Dr. W. Glenn Steele for his encouragement and financial support in my continuing graduate studies in the Department of Mechanical Engineering. I also wish to thank all the faculty and staff of the Mechanical Engineering Department for their help and support.

Finally, a very special expression of appreciation is extended to my wife, Julie, and my son, Steven. Without their encouragement, support and understanding this endeavor would not have been possible.

## TABLE OF CONTENTS

|  | Page      |
|--|-----------|
| ACKNOWLEDGMENTS .....                                      | ii        |
| LIST OF TABLES .....                                       | v         |
| LIST OF FIGURES .....                                      | vi        |
| NOMENCLATURE .....   | ix        |
| <b>CHAPTER</b>   |           |
| <b>I. INTRODUCTION .....</b>                               | <b>1</b>  |
| Torsional Vibrations in Ship Propulsion Systems .....      | 1         |
| Background .....   | 2         |
| Objectives .....   | 4         |
| Overview .....   | 5         |
| <b>II. MODELING THE TORSIONAL VIBRATION SYSTEM .....</b>   | <b>6</b>  |
| Method of Bond Graph .....                                 | 6         |
| Modeling of the Propulsion System by Bond Graph .....      | 11        |
| State Space Formulation of Bond Graph Model .....          | 11        |
| <b>III. CHARACTERISTICS OF THE SYSTEM COMPONENTS .....</b> | <b>16</b> |
| Introduction .....   | 16        |
| Excitations .....  | 17        |
| Diesel Engine Excitations .....                            | 17        |
| Propeller Excitations .....                                | 20        |
| Damping .....  | 21        |
| Inertia .....  | 23        |
| Stiffness .....  | 24        |
| <b>IV. DESIGN OF THE DYNAMIC TEST STAND .....</b>          | <b>29</b> |
| Introduction .....   | 29        |
| Description of Dynamic Test Stand .....                    | 32        |
| Dynamic Analysis of Test Stand .....                       | 38        |
| Design of Hydraulic System .....                           | 41        |
| Instrumentation of Testing System .....                    | 44        |
| Signal Processing .....                                    | 49        |



| CHAPTER   | Page |
|---|------|
| V. ANALYSIS OF RESULTS . . . . .  | 54   |
| Modeling the HRC Elastic Coupling . . . . .   | 54   |
| Data Processing . . . . .   | 58   |
| Dynamic Stiffness . . . . .   | 61   |
| Damping . . . . .   | 66   |
| Conclusions . . . . .   | 67   |
| VI. SIMULATION OF THE PROPULSION SYSTEM . . . . .   | 73   |
| Introduction . . . . .  | 73   |
| Simulation Program Development . . . . .  | 73   |
| Simulation Results . . . . .  | 76   |
| VII. CONCLUSIONS AND RECOMMENDATIONS . . . . .  | 85   |
| Time Domain Torsional Vibrations Simulation . . . . .   | 85   |
| Dynamic Properties of HRC Elastic Coupling . . . . .  | 86   |
| APPENDIX  |      |
| A. DESCRIPTION OF A TYPICAL MARINE PROPULSION SYSTEM . . . . .  | 88   |
| B. PROGRAM FOR FORMATION OF JUNCTION STRUCTURE MATRICES<br>FOR BOND GRAPH SHOWN IN FIGURE A.3 . . . . . | 92   |
| C. PROGRAM FOR TEST STAND DYNAMIC ANALYSIS . . . . .  | 96   |
| D. PROGRAM FOR DATA ACQUISITION SYSTEM . . . . .  | 100  |
| E. PROGRAM FOR TEST DATA POST PROCESSING . . . . .  | 106  |
| BIBLIOGRAPHY . . . . .  | 112  |

## LIST OF TABLES

| Table |  | Page |
|-------|--|------|
| 2.1   | Power and Energy Variables for Mechanical Rotational Ports . . . . .   | 7    |
| 3.1   | Constitutive Equations for Four Basic Elements . . . . .   | 16   |
| 3.2   | Propeller Variable Torque Excitation Factors . . . . .   | 21   |
| 4.1   | Vibration Analysis Results of the Dynamic Test Rig for HRC-63K<br>Coupling with Half Rubber Elements . . . . . | 40   |
| 4.2   | JSB Gear Pump Specifications . . . . .   | 42   |
| 4.3   | Fluid Motor Performance Data . . . . .   | 42   |

## LIST OF FIGURES

| Figure |   | Page |
|--------|---|------|
| 1.1    | Influence of Alternating Component of Torque on Shaft Fatigue Life . .                            | 2    |
| 2.1    | Tetrahedron of State . . . . .  | 7    |
| 2.2    | Constitutive Equations of Three One-port Elements:<br>Resistor, Capacitor, and Inductor . . . . . | 8    |
| 2.3    | Effort and Flow Sources . . . . .   | 8    |
| 2.4    | Constitutive Equations of Two-port Elements:<br>Transformer and Gyrator . . . . .                 | 10   |
| 2.5    | Constitutive Equations of Parallel and Series Junctions . . . . .                                 | 10   |
| 2.6    | Significant Vectors for Systems Having Integration<br>Causality . . . . .                         | 12   |
| 2.7    | Simulink Block Diagram of Equation (2.12) . . . . .   | 15   |
| 3.1    | Crank Mechanism . . . . .   | 18   |
| 3.2    | Timoshenko and Baud Gear Tooth Model . . . . .  | 24   |
| 3.3    | Torsional Stiffness of Spur Gear with Different Contact<br>Ratio . . . . .                        | 26   |
| 3.4    | Approximation of Torsional Stiffness of Spur Gear . . . . .                                       | 27   |
| 3.5    | Step Response of Single DOF System . . . . .  | 27   |
| 4.1    | Assembly Details of HRC Coupling . . . . .  | 31   |
| 4.2    | HRC Coupling Dynamic Test Stand . . . . .   | 33   |
| 4.3    | Left Side View of Dynamic Test Stand . . . . .  | 34   |
| 4.4    | Right Side View of Test Stand . . . . .   | 35   |
| 4.5    | Dynamic Test Stand Shaft Details . . . . .  | 36   |

| Figure | Page   |
|--------|--|
| 4.6    | Test Stand Housing . . . . . 37  |
| 4.7    | Torsional Vibration Model of Test Stand . . . . . 39   |
| 4.8    | Test Stand Hydraulic System . . . . . 41   |
| 4.9    | Wiring Diagram of Four Strain Gages . . . . . 44   |
| 4.10   | Signal Processing Circuit for Strain Gages . . . . . 46  |
| 4.11   | LVDT Circuit . . . . . 47  |
| 4.12   | Test Stand Data Acquisition System . . . . . 49  |
| 4.13   | Relation Between LVDT Linear Displacement and Coupling<br>Angular Twist . . . . . 52   |
| 5.1    | Kelvin-Voigt Model . . . . . 54  |
| 5.2    | Oscillatory Torque and Angular Displacement at A Given<br>Operating Point . . . . . 55   |
| 5.3    | Phase Diagram of Torque . . . . . 55   |
| 5.4    | Hysteresis Loop . . . . . 57   |
| 5.5    | Measured Vibratory Torque and Displacement . . . . . 59  |
| 5.6    | Phase Difference Between Vibratory Torque and Angle<br>of Twist . . . . . 60   |
| 5.7    | Torque Versus Displacement for Static Conditions . . . . . 64  |
| 5.8    | Comparison of Measured Data and Calculated Data at<br>Temperature $\theta = 110$ °F . . . . . 64                                 |
| 5.9    | Histogram of Error of Dynamic Stiffness Between Measured<br>Values and Values Predicted by Equation (5.17) . . . . . 65          |
| 5.10   | Histogram of Error of Dynamic Stiffness Between Measured<br>Values and Values Predicted by Equation (5.20) . . . . . 65          |
| 5.11   | Histogram of Error of Relative Damping Between Measured<br>Values and Values Predicted by Equation (5.21) . . . . . 66           |
| 5.12   | Histogram of Error of Equivalent Viscous Damping Between<br>Measured Values and Values Predicted by Equation (5.25) . . . . . 69 |

| Figure | Page  |
|--------|---|
| 5.13   | Influence of Temperature on Dynamic Stiffness . . . . . 69                          |
| 5.14   | Influence of Temperature on Relative Damping . . . . . 70                           |
| 5.15   | Influence of Frequency on Dynamic Stiffness . . . . . 70                            |
| 5.16   | Influence of Frequency on Relative Damping . . . . . 71                             |
| 5.17   | Influence of Vibration Amplitude on Dynamic Stiffness . . . . . 71                  |
| 5.18   | Influence of Vibration Amplitude on Relative Damping . . . . . 72                   |
| 6.1    | Simulation Block Diagram of the Storage Field . . . . . 77                          |
| 6.2    | Simulation Block Diagram of the Dissipation Field . . . . . 78                      |
| 6.3    | System Inputs: Excitations . . . . . 79   |
| 6.4    | System Outputs: Torque on the Shaft . . . . . 80                                    |
| 6.5    | Simulation Block Diagram of A Typical Marine Propulsion System . . . . . 81         |
| 6.6    | Vibratory Torque on Gear Box Input Shaft Due to Propeller Excitation . . . . . 82   |
| 6.7    | Torque on the Gear Box Input Shaft Due to Propeller Excitation . . . . . 82         |
| 6.8    | Vibratory Torque on the Propeller Shaft Due to Propeller Excitation . . . . . 83    |
| 6.9    | Torque on the Propeller Shaft Due to Propeller Excitation . . . . . 83              |
| 6.10   | Vibratory Torque on the Shaft 10 Due to Engine 5th Harmonic Excitation . . . . . 84 |
| 6.11   | Torque on the Shaft 10 Due to Engine 5th Harmonic Excitation . . . . . 84           |
| A.1    | A Typical Marine Propulsion System . . . . . 89                                     |
| A.2    | Mass-spring Model of the Marine Propulsion System . . . . . 90                      |
| A.3    | Bond Graph Representation of the Marine Propulsion System . . . . . 91              |

## NOMENCLATURE

|              |  |
|--------------|--|
| $A$          | state matrix<br>piston face area       |
| $a_i$        | harmonic coefficient                   |
| $B$          | input matrix                           |
| $b$          | gear face width                        |
| $b_i$        | harmonic coefficient                   |
| $b_p$        | propeller damping coefficient          |
| $bhp$        | brake horsepower                       |
| $C_E$        | equivalent viscous damping coefficient |
| $c$          | center distance between gears          |
| $D_{in}$     | dissipation field input vector         |
| $D_{out}$    | dissipation field output vector        |
| $d$          | piston diameter<br>shaft diameter      |
| $E$          | modulus of elasticity                  |
| $e$          | general effort                         |
| $F_t$        | gear tangential force                  |
| $F_n$        | gear normal force                      |
| $f$          | general flow<br>frequency              |
| $G$          | shear modulus of elasticity            |
| $GF$         | gage factor                            |
| $HP_{rated}$ | engine rated horsepower                |

|             |  |
|-------------|--|
| I           | inertia  |
| $I_{eq}$    | equivalent moment of inertia                                   |
| $I_{rot}$   | rotating inertia   |
| ihp         | indicated horsepower   |
| J           | junction matrix<br>moment of inertia                           |
| $J_s$       | polar moment of inertia of the shaft                           |
| j           | $\sqrt{-1}$  |
| K           | spring ratio<br>dynamic torsional stiffness                    |
| $K^*$       | complex stiffness  |
| L           | length of stroke   |
| l           | length of connecting rod                                       |
| m           | mass   |
| $m_{rec}$   | reciprocating mass   |
| N           | number of cylinder in the engine                               |
| n           | engine speed   |
| $n_{rated}$ | rated engine speed   |
| $n_x$       | number of revolutions required for each power stroke delivered |
| P           | power  |
| p           | general momentum<br>pressure                                   |
| $p_b$       | brake mean effective pressure                                  |
| $p_g$       | gas pressure   |
| $p_t$       | tangential pressure  |
| Q           | flow rate  |
| q           | general displacement   |

|             |                                       |
|-------------|---------------------------------------|
| $R$         | radius where the LVDT is mounted      |
| $R_1$       | pinion pitch radius                   |
| $r$         | crank radius                          |
| ratio       | gear ratio                            |
| $r_p$       | propeller torque excitation factor    |
| SF          | LVDT scale factor                     |
| $T$         | torque                                |
| $T_K$       | spring torque                         |
| $T_C$       | damping torque                        |
| $T_{ep}$    | propeller excitation torque           |
| $T_m$       | mean torque                           |
| $T_{rated}$ | rated engine torque                   |
| $T_v$       | vibratory torque                      |
| $t$         | time                                  |
| $U$         | source vector<br>input vector         |
| $V_{in}$    | bridge excitation voltage             |
| $V_{out}$   | bridge output voltage                 |
| $V_r$       | ratio of change in voltage            |
| $v$         | fluid velocity                        |
| $W_d$       | energy dissipated by relative damping |
| $W_e$       | flexible strain energy                |
| $X$         | state vector                          |
| $Y$         | output vector                         |
| $Z$         | storage field output vector           |
| $z$         | number of propeller blades            |



|                           |  |
|---------------------------|--|
| $\alpha$                  | crank angle from top dead center   |
| $\beta$                   | connecting rod angle<br>gear pressure angle  |
| $\beta_h$                 | helix angle  |
| $\gamma$                  | shear strain   |
| $\delta$                  | tooth deflection   |
| $\delta_{bs}$             | tooth bending and shear deflection   |
| $\delta_c$                | tooth deflection due to contact  |
| $\delta_\varphi$          | relative angular displacement between inner hub and outer hub of elastic coupling  |
| $\eta$                    | efficiency<br>loss factor resulting from the deformation of the elastic element lagging the applied force during sinusoidal motion |
| $\eta_m$                  | engine mechanical efficiency   |
| $\theta$                  | temperature  |
| $\mu$                     | poisson's ratio  |
| $\tau$                    | torsional stress   |
| $\varphi$                 | angular displacement   |
| $\varphi_m$               | meant angular displacement   |
| $\varphi_v$               | vibratory angular displacement   |
| $\psi$                    | relative damping ratio   |
| $\omega$                  | angular velocity<br>angular vibration frequency  |
| $\omega_p$                | propeller rotation speed   |
| $\omega_{vib}$            | vibration frequency  |
| $\varepsilon$             | phase angle  |
| $\varepsilon_{@45^\circ}$ | shaft strain at a 45° angle  |

## CHAPTER I INTRODUCTION

### Torsional Vibrations in Ship Propulsion Systems

The work boat makes a significant contribution to the American economy. According to the Army Corps of Engineers' 1992 Inland Waterway Review, in 1989 there were approximately 5,250 work boats in the U.S. fleet, with a combined propulsion output of 8.7 million horsepower, or an average of just over 1,650 horsepower per vessel. Since 1950 the total horsepower has increased 400 percent, up from 1.7 million.

The propulsion system for a typical work boat consists of an internal combustion engine, a coupling, reduction gears, and a propeller as shown in Figure A.1. This mass-spring system has the potential to vibrate torsionally. When the system is excited at one of its torsional natural frequencies the resonance vibration produces large vibratory torques which may cause fatigue failure of shafting and/or hammering of gear teeth. Figure 1.1, for example, shows how the factor of safety of the shaft decreases rapidly when the alternating component of torque is increased while the mean torque remains constant (Jones et al. 1994). The same alternating torque increases the bending and compressive stresses in the gear teeth. If the vibratory torque exceeds the mean torque, the gear teeth will separate during the cycle of vibration and will produce impact loading, gear tooth hammering, which may result in excessive noise or chatter.

Several sources of excitation torque exist for powering the resonant vibrations in a typical marine vessel. The non-uniformity in the driving torque, due to the internal combustion engine, is the main source of the excitation. The excitation torque resulting

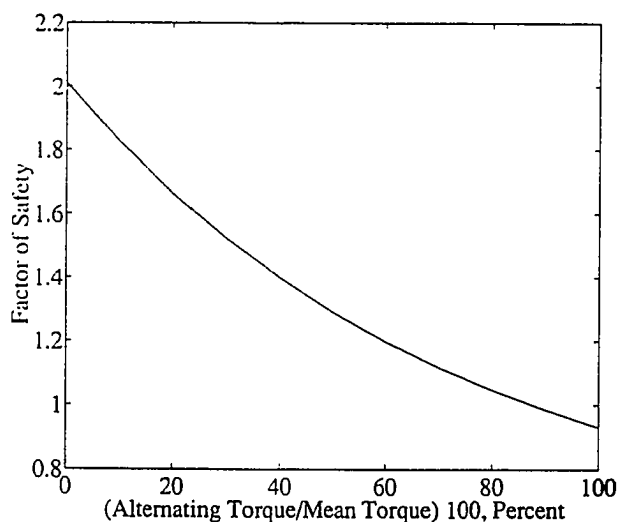


Figure 1.1 Influence of Alternating Component of Torque on Shaft Fatigue Life

from the propeller operating in a nonuniform wake is also significant. The manufacturing error of the meshing gear pairs and the variation of the gear pair meshing stiffness may excite the high frequency vibrations.

### Background

Torsional oscillations of the internal combustion engine driven system have been studied for a long time as indicated by Porter's (1927) discussion of the severity of torsional vibrations. The system is normally modeled as a lumped mass-spring linear system. The traditional analysis of the torsional vibration was conducted by Holzer. The Holzer method gives the system natural frequencies and normalized mode shapes by iterative calculation. Den Hartog (1956) describes the approach in detail in his book. The actual vibration amplitudes may be calculated by the energy method. The finite element method provides for the solution of the forced, damped system. The means of mitigating torsional vibration are also discussed by Den Hartog (1956). Jones et al. (1982) analyzed the torsional vibrations in work boat power trains and suggests that system tuning be

accomplished by sensitivity studies. Each vessel's power train has its own characteristic vibration signature.

In recent years, due to the fast growth in modern control research and the ready availability of high speed computers, some new developments have occurred in the numerical analysis area, especially in matrix computation. To apply the approach used in the modern control area to the study of torsional vibrations and to introduce modern control theory to vibration control is a new challenge. A few examples may be found in the dynamic analysis and control of the automobile power train system by using this technique (Cho et al. 1989, Choy et al 1991). Numerous papers are devoted to the study of the semi-active or active control of the car suspension system (Karnopp et al 1974, 1990).

The ship's power train system is a nonlinear system. For example, the torsional stiffness of gear teeth varies with angular position. The gear backlash has strong nonlinear properties. The traditional way of transforming a nonlinear system into an equivalent linear system has some drawbacks. How these simplifications affect the results is still unknown. No analytical solution has been found for nonlinear systems except in a few special situations. Several publications present studies of the dynamic properties of the gear pair by using a nonlinear model. For example, Singh et al. (1989) investigated the automotive neutral gear rattle due to backlash by numerical simulation. Kahraman and Singh (1990) studied the nonlinear dynamics of a spur gear pair by a very simple model. No reports have been located about the study of nonlinear torsional vibrations in boat propulsion systems.

The torsional elastic couplings used in ship drive trains are normally nonlinear. The dynamic properties for the HRC elastic coupling manufactured by Marine Gears, Inc., are unknown. Its characteristics depend mainly on the rubber elements and coupling geometry. Previous study shows that the dynamic properties of the HRC

coupling may depend on the mean torque, vibration frequency, vibration amplitude and temperature.

The mechanical properties of the elastomer material have been studied for a long time (Bert, 1973), and various models have been proposed to describe the elastomer behaviors. Some models are too simple to represent the elastomer material behaviors. Others are too complex to be used practically. Besides, almost all the studies are limited to the linear or linearized model with harmonic vibration. Since the elastomer material's mechanical properties depend on the composition, the method of processing, the size and shape, and the manner in which it is used, the dynamic measurement of the coupling itself is necessary. The mathematical model which describes the coupling's mechanical properties has to be simple for practical use yet be able to represent the real behavior of the coupling in its working range.

### Objectives

The first objective of this research was to develop a time domain simulation model for torsional vibration analysis. The model should simulate both linear and nonlinear cases. The model is to be used to predict the severity of the torsional vibrations of the system. The nonlinear simulation will offer an optional method of analysis and will suggest the need for a different input data base. A typical marine propulsion system will be used through this paper to illustrate the method of analysis.

A second objective was to design a dynamic test stand and complete dynamic tests of the elastic coupling. The elastic coupling is an important component in the power train system as it not only transmits power, but also isolates engine excitation from other parts of the system and dissipates vibratory energy by damping. Knowledge of its dynamic properties is critical for successful simulation.<sup>1</sup>

### Overview

In Chapter II of this paper, A Bond graph model of the marine propulsion system is proposed. By combining the Bond graph and SIMULINK™ software, a unique approach is introduced for time domain nonlinear simulation. The approach is shown to be very effective. Chapter III addresses the system's component characteristics for time domain nonlinear simulation purposes. Chapter IV describes the design of the elastic coupling dynamic test rig and data acquisition system. In Chapter V, the test results are processed and presented in two different forms. Chapter VI develops the simulation program. A typical marine propulsion system is used as an example to describe the approach developed in this paper. Chapter VII presents conclusions and recommendations.

## CHAPTER II

### MODELING THE TORSIONAL VIBRATION SYSTEM

Although all systems existing in the world are distributed, ideal elements are usually created to model real systems in order to simplify the calculations. This leads to a lumped model. From the energy point of view, a dynamic system will transmit, store and dissipate energy. Therefore, a few ideal elements, together with the topological structure, are sufficient to describe a dynamic system.

#### Method of Bond Graph

The Bond graph method, which was originated by Paynter and developed by Karnopp and Rosenberg, is used here to describe the lumped system. Four variables, effort  $e(t)$ , flow  $f(t)$ , momentum  $p(t)$  and displacement  $q(t)$ , are used in the Bond graph to describe the power flowing in the system. The relationships between these four variables are shown in Figure 2.1. For mechanical rotational ports, the variables are listed in Table 2.1. There are three one-port elements in the Figure 2.1, namely, resistor R, capacitor C and inductor I.

The constitutive equation for the R-element is between effort and flow in general and may be linear or not. The R-element dissipates and produces heat, or precisely entropy-flow. Power always enters and never returns. R-elements are irreversible. The Bond graph and block diagram for the R-element are shown in Figure 2.2(a).

The constitutive equation for the C-element is between effort and displacement. C-elements are energy conserving. The Bond graph and block diagram are shown in

Table 2.1 Power and Energy Variables for Mechanical Rotational Ports

| Generalized Variables | Mechanical Rotation                            | English Units |
|-----------------------|--|---------------|
| Effort, $e$           | Torque, $T$                                    | [in-lb]       |
| Flow, $f$             | Angular velocity, $\omega$                     | [rad/sec]     |
| Momentum, $p$         | Angular momentum, $p_T$                        | [in-lb-sec]   |
| Displacement, $q$     | Angular, $\varphi$                             | [rad]         |
| Power, $P$            | $T(t)\omega(t)$                                | [(in-lb)/sec] |
| Energy, $E$           | $\int \omega T d\varphi, \int p_T \omega dp_T$ | [in-lb]       |

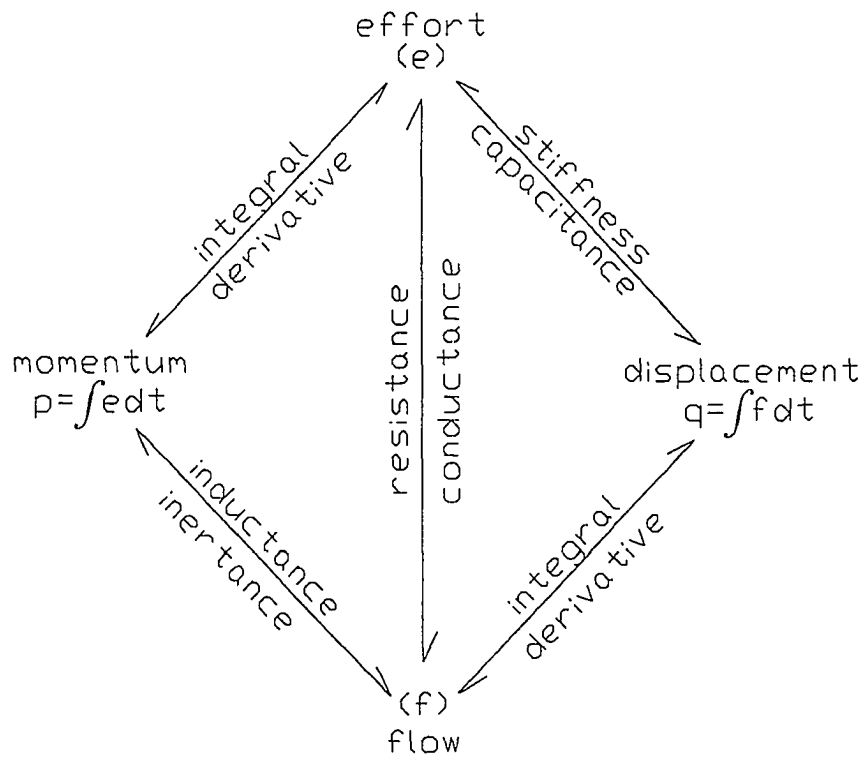


Figure 2.1 Tetrahedron of State



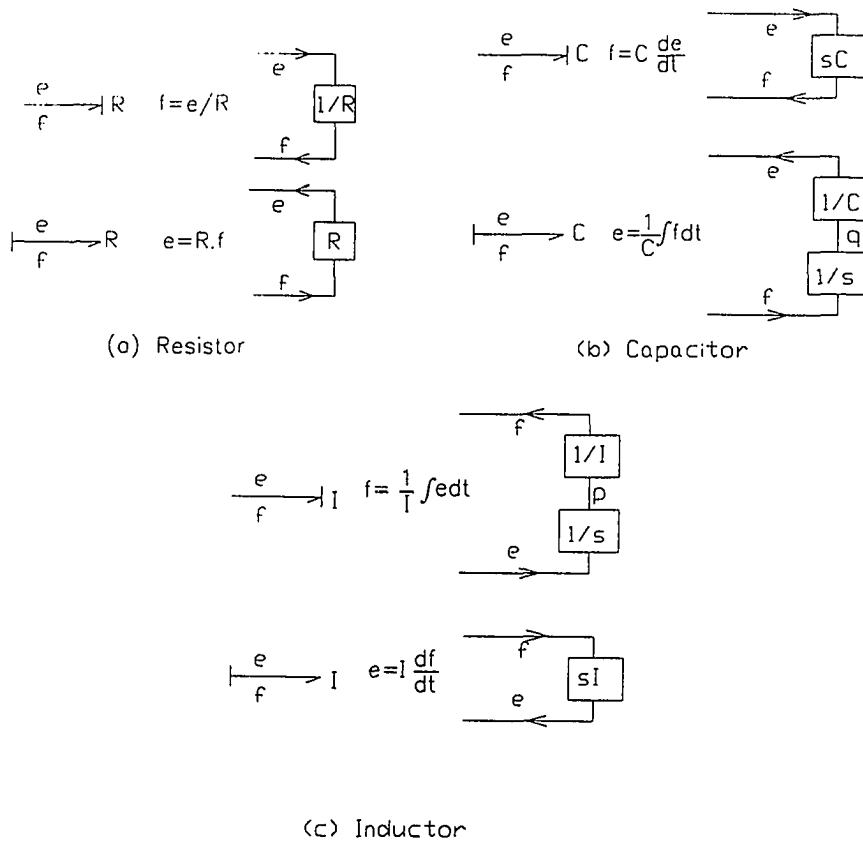


Figure 2.2 Constitutive Equations of Three One-port Elements: Resistor, Capacitor, and Inductor

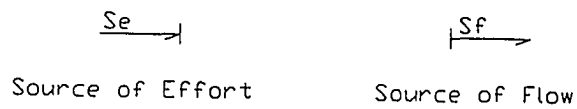


Figure 2.3 Effort and Flow Sources

Figure 2.2(b). Both derivative and integral causalities are possible for the C-element. Computers can integrate easily, but they take derivatives only with great difficulty.

I-elements are also energy storing. The constitutive equation is between momentum and flow. The block diagram and Bond graph are shown in Figure 2.2(c) with both derivative and integral causalities.

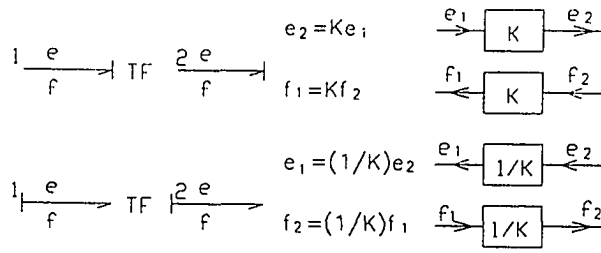
Two additional elements, effort and flow sources,  $S_e$ ,  $S_f$ , are used to model the interaction between the system and the outside world. The effort source gives effort independent of flow. The flow source gives flow independent of effort. In the context of thermodynamics, effort and flow sources are reversible. The Bond graphs for  $S_e$  and  $S_f$  are shown in Figure 2.3. The causalities are mandatory.

The above five elements, including the two sources, are all one-port. They will be connected by the other elements, namely two-port, three-port and partly multi-port. These elements are used to describe the system structure.

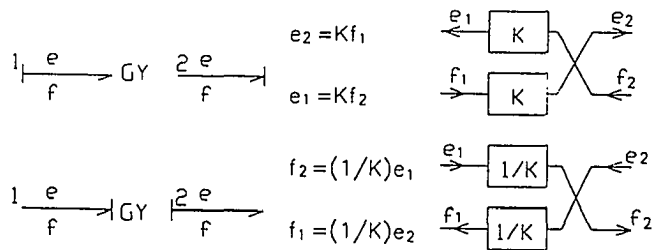
The Transformer, TF, or Modulated Transformer is shown in Figure 2.4(a). Both efforts and both flows are proportional. Transformers conserve power and are reversible.

Gyrators, GY, are similar two-port elements, also called over crossed transformers, since effort in one bond is proportional to flow in the other. The Bond graph and block diagram for gyrator are shown in Figure 2.4(b).

The parallel junctions (or p-junctions) and series junctions (or s-junctions) are illustrated in Figure 2.5. They conserve power and are reversible. Parallel junctions have equal efforts while the flows add up to zero. Series junctions have equal flows and the efforts add up to zero. The causal pattern of junctions is always same: At a p-junction one effort pushes inward, all others outward. At a s-junction one flow points inward, all others point outward.



(a) Transformer



(b) Gyrator

Figure 2.4 Constitutive Equations of Two-port Elements: Transformer and Gyrator

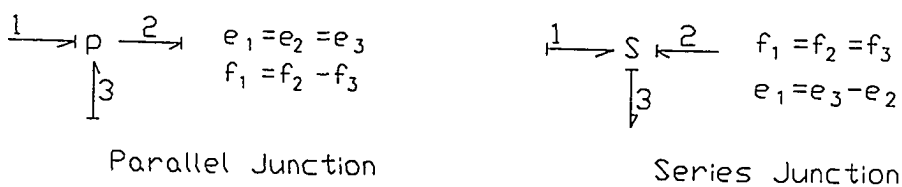


Figure 2.5 Constitutive Equations of Parallel and Series Junctions

### Modeling of the Propulsion System by Bond Graph

For a torsional system, there are two types of energy storage elements, spring and inertia, and one type of energy dissipation element, damper. A typical marine propulsion system shown in Appendix Figure A.1 may be modeled as a mass-elastic system for torsional analysis as shown in Figure A.2.

To transform the above model of a torsional mechanical system into a Bond graph, the effort is torque and the flow is angular velocity. The C-element represents a torsional spring, the I-element represents the inertia, and the R-element represents a damper. The effort source is torque applied to the system. The Bond graph, which is based on the model of Figure A.2, is shown in Figure A.3.

### State Space Formation of Bond Graph Model

In order to simulate the system, the Bond graph presentation of the model must be transformed into one of two state space forms, namely,

$$\dot{X} = AX + BU \quad (2.1)$$

or

$$\dot{X} = \Phi (X, U) \quad (2.2)$$

where X is called the state vector, A is the state matrix, B is the input matrix, and U is the input vector.

Actually, any Bond graph composed of elements from the basic set may be organized into the form shown in Figure 2.6. The five vectors shown in Figure 2.6 are  $\dot{X}$  = storage field input vector, Z = storage field output vector,  $D_{in}$  = dissipation field input vector,  $D_{out}$  = dissipation field output vector, U = source vector.

The constitutive equations for the storage field, if it is nonlinear, are

$$Z = \phi_s(X) \quad (2.3)$$

If the storage field is linear, the constitutive equations are

$$Z = SX \quad (2.4)$$

For the dissipation field in the nonlinear case

$$D_{out} = \phi_L(D_{in}) \quad (2.5)$$

and in the linear case

$$D_{out} = LD_{in} \quad (2.6)$$

where S and L are square matrices.

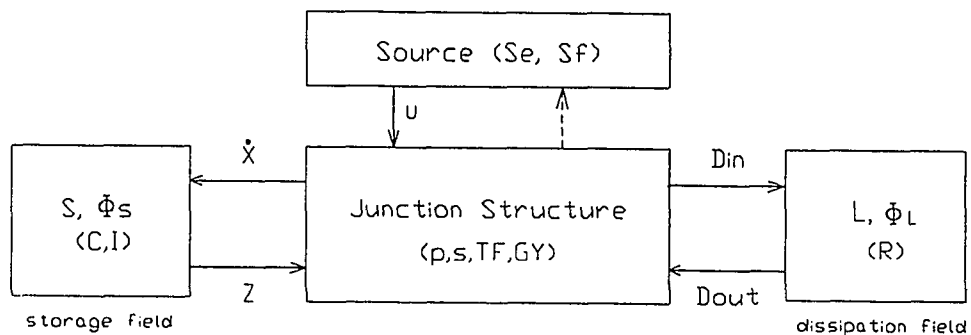


Figure 2.6 Significant Vectors for Systems Having Integration Causality

The junction structure yields expressions for the  $\dot{X}$  and  $D_{in}$  vectors in terms of the inputs to the junction structure, namely,  $Z$ ,  $D_{out}$ , and  $U$ . Provided that elements TF and GY all have constant moduli, this expression is

$$\begin{bmatrix} \dot{X} \\ D_{in} \end{bmatrix} = [J] \begin{bmatrix} Z \\ D_{out} \\ U \end{bmatrix} = \begin{bmatrix} J_{SS} & J_{SL} & J_{SU} \\ J_{LS} & J_{LL} & J_{LU} \end{bmatrix} \begin{bmatrix} Z \\ D_{out} \\ U \end{bmatrix} \quad (2.7)$$

The matrix  $J$  is always skew-symmetric, because the junction structure is energy conserving. If there are no algebraic loops, the matrix  $J_{LL}$  is zero.

If the system is linear, and the matrix  $J_{LL}$  is null, the state space equations are

$$\dot{X} = AX + BU \quad (2.8)$$

where

$$A = (J_{SS} + J_{SL}LJ_{LS})S \quad (2.9)$$

and

$$B = J_{SL}LJ_{LU} + J_{SU} \quad (2.10)$$

If the system is nonlinear, the state space equations are

$$\dot{X} = J_{SS}Z + J_{SL}D_{out} + J_{SU}U \quad (2.11)$$

that is

$$\dot{X} = J_{SS}\phi_S(X) + J_{SL}\phi_L(J_{LS}\phi_S(X) + J_{LU}U) + J_{SU}U \quad (2.12)$$

Any dynamic system may be expressed by the equation (2.12), no matter if the system is linear or nonlinear. The theoretical solution for equation (2.12) is very difficult to obtain for the nonlinear case. For numerical simulation, the Equation (2.12) could be expressed in a block diagram as shown in Figure 2.7. This block diagram may be

directly expressed in a simulation software, such as SIMULINK™, thus greatly simplifying the program development. For the nonlinear case in the block diagram,  $Y$  is the output vector, which is the function of state vector  $X$ , i.e.

$$Y = f(X) \quad (2.13)$$

For the linear case

$$Y = CX \quad (2.14)$$

where  $C$  is a matrix.

The constitutive functions  $\phi_S$  and  $\phi_L$  will be studied in the next three chapters. The formation of junction structure matrix could be completed by a computer program. The junction structure matrix only depends on the system structure. Once the system is defined, the junction structure is defined.

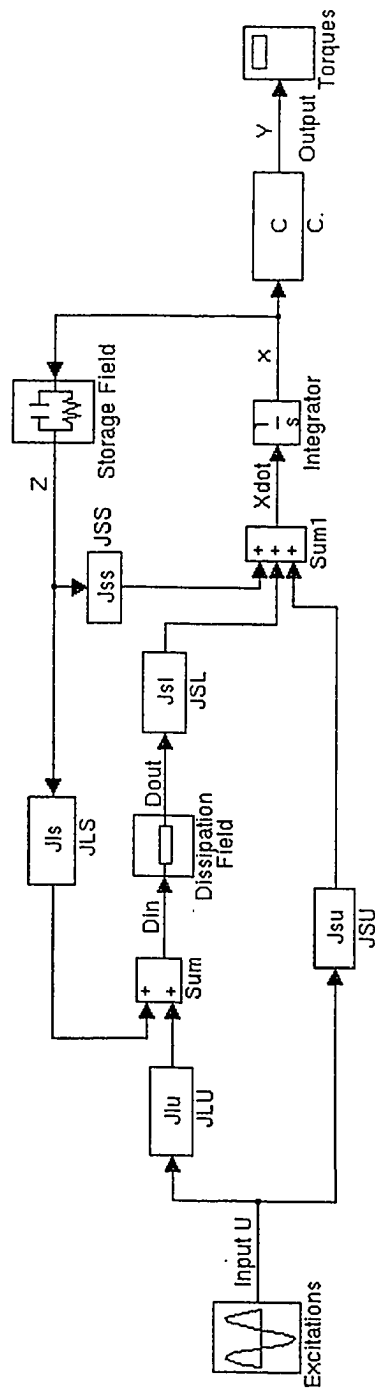


Figure 2.7 Simulation Block Diagram of Equation (2.12)



CHAPTER III  
CHARACTERISTICS OF THE SYSTEM COMPONENTS

Introduction

Several references (B.I.C.E.R.A., Den Hartog, etc) give detailed information about the characteristics of the components of the propulsion power train system. The information is tailored to fit the linear system, frequency domain analysis requirements. For example, the damping is given in the energy dissipation form. Stiffness and inertia are simplified to be constant. Excitation forces are decomposed into harmonic components. For the time domain, nonlinear simulation using the method developed in the chapter II, the constitutive equations for the components have to be prepared as shown in Table 3.1. This chapter discusses the constitutive equations in general. The characteristics of the elastic coupling will be investigated in the next two chapters.

Table 3.1 Constitutive Equations for Four Basic Elements

| element    | input                                     | output                                    | constitutive equation           |  |
|------------|---|---|---------------------------------|--|
|            |   |   | linear                          | nonlinear                              |
| excitation | torque, $T$                               |   |                                 | $T = f_T(t)$                           |
| inertia    | angular velocity, $\omega$                | angular momentum, $p_r$                   | $p_r = I\omega$                 | $p_r = f_I(\omega)$                    |
| spring     | angular displacement, $\varphi$           | torque, $T$                               | $T = K\varphi$                  | $T = f_K(\varphi)$                     |
| damper     | angular velocity, $\omega$ or torque, $T$ | torque, $T$ or angular velocity, $\omega$ | $T = b\omega$ or $\omega = T/b$ | $T = f_b(\omega)$ or $\omega = f_b(T)$ |

### Excitations

There are two types of excitations in the propulsion system. The external excitations of diesel engine and propeller are the sources of vibrations at one to twelve times crankshaft speed or one to three times blade passage frequency, respectively. The internal excitations are the source of vibrations at the frequency of tooth meshing, while eccentricity of gear, misalignment of gear, and tooth errors may appear at shaft frequency.

#### Diesel Engine Excitations

Diesel engine excitations are due to the combined effect of varying gas pressure and the variation in the effective reciprocating mass. The inertia torque is as follows (Den Hartog, 1956):

$$T_i = \frac{1}{2} m_{rec} \omega^2 r^2 \left( \frac{r}{2l} \sin \omega t - \sin 2\omega t - \frac{3r}{2l} \sin 3\omega t \right) \quad (3.1)$$

where

$m_{rec}$  = reciprocating mass,

$\omega t$  = crank angle from top dead center,

$r$  = crank radius,

$l$  = length of connecting rod.

Torque on the crank due to gas pressure is a periodic function, which may be derived by thermodynamic analysis, but it is usually provided by the engine manufacturers. Tangential pressure on the crank,  $p_t$ , is the function of gas pressure and the position of the piston

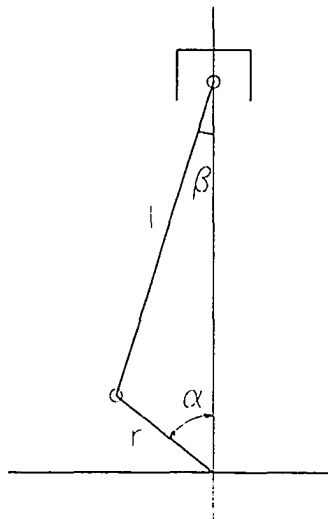


Figure 3.1 Crank Mechanism

$$P_t = \frac{\sin(\alpha + \beta)}{\cos \beta} P_g \quad (3.2)$$

where

$p_g$  = gas pressure (psi),

$\alpha$  = crank angle from top dead center,

$\beta$  = connecting rod angle (see Figure 3.1).

The gas pressure  $p_g$  is a periodic function repeating itself every cycle of the engine or every one or two revolutions of the shaft for two- or four-cycle engines, respectively. The torque due to gas pressure is expressed as

$$T_g = \frac{\pi}{4} d^2 r P_t \quad (3.3)$$

where

$d$  = piston diameter

In the absence of test data for an engine, Porter's data is recommended. When using that data, mean indicated pressure (mip or imep) is needed. The formula

calculating mip is given as follows (Obert)

$$p_b = bmep = \frac{12 \cdot bhp \cdot 33,000 \cdot n_x}{D n} \quad (3.4)$$

$$imep = \frac{bmep}{\eta_m}$$

where

$D = A L N$ , total piston displacement, in<sup>3</sup>

$p_b = bmep$  = brake mean effective pressure, psi

$A$  = piston-face area, in<sup>2</sup>

$L$  = length of stroke, in

$n_x$  = number of revolutions required for each power stroke delivered. 2 for a four-stroke-cycle engine and 1 for a two-stroke-cycle

$N$  = number of cylinder (or pistons) in the engine

$n$  = rpm,

$\eta_m$  = bhp/ihp, mechanical efficiency

bhp = brake horsepower

ihp = indicated horsepower

For time domain simulation, the gas torque may be rebuilt from Porter's harmonic data by the following formula

$$T_g = Ar \left[ b_0 + \sum_{i=1}^n b_i \cos(iy) + \sum_{i=1}^n a_i \sin(iy) \right] \quad (3.5)$$

where

$y = \omega t$  for two-stroke cycle engine,  $\frac{1}{2}\omega t$  for four-stroke cycle engine.

$a_i, b_i$  = harmonic coefficients.

$r$  = crank radius, in

$A$  = piston face area, in<sup>2</sup>

For torsional vibration simulation,  $b_0$  may be excluded from the above formula if the mean load torque is not included in the analysis.

For the multi-cylinder engine, the excitation torque for every cylinder is the same except for the phase angles. These phase angles are determined by the firing order and crank vector relationships. For misfiring simulation, the  $a_i$  and  $b_i$  corresponding to the nonworking cylinder has to be replaced with new values which represent the compression and expansion of the unburned mixture.

### Propeller Excitations

The propeller blades produce alternating torque as they pass through the variable wake. Fluid mechanics analysis and actual measurements may be necessary to determine the propeller load characteristic. In the absence of the measured data, the following formulas may be used to calculate the rated engine torque,  $T_{rated}$ , at rated speed,  $n_{rated}$ , and the mean engine torque,  $T_m$ , at speed  $n$ .

$$T_{rated} = 63025 \frac{HP_{rated}}{n_{rated}} \quad (3.6)$$

$$T_m = T_{rated} \left( \frac{n}{n_{rated}} \right)^2 \quad (3.7)$$

where

$HP_{rated}$  = engine rated horsepower at speed,  $n_{rated}$

$T_{rated}$  = engine rated torque (lb in) at speed,  $n_{rated}$

$n_{rated}$  = engine rated speed (rpm),

$n$  = engine speed (rpm).

The following formula may be used to estimate the propeller excitation torque,  $T_{cp}$ .

$$T_{ep} = r_p T_m \text{ratio} \sin(z\omega_p t) \quad (3.8)$$

$$\omega_p = \frac{2\pi n}{60 \text{ratio}}$$

where

$r_p$  = amplitude of alternating component of torque produced by the propeller blades at frequency  $z\omega_p$  divided by  $T_m$  = propeller torque excitation factor,

$z$  = number of propeller blades,

ratio = gear ratio,

$\omega_p$  = propeller rotation speed, rad/sec,

$t$  = time, sec.

The excitation factors are dependent on type of vessel and number of blades. The ranges of alternating propeller loads are given in Table 3.2. (Harrington)

Table 3.2 Propeller Torque Excitation Factors ( $r_p$ )

| No. of propeller blades         | 3           | 4           | 5           |
|---------------------------------|-------------|-------------|-------------|
| single-screw vessels            | 0.07 ~ 0.12 | 0.10 ~ 0.15 | 0.06 ~ 0.10 |
| twin-screw vessels with struts  | 0.02 ~ 0.05 | 0.02 ~ 0.05 | 0.02 ~ 0.4  |
| twin-screw vessels with bossing | 0.04 ~ 0.08 | 0.04 ~ 0.06 | 0.04 ~ 0.05 |

### Damping

System damping dissipates the continuous flow of excitation energy into the system. Its value influences the vibratory amplitude significantly at resonance. The empirical data are available in several reference books (for example, Nestorides, Wang, Q.).

Propeller torsional damping is produced by the action of the water on the

vibrating propeller. In general, the propeller damping coefficient,  $b_p$ , may be expressed as (Harrington)

$$b_p = \frac{C_p T_m \text{ ratio}}{\omega_p} \quad \frac{\text{in lb sec}}{\text{rad}} \quad (3.9)$$

where

$C_p$  = a constant.

As an approximation for many propellers,  $C_p = 3.7$  to  $4.0$ , which may be used in the absence of other data.

The energy loss in the bearings, gear mesh and shaft flexing is assumed to be hysteretic in nature and is expressed as follows

$$W_d = \frac{1}{2} \psi K (\varphi_{n-1} - \varphi_n) \quad (3.10)$$

where

$W_d$  = energy dissipated per cycle of vibration, lb in/cycle,

$\psi$  = relative damping factor,

$K$  = torsional stiffness of shaft, lb in/radian,

$(\varphi_{n-1} - \varphi_n)$  = angle of twist of shaft  $n$ , radian.

The equivalent viscous damping coefficient,  $C_E$ , may be calculated by equating the energy dissipated by hysteresis damping to the energy dissipated per cycle by viscous damping. Of course, this relationship is only valid at one frequency of vibration,  $\omega_{vib}$ , and assumes no other frequencies offer significant dissipation of energy.

$$C_E = \frac{\psi K}{2 \pi \omega_{vib}} \quad (3.11)$$

where

$\omega_{vib}$  = vibration frequency, rad/sec.

### Inertia

For most elements which store kinetic energy in the system, the constitutive equations are linear. The equivalent inertia of a simplified system must have the same kinetic energy as the original system. For example, the equivalent moment of inertia of each crank mechanism is the function of crank angle:

$$I_{eq} = I_{rot} + \frac{1}{2} m_{rec} (r \cos \omega t)^2 \quad (3.12)$$

where

$I_{rot}$  = rotating inertia, lb in sec<sup>2</sup>

$m_{rec}$  = reciprocating mass, lb sec<sup>2</sup> /in

$r$  = crank radius, in

$\omega t$  = crank angle from top dead center, radian.

The equivalent moment of inertia of engine damper may be a function of vibration frequency (Den Hartog):

$$I_{eq} = \frac{I_d}{1 + (I_d \omega_{vib} / C)^2} \quad (3.13)$$

where

$I_d$  = inertia of damper flywheel, lb in sec<sup>2</sup>

$\omega_{vib}$  = vibration frequency, rad/sec

$C$  = viscous friction coefficient of the damper, lb in sec.



### Stiffness

The torsional spring constant,  $K$ , may be evaluated by employing applied elasticity theory, testing, or finite element analysis. For example, the torsional stiffness for a spur gear may be calculated as follows:

For a spur gear, the actual gear tooth may be approximated by a tapered cantilever beam as shown in Figure 3.2 (Timoshenko and Baud). The tangential deflection due to bending and shear is  $\delta_{bs}$

$$\delta_{bs} = \frac{12F_n \cos \beta L^3}{Eh_0^3 b} \left[ \left( \frac{3}{2} - \frac{a}{2L} \right) \left( \frac{a}{L} - 1 \right) + \log_e \frac{L}{a} \right] + \frac{4F_n \cos \beta (L-a) (1+\mu)}{(h+h_0) Eb} \quad (3.14)$$

where

$\delta_{bs}$  = bending and shear deflection, in.

$E$  = modulus of elasticity, psi

$\mu$  = Poisson's ratio

and the other variables are defined in Figure 3.2.

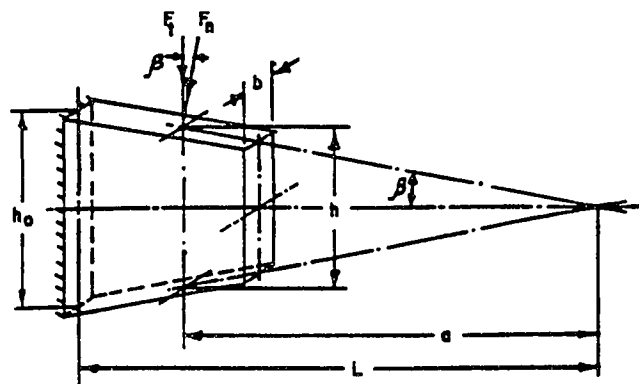


Figure 3.2 Timoshenko and Baud Gear Tooth Model

The local total deformation due to contact stress is (Furrow and Mabie)

$$\delta_c = \frac{2(1-\mu^2)}{Eb} \frac{F_n}{\pi} \left[ \frac{2}{3} + \log_e \frac{1.731 E b c \sin \phi}{F_n} \right] \quad (3.15)$$

where

$\delta_c$  = deflection due to contact, in.

$c$  = center distance between gears, in.

$\phi$  = pressure angle, degrees.

Assuming that contact deflection is divided equally between two teeth in the mesh and using only that component of contact deflection which is perpendicular to the tooth centerline, the contact deflection for pinion and gear is

$$\delta_{ci} = \frac{1}{2} \delta_c \cos \beta_i \quad (3.16)$$

where  $i = 1$  for pinion,  $i = 2$  for gear. The combined stiffness for pinion and gear is

$$k_i = \frac{(\delta_{bsi} + \delta_{ci})}{F_n \cos \beta_i} \quad (3.17)$$

The torsional stiffness with reference to the pinion side is

$$K_1 = \frac{R_1^2}{k_1 + k_2} \quad (3.18)$$

where  $R_1$  is the distance from the center of the pinion to the point where the force is applied.

For a gear set, the number of pairs of gear teeth vary as the gear rotates. The contact ratio is the average number of pairs of teeth in contact. For a gear set with contact ranging between 1 pair and 2 pairs of teeth, the combined stiffness for different contact ratios is shown in Figure 3.3. This indicates that the spur gear pair torsional stiffness may be approximated with two different spring constants  $K_1$  and  $K_2$  as shown

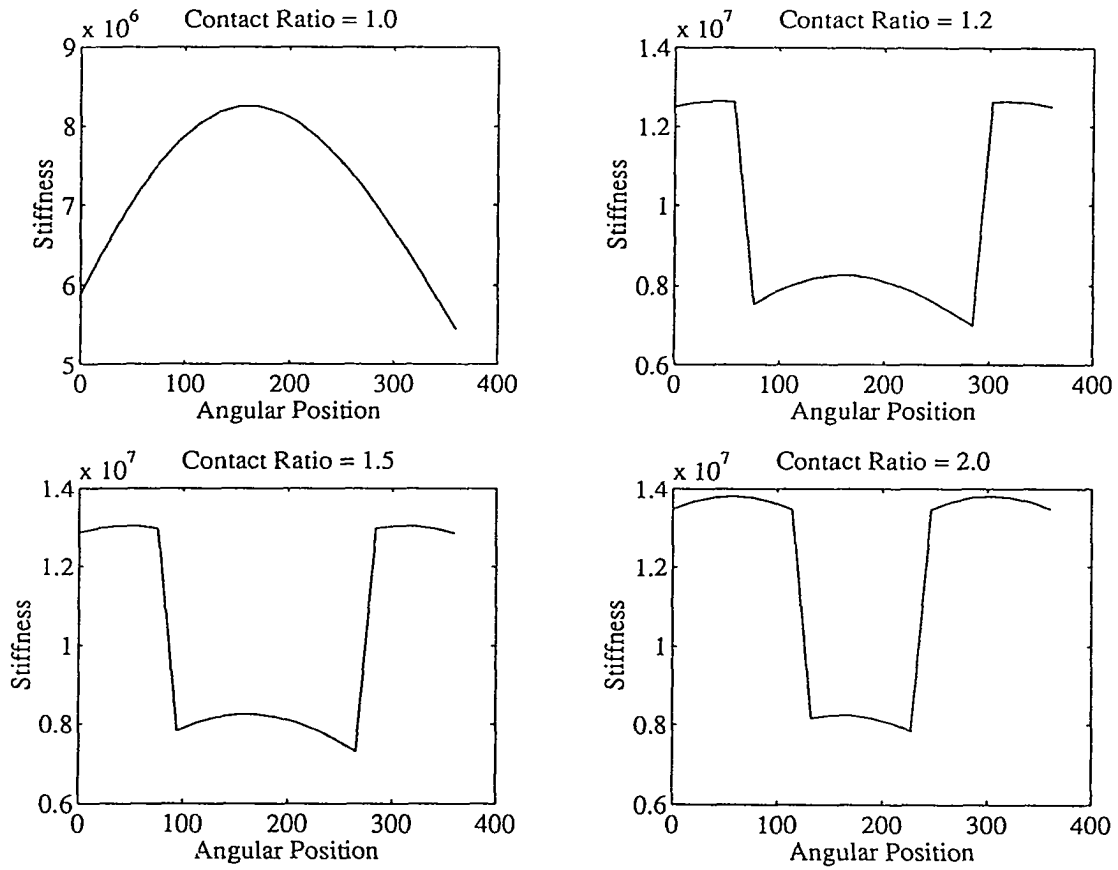


Figure 3.3 Torsional Stiffness of Spur Gear with Different Contact Ratio

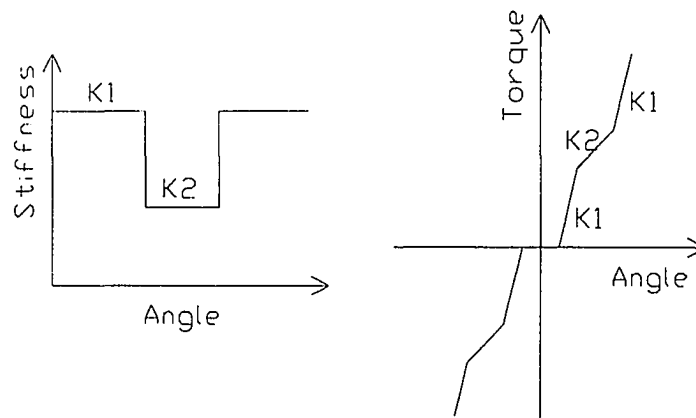


Figure 3.4 Approximation of Torsional Stiffness of Spur Gear

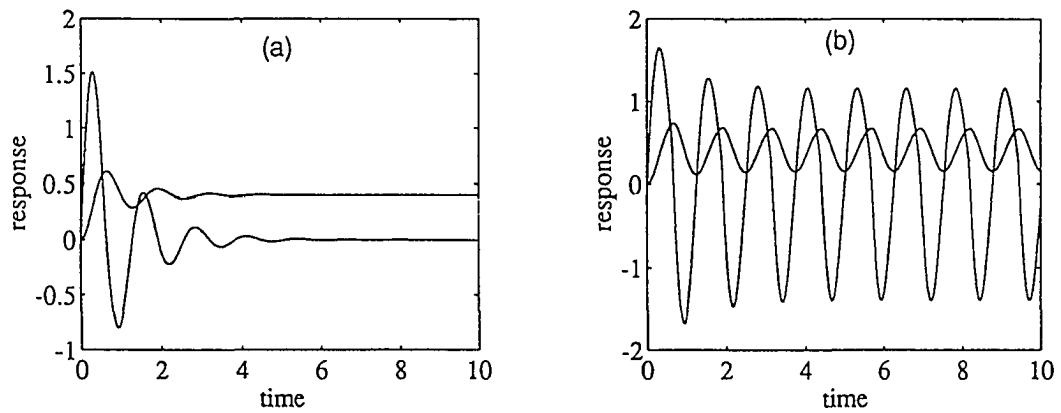


Figure 3.5 Step Response of Single DOF System  
 (a) Constant Stiffness (b) Position-varying Stiffness

in Figure 3.4(a). If the gear backlash is considered, the relationship between torque and angle of displacement for spur gears may be expressed as Figure 3.4(b).

The position-varying gear torsional stiffness produces a time-varying torsional stiffness for constant speed, which may cause self-excited vibration. Figure 3.4 shows the step response of a one-degree-freedom mass-spring system with a constant stiffness and a time-varying stiffness.

For helical gear pair, finite element analysis is necessary to get the compliance of the teeth. Zhang's results show that "The local compliance has a major influence on the total compliance. The compliance due to the effect of beam and foundation deformation is much smaller". The variation of the compliance is smaller compared with the spur gear pair. The flexibility due to total deflection may be approximated (B.I.C.E.R.A.) :

$$\frac{1}{K_{total}} = \frac{\delta}{P_t} = \frac{9}{b} \left[ \frac{1}{E_1} + \frac{1}{E_2} \right] \times \frac{1}{\cos \beta_n} \quad (3.19)$$

where

$\beta_n$  = helix angle at pitch line,

$E_1, E_2$  = modulus of elasticity, psi

$P_t$  = tangential force, lb

$\delta$  = tooth deflection, in

$b$  = face width, in.

The torsional stiffness of a single pair of helical gear with reference to the pinion side is  $K_1$ .

$$K_1 = \frac{R_1^2}{K_{total}} \quad (3.20)$$

Multiplying this by the contact ratio may give an approximation of the average stiffness.

## CHAPTER IV

### DESIGN OF THE DYNAMIC TEST STAND

#### Introduction

In the field of torsional vibrations, investigators are interested in the static and dynamic characteristics of the elastic coupling. Previous studies show that the dynamic properties may depend on the preload (mean torque), vibratory torque amplitude, frequency and temperature. The static stiffness values of HRC elastic couplings were measured by Elahi (1985). The results indicate that the static stiffness of the HRC elastic coupling is a strong function of the mean torque. The dynamic characteristics of HRC couplings are not available.

A typical HRC elastic coupling used in marine vessels consists of inner hub, cover flange, front plate and rubber elements as shown in Figure 4.1. There are six to twelve rubber elements in one coupling depending on the type and the capacity of the coupling. The rubber element is not a pure rubber material but a composite. It is reinforced with chords. The torque is transmitted from one side to another through the rubber elements which connect the inner hub to the cover flange with pins. There are a number of different configurations for elastic couplings in production.

In order to evaluate the influence of various parameters on the dynamic properties of the elastic coupling, the test stand design must provide for measurement of mean torque, damping, vibration torque, temperature, frequency and vibratory torque amplitude over the operating ranges. Namely, it has to meet the following requirements:

- (1) Provide the required mean torque from 20% to 110% of rated torque,
- (2) Simulate the ambient operation temperature from 70°F to 120°F,
- (3) Generate the vibratory torque with frequency from 0 to 50 hz,
- (4) Vary the vibratory torque amplitudes from 5% to 50% of mean torque.
- (5) Record two signals: the torque transmitted by the coupling and the angular displacement across the coupling, at the same time with a relative high sample rate.

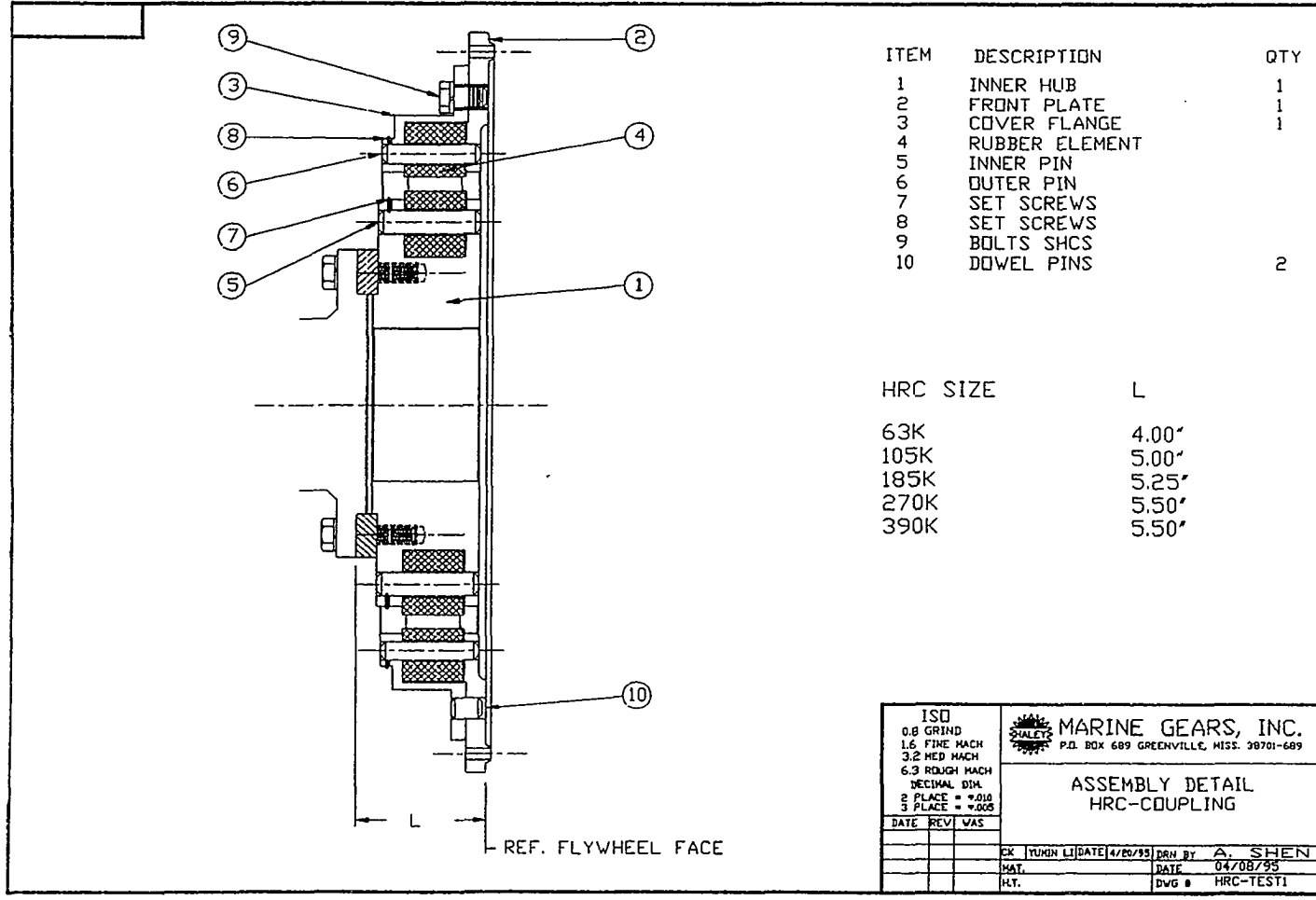


Figure 4.1 Assembly Details of HRC Coupling



### Description of Dynamic Test Stand

The test stand consists of mechanical, hydraulic, and electronic systems (Figure 4.2). Figure 4.3 shows the left side view of the dynamic test stand. The test stand is symmetric with two identical elastic couplings. Using two couplings allows the preload torque of one coupling to react to the preload of the other coupling like a "four square test stand". The coupling inner hubs are mounted on the shaft. The front plate of the right coupling is connected to the frame. By twisting the front plate of the left coupling through a chain hoist, mean torque is applied. Then the front plate of the left coupling is locked down to the frame. The vibratory torque is generated by a rotating mass driven by a hydraulic motor, which is attached to a beam. The rotating mass is connected to the left coupling hub through a 30 inch long rectangular beam as shown in Figure 4.4. The required vibration frequency is achieved by adjusting the flow rate, which goes to the hydraulic motor from the hydraulic pump. The eccentric weight and its eccentric radius determine the vibratory amplitude. All the machine components are designed to withstand both static and dynamic requirements. For example, the shaft, which is shown in Figure 4.5, is designed to satisfy the strength requirement. At the same time, it must have a significant strain output to be measurable. The strain gages are attached on the surface of the shaft between the inner hubs to measure the strain, which can be converted to torque. Three Linear Differential Transformers (LVDT) are mounted at 120° apart. The LVDT core is connected to the inner hub through a tripod, the LVDT housing is connected to the front plate through a bracket.(see Figure 4.3).

For high temperature tests, a small insulated house covers the test stand (Figure 4.6). The house is heated by several electrical heaters to achieve the required the temperature.

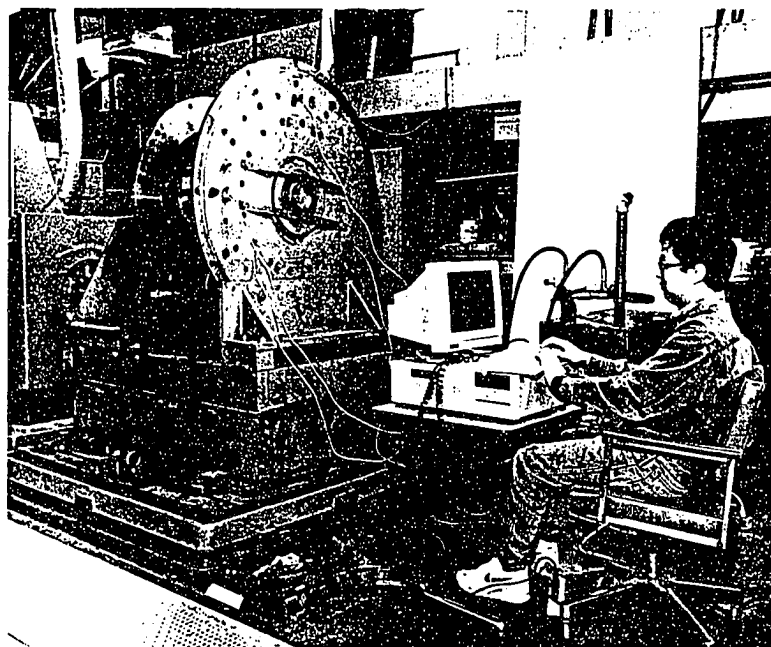


Figure 4.2 HRC Coupling Dynamic Test Stand

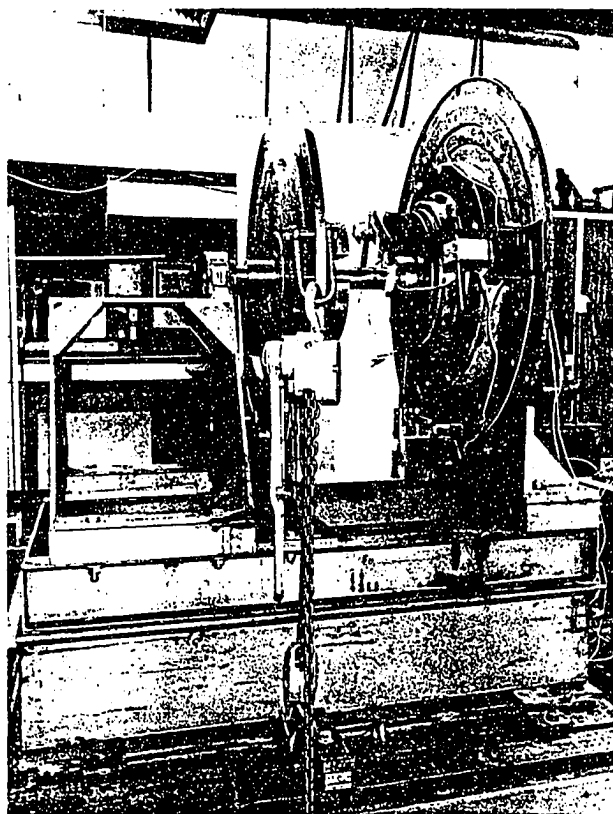


Figure 4.3 Left Side View of Dynamic Test Stand

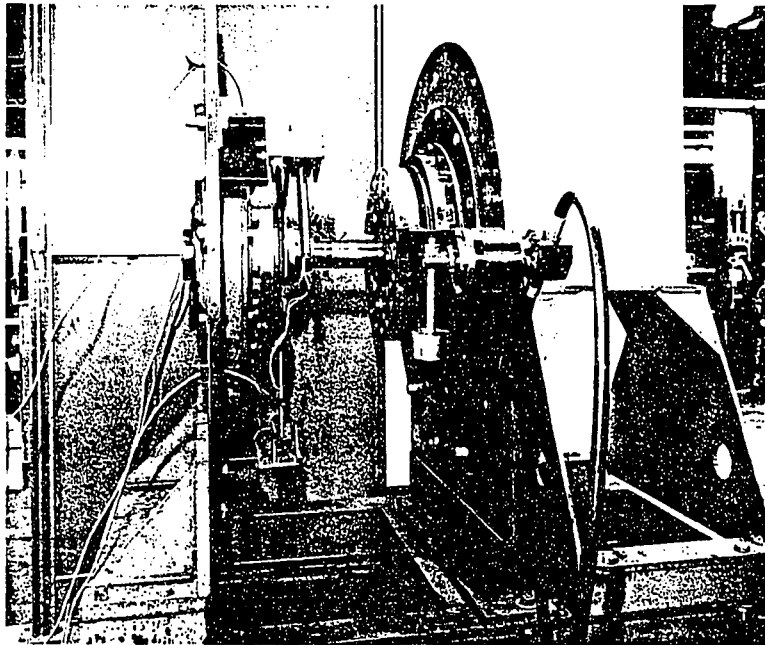


Figure 4.4 Right Side View of Test Stand

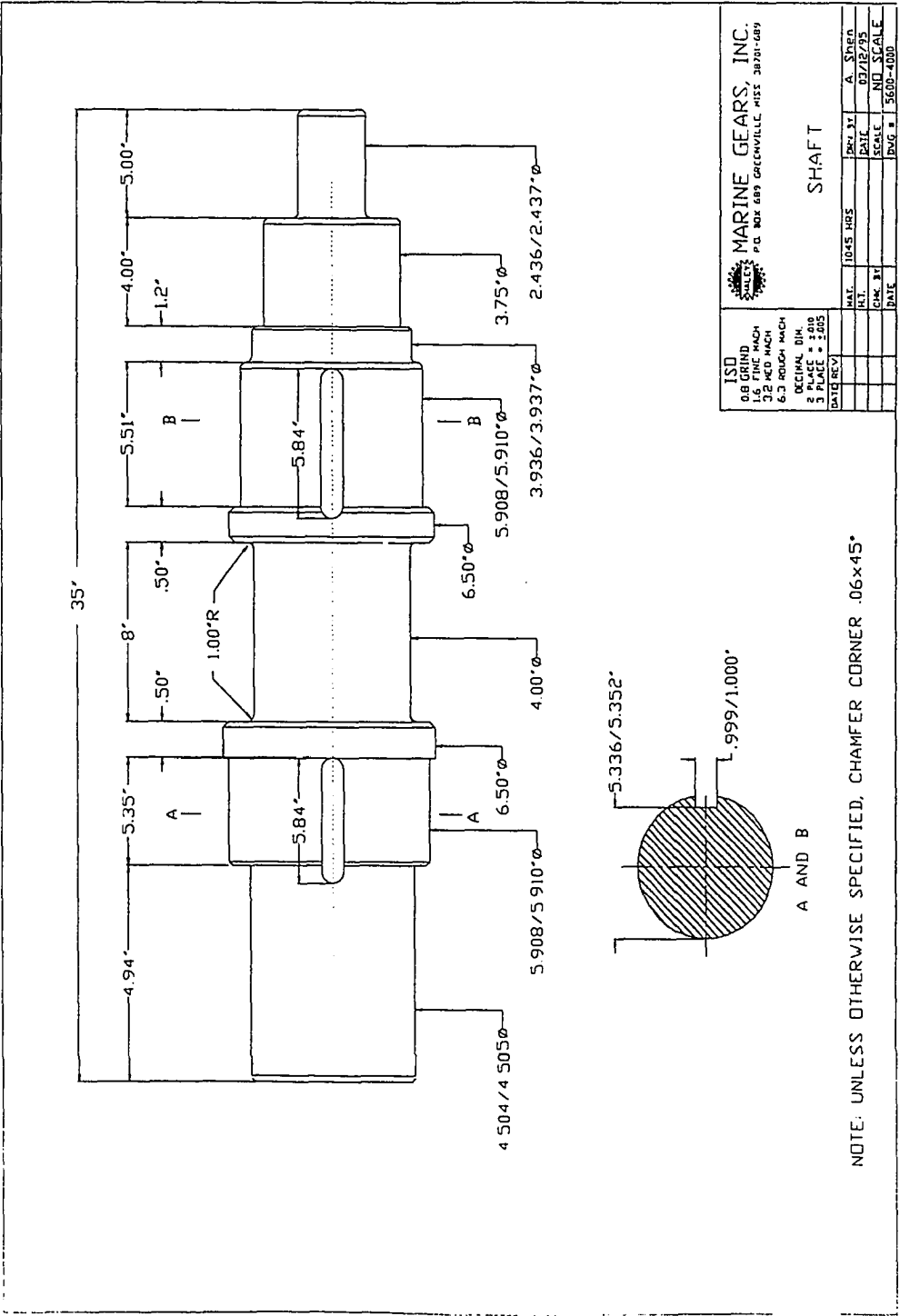


Figure 4.5 Dynamic Test Stand Shaft Details

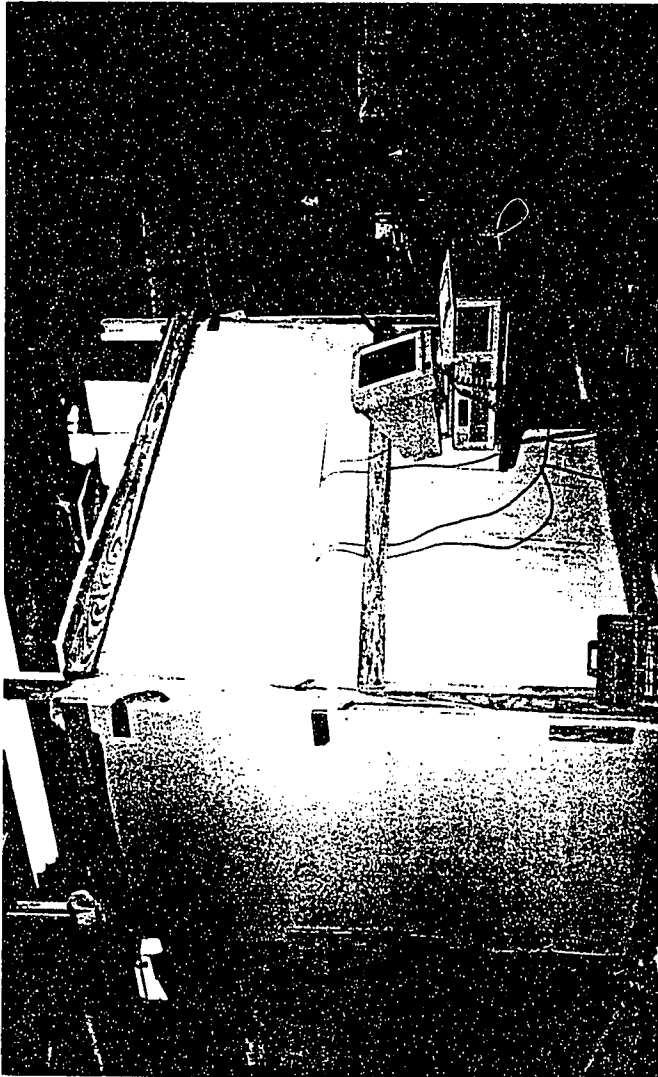


Figure 4.6 Test Stand Housing

### Dynamic Analysis of Test Stand

Dynamic analysis of the test stand will provide the necessary data for checking components' strength, estimation of the shaker force, design of hydraulic system and the calculation of the torque transmitted through the rubber elements.

The test stand may be modeled as a lumped system as shown in Figure 4.7. The torsional stiffness of the elastic coupling is  $K_r$ . Its value is unknown but can be estimated based on existing zero frequency test data. The coupling damping is  $C_r$ .  $J_1$  represents the inertia of right inner hub and the LVDT mounting device.  $J_2$  the inertia of the left inner hub and part of the shaker arm. The equivalent inertia of the shaker and part of the arm is  $J_3$ . The torsional stiffness of the shaft is  $K_1$ . The equivalent torsional stiffness of the shaker arm is  $K_2$ . The data are as follows:

$$J_1 = J_{hub} + 2.5 \text{ lb-in-s}^2$$

$$J_2 = J_{hub} + J_{arm}$$

$J_{hub} = 1.86 \text{ lb in s}^2$  for HRC-63K,  $5.0 \text{ lb in s}^2$  for HRC-105K,  $41.6 \text{ lb in s}^2$  for HRC-390K

$$J_3 = J_{arm} + J_{shaker} = 9.8 + m_s 30^2$$

where  $m_s$  is the weight of shaker and eccentric weight

$$K_1 = 5.13 \times 10^6 \text{ lb in/radian}$$

$$K_2 = 3.83 \times 10^7 \text{ lb in/radian}$$

$K_r = 5.714 \times 10^5$  (HRC-63K),  $9.69375 \times 10^5$  (HRC-105K),  $4.76375 \times 10^6$  (HRC-390K)

$$C_r = (K_r \psi_r) / (2\pi\omega_r), \psi = 1.1, \omega = 2\pi f$$

The system differential equations are

$$J\ddot{\Theta} + C\dot{\Theta} + K\Theta = T \quad (4.1)$$

where

$$J = \begin{bmatrix} J_1 & 0 & 0 \\ 0 & J_2 & 0 \\ 0 & 0 & J_3 \end{bmatrix}$$

$$C = \begin{bmatrix} C_r & 0 & 0 \\ 0 & C_r & 0 \\ 0 & 0 & 0 \end{bmatrix}$$

$$K = \begin{bmatrix} k_1 + k_r & -k_1 & 0 \\ -k_1 & k_1 + k_2 + k_r & -k_2 \\ 0 & -k_2 & k_2 \end{bmatrix}$$

$$T = \begin{bmatrix} 0 \\ 0 \\ T_2 \end{bmatrix}$$

The computer program is attached in Appendix C. The analysis results for the HRC-63K coupling are shown in Table 4.1.

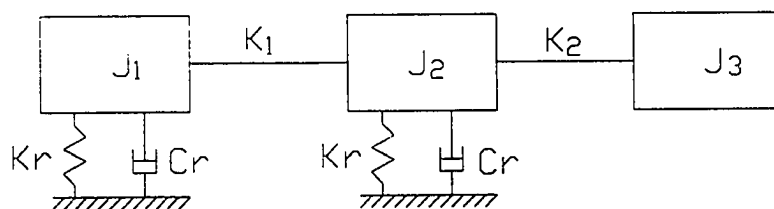


Figure 4.7 Torsional Vibration Model of Test Stand



Table 4.1 Vibration Analysis Results of the Dynamic Test Rig for HRC-63K Coupling with Half Rubber Elements

| Vibration Frequency (f, hz) | Excitation Torque (Te,lb-in) | Excitation Force (Fe,lb) | Coupling Vibratory Torque (Tc,lb-in) | Tc over Trated (%) | Shaft Vibratory Torque (Ts,lb-in) | Shaft Surface Strain (10 <sup>-6</sup> ) | LVDT Stroke (inches) | Eccentric weight-radius (WR,lb-in) | Eccentric Weight (W,lbs) | Eccentric Radius (R,inches) |
|-----------------------------|------------------------------|--------------------------|--------------------------------------|--------------------|-----------------------------------|--|----------------------|------------------------------------|--------------------------|-----------------------------|
| 5                           | 7875.00                      | 262.50                   | 3642.88                              | 46.26              | 3684.78                           | 52.22                                    | .0510                | 102.77                             | 10                       | 10.28                       |
| 5                           | 17325.00                     | 577.50                   | 8014.34                              | 101.77             | 8106.51                           | 114.88                                   | .1122                | 226.09                             | 10                       | 22.61                       |
| 10                          | 7875.00                      | 262.50                   | 4082.50                              | 51.84              | 4084.04                           | 57.88                                    | .0572                | 25.69                              | 5                        | 5.14                        |
| 10                          | 15198.75                     | 506.62                   | 8005.97                              | 101.66             | 8008.98                           | 113.50                                   | .1121                | 49.59                              | 8                        | 6.20                        |
| 20                          | 7875.00                      | 262.50                   | 7198.44                              | 91.41              | 6881.14                           | 97.52                                    | .1008                | 6.42                               | 2                        | 3.21                        |
| 20                          | 8662.50                      | 288.75                   | 7918.29                              | 100.55             | 7569.26                           | 107.27                                   | .1109                | 7.07                               | 2                        | 3.53                        |
| 30                          | 7875.00                      | 262.50                   | 17084.33                             | 216.94             | 15068.27                          | 213.54                                   | .2392                | 2.85                               | 1                        | 2.85                        |
| 30                          | 3780.00                      | 126.00                   | 8200.48                              | 104.13             | 7232.77                           | 102.50                                   | .1148                | 1.37                               | 1                        | 1.37                        |
| 40                          | 7875.00                      | 262.50                   | 3599.39                              | 45.71              | 2803.71                           | 39.73                                    | .0504                | 1.61                               | 1                        | 1.61                        |
| 40                          | 17325.00                     | 577.50                   | 7918.67                              | 100.55             | 6168.17                           | 87.41                                    | .1109                | 3.53                               | 1                        | 3.53                        |
| 50                          | 7875.00                      | 262.50                   | 1789.63                              | 22.73              | 1158.91                           | 16.42                                    | .0251                | 1.03                               | 1                        | 1.03                        |
| 50                          | 35437.50                     | 1181.25                  | 8053.32                              | 102.26             | 5215.09                           | 73.91                                    | .1128                | 4.62                               | 1                        | 4.62                        |

### Design of Hydraulic System

The vibratory torque is generated by a rotating mass which is driven by a hydraulic motor. Figure 4.8 shows the schematic drawing of the hydraulic system. The three phase electric motor operates at 1800 rpm. The specifications of the JSB Hydraulic Gear pump are listed in Table 4.2. The Dayton Fluid Motor performance data are listed in Table 4.3.

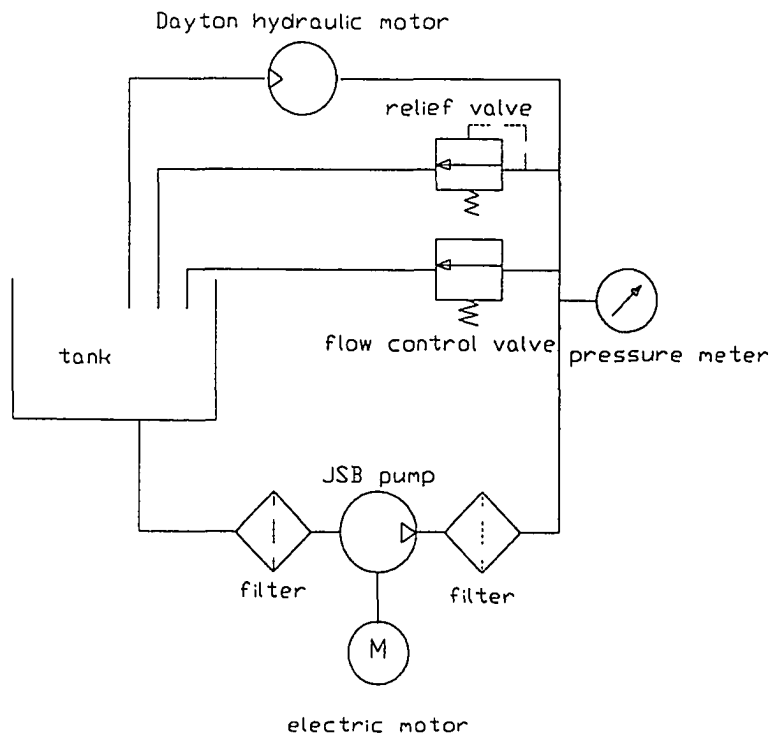


Figure 4.8 Test Stand Hydraulic System

Table 4.2 JSB Gear Pump Specifications

| Output Normal GPM | Output Cubic inches per Rev | GPM@RPM  |          | Max. Pressure (psi) |                   | Stock Number |
|-------------------|-----------------------------|----------|----------|---------------------|-------------------|--------------|
|                   |                             | 1800 RPM | 3600 RPM | Continuous Duty     | Intermittent Duty |              |
| 9                 | 1.16                        | 9.03     | 18.06    | 4000                | 4400              | 4F671        |

Table 4.3 Fluid Motor Performance Data

| Model | Flow Range GPM | Inlet Pressure |           |               |           |               |           |               |           |               |           |
|-------|----------------|----------------|-----------|---------------|-----------|---------------|-----------|---------------|-----------|---------------|-----------|
|       |                | 500 psi        |           | 1000 psi      |           | 1500 psi      |           | 2000 psi      |           | 2500 psi      |           |
|       |                | Torque in-lbs  | Speed RPM | Torque in-lbs | Speed RPM | Torque in-lbs | Speed RPM | Torque in-lbs | Speed RPM | Torque in-lbs | Speed RPM |
| 4F656 | 4              | 28             | 1951      | 60            | 1862      | 93            | 1774      | 126           | 1686      | 159           | 1597      |
|       | 6              | 28             | 2971      | 60            | 2882      | 93            | 2974      | 126           | 2706      | 159           | 2617      |
|       | 8              | 28             | 3991      | 60            | 3902      | 93            | 3814      | 126           | 3725      | 159           | 3637      |
|       | 10             | 28             | 5000      | 60            | 4922      | 93            | 4834      | 126           | 4745      | 159           | 4657      |

The highest frequency to be operated is 50 HZ, which requires 3000 rpm for motor speed. The Dayton fluid motor 4F656 will give this speed if the flow rate is about 8GPM. This 8GPM flow rate is supplied by the JSB hydraulic gear pump 4F671 @ 1800 RPM. Results of the dynamic analysis show the maximum required torque (which is the weight times radius) to excite the system for HRC-63K, HRC-105K and HRC-390K couplings is 50 in lbs, 40 in lbs and 210 in lbs, respectively. The Dayton 4F656 motor, which generates 126 in-lbs torque at pressure 2000 psi is enough for HRC-63K and HRC-105K tests, but is not sufficient for testing the HRC-390K coupling. Therefore, for testing the HRC-390K coupling, the eccentric weight is raised to the highest point and released.

To estimate the horse power needed for the system, take the HRC-390K coupling with 1/4 of the elements installed as an example. The energy dissipated by the elastic

coupling is:

$$W_d = \frac{1}{2} \psi_r K \phi^2 = \frac{1}{2} \psi_r T \phi \quad (4.2)$$

where

$K$  = coupling stiffness =  $4.76 \times 10^6$  lb in /radian,

$\psi_r$  = relative damping = 1.2,

$\phi$  = vibratory amplitude = 0.05 inches,

$T$  = rated torque = 97500 lb in.

Substituting the above values yields  $W_d = 292.5$  lb in/cycle. Considering two elastic couplings, the total dissipated energy is  $W_d = 585$  lb in/cycle. The maximum power which occurs at 50 Hz frequency is

$$Power = W_d \times f_{\max} = \frac{585 \frac{lb-in}{cyle} \cdot 50 \frac{cycles}{sec}}{12 \frac{in}{ft} \cdot \frac{550 ft-lb}{sec HP}} = 4.43 HP.$$

The power provided by the Dayton fluid motor at 7 GPM with 2000 psi pressure and an efficiency of 80% is

$$Power = \frac{Q p}{1714 \eta} = \frac{(7 GPM) (2000 psi)}{1714 \times 0.8} = 10.21 HP$$

which is sufficient to drive the shaker.

The pump's inlet pipe has a diameter 3/4" which gives a cross sectional area of 0.44 in<sup>2</sup>. With 8 GPM flow rate the average fluid velocity in the suction line is

$$v_{in} = 8 \frac{Gallon}{min} \cdot \frac{231 in^3}{Gallon} \cdot \frac{min}{60 sec} \cdot \frac{ft}{12} \cdot \frac{1}{.44} = 5.83 ft/sec$$

The pump's outlet pipe has a diameter 1/2" which gives a cross sectional area of

0.196 in<sup>2</sup>. With 8 GPM flow rate the average fluid velocity in the high pressure line is 13.1 ft/sec. Both velocities meet the design requirements of 6 fps in the inlet and 15 fps in the outlet for the pump.

### Instrumentation of Testing System

In order to evaluate the coupling's dynamic stiffness and damping, two signals, torque transmitted by coupling and the relative angular displacement of the coupling, must be recorded in the time domain. The torque transmitted by the coupling may be indirectly obtained by measuring the strain on the surface of the shaft. The relative angular displacement may be evaluated by measuring the change in length between points on the inner hub and the outer hub of the elastic coupling at a specific radius.

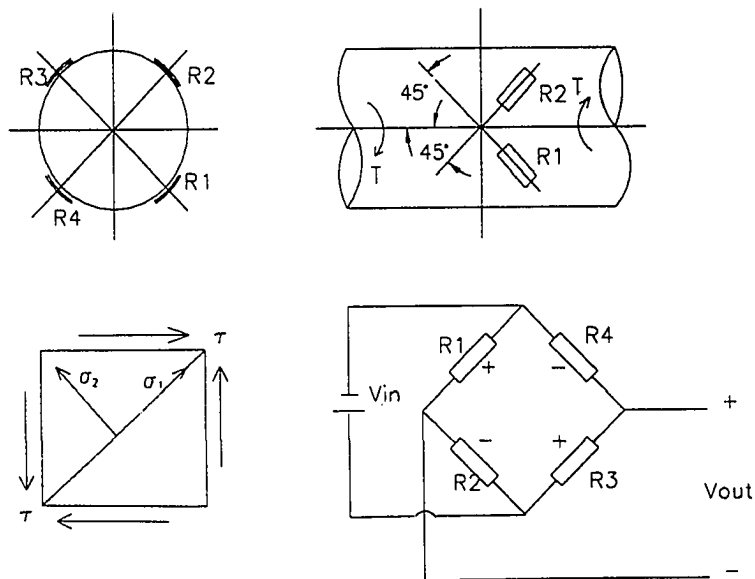


Figure 4.9 Wiring Diagram of Four Strain Gages

Figure 4.9 shows the connection of strain gages in a Wheatstone bridge for measuring the torsional strains. The gages are mounted at a  $45^\circ$  angle with the shaft axis. Gages  $R_1$  and  $R_3$  are diametrically opposite on the shaft surface, and the same restriction holds with gages  $R_2$  and  $R_4$ . The full wheatstone type bridge system results in automatic temperature compensation for all gages and elimination of the effects of all strains other than torsional strain. Two Micro-Measurements 2-element  $90^\circ$  rosette are used in this circuit. The specifications are as follows:

Type: CEA-06-187UV-350

Resistance:  $350.0 \pm 0.4\%$  ohms at  $24^\circ\text{C}$

Gage factor:  $2.065 \pm 0.5\%$  at  $24^\circ\text{C}$

Since the strain gage signal is relatively small, electrical noise at 60 Hz may occur and a d.c. offset voltage may exist, a signal conditioner is employed to amplify the output, to filter out the noise, and to balance the bridge. Figure 4.10 shows the circuit of the signal conditioner which was designed and built by Jeff Rayburn and modified by the author. The amplifier section of the circuit has two different gains 100 and 250. The null balance section of the circuit shown in Figure 4.10 is used to balance (i.e., "zero") the bridge. It consists of a  $50\text{ k}\Omega$  potentiometer and two  $10\text{ k}\Omega$  resistors. This compensates for differences in resistance due to the lead wire lengths, thermal strains, solder joints, etc. The signal conditioner has two outputs, one passes through the low pass filter, and the other is unfiltered. The low pass filter is designed to achieve the cleanest possible signal without attenuating the strain gage signals of 0 to 50 Hz by setting the break frequency at 1000 cps.

The circuit and block diagram for measuring the relative angular movement between the inner and outer hubs is shown in Figure 4.11. The angular movement is evaluated from changes in chord length as measured by LVDTs. Three LUCAS 1000 DC-E Liner Variable Differential Transformers (LVDT) are used in this experiment.

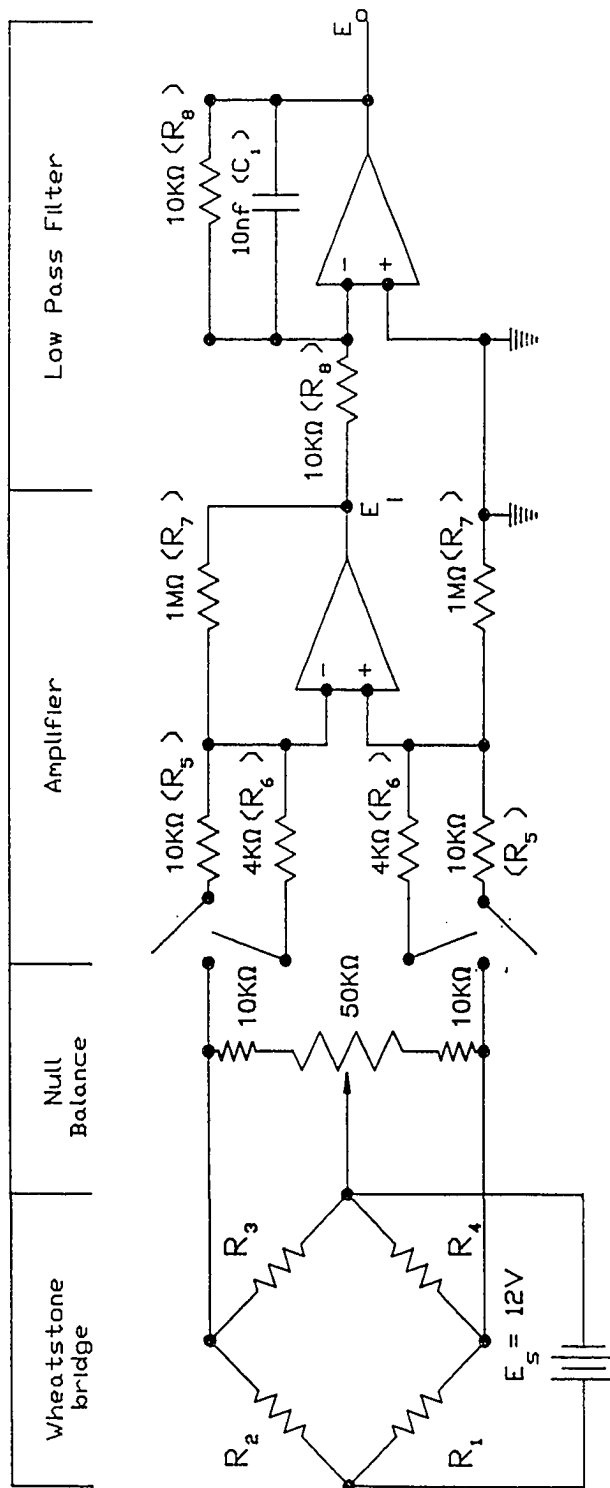


Figure 4.10 Signal Processing Circuit for Strain Gages

The specifications are:

- Input:  $\pm 15\text{V DC}$  (nominal),  $\pm 20\text{ ma}$
- Operating Temperature Range:  $32^\circ\text{F}$  to  $+160^\circ\text{F}$
- Survival Temperature Range:  $-65^\circ\text{F}$  to  $+200^\circ\text{F}$
- Shock Survival: 250g for 11 milliseconds
- Vibration Tolerance: 10g up to 2KHZ
- Output Impedance: less than 1 Ohm
- Nominal Liner Range:  $\pm 1.000$  inches
- Scale Factor: 10.0
- Response -3dB: 200HZ

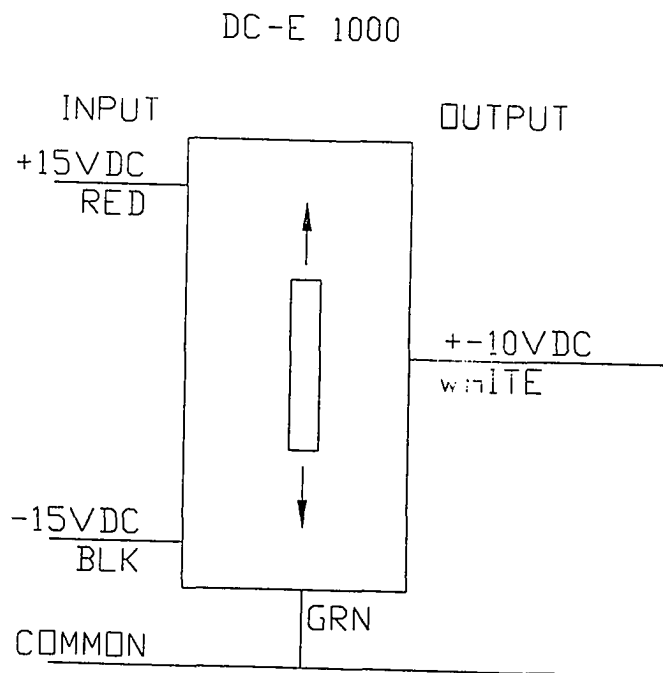


Figure 4.11 LVDT Circuit



The scale factor is calibrated for each LVDT by the manufacturer. The serial numbers, S/N, and scale factor, SF, are: S/N 8178 SF = 10.385 V/in, S/N 8176 SF = 10.419 V/in, S/N 8171 SF = 10.361 V/in.

Both strain and displacement are measured at the same time at high speed. The computer data acquisition system board DAS1402 is used to receive the signals. DAS1402 board is multi-function, high speed, analog and digital interface board for the PC computers. The DAS1402 offers 8 differential or 16 single-ended analog input channels with 12-bit resolution at 100,000 samples/sec. Input ranges are software-programmable. The DAS1402 offers gains of 1, 2, 4, and 8. The input ranges for the bipolar setting are respectively:  $\pm 10V$ ,  $\pm 5V$ ,  $\pm 2.5V$ ,  $\pm 1.25V$ .

Figure 4.12 shows the configuration of the test stand data acquisition system. Channel 0 reads filtered strain gage signals, channel 1 receives unfiltered strain gage signals, channels 3, 4, 5 receive the LVDT signals. Two computer programs, "Static.bas" and "Dynamic.bas", which were used in this test, are attached in Appendix D. The programs record the readings at a high speed and save them to a data file.

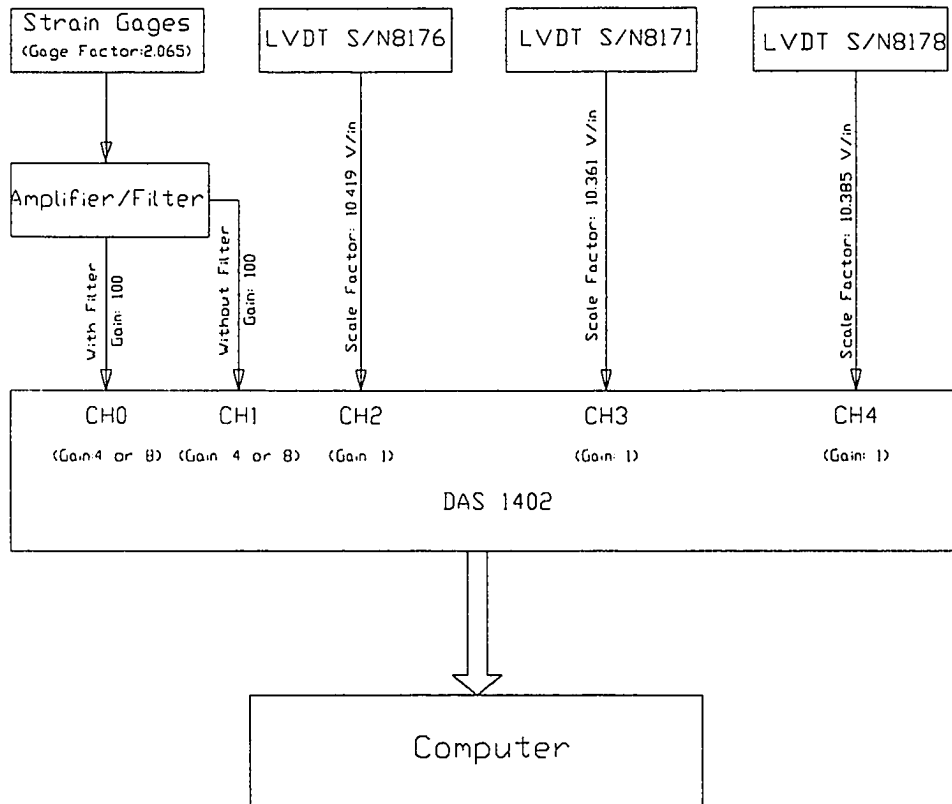


Figure 4.12 Test Stand Data Acquisition System

### Signal Processing

The data recorded from the A/D board are voltage signals and must be converted to the corresponding torque and angular displacement values.

The strain on the surface of the shaft at  $45^\circ$ ,  $\epsilon_{@45^\circ}$ , can be calculated as follows for a four active arm bridge made of strain gages having the same resistance:

$$\varepsilon_{@45^\circ} = \frac{-V_r}{GF} \quad (4.3)$$

$$V_r = \left[ \left( \frac{V_{out}}{V_{in}} \right)_{strained} - \left( \frac{V_{out}}{V_{in}} \right)_{unstrained} \right] \quad (4.4)$$

where

GF = gage factor,

$V_r$  = ratio of change in voltage,

$V_{in}$  = bridge excitation voltage,

$V_{out}$  = bridge output voltage.

The shear strain  $\gamma$  is

$$\gamma = 2 \times \varepsilon_{@45^\circ} = \frac{\tau}{G} \quad (4.5)$$

where

$$\tau = \text{torsional stress} = \frac{T d/2}{J}$$

T = torque on the shaft,

J = polar moment of inertia of the shaft.

For a solid circular shaft, torque on the shaft is

$$T = \frac{\gamma G \pi d^3}{16} \quad (4.6)$$

where

G = shear modulus of elasticity,

d = shaft diameter.

For a gage factor, GF, of 2.065, a bridge excitation voltage  $V_{in}$ , a shaft diameter, d, of 2.5" and a steel shaft with  $G = 11.5 \times 10^6$  psi, the torque, T, transmitted by the shaft is given below, if the bridge is initially balanced, and  $V_r = (V_{out} / V_{in})_{strained}$ .

$$T = \frac{\gamma G \pi d^3}{16} = \frac{2 \varepsilon_{\theta 45} G \pi d^3}{16} = -\frac{V_r G \pi d^3}{8 G F} \quad (4.7)$$

$$T = -\frac{11.5 \times 10^6 \times \pi \times 2.5^3}{2.065 \times V_{in} \times 8} \times V_{out} = -34.171 \times 10^6 \frac{V_{out}}{V_{in}}$$

Let  $V_{i0}$ ,  $V_{i1}$  represent the initial reading of the strain gage channels 0 and 1, let  $V_0$ ,  $V_1$  represent the channels 0 and 1 readings. The amplifier gain for the strain gage bridge was set to 100. The gain of the DAS1402 board for strain gage data channels 0 and 1 is 8 ( $\pm 1.25$  V). The mean torque is evaluated as follows:

$$T_{mean} = 34.171 \times 10^6 \times V_{i0} \times \frac{1.25}{2048} \times \frac{1}{100} \times \frac{1}{V_{in}} \quad (4.10)$$

$$= 208.56324 V_{i0}/V_{in} \quad (in-lbs)$$

where

$V_{in}$  = bridge excitation voltage.

The vibratory torque is calculated as follows:

$$T_{vibratory} = 208.56324 (V_0 - V_{i0}) / V_{in} \quad (in-lbs) \quad (4.11)$$

The relative angular displacement between inner hub and outer hub of coupling from Figure 4.13 is  $\delta\theta$

$$\delta\theta = 2 \left[ \arcsin\left(\frac{l_1 + \delta l}{2R}\right) - \arcsin\left(\frac{l_1}{2R}\right) \right] \quad (4.8)$$

where

$R = 16"$ , radius where is the LVDT is mounted,

$l_1$  = initial distance between two mounting points,

$\delta l = l_2 - l_1$ , relative displacement between two mounting points.

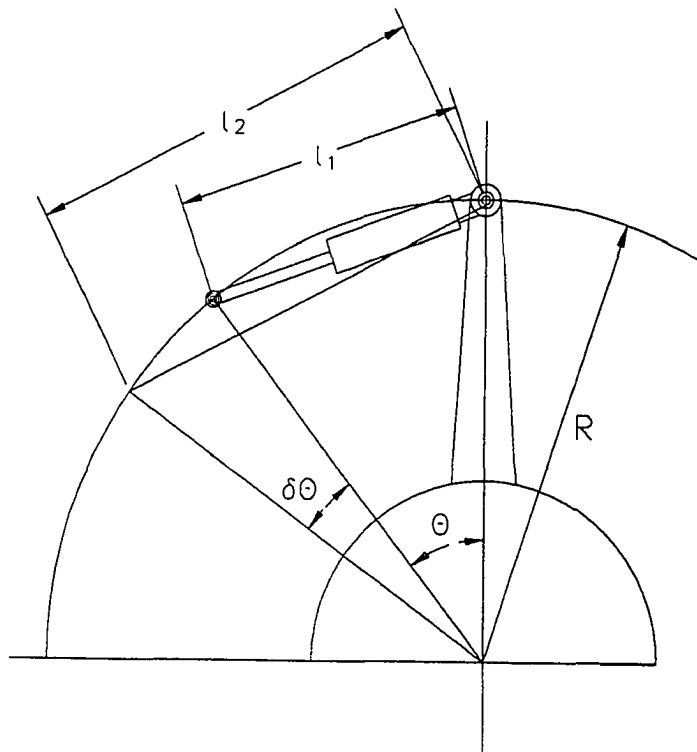


Figure 4.13 Relationship Between LVDT Linear Displacement and Coupling Angular Twist

The relationship between the relative displacement and output voltage is

$$\delta l = \frac{(V_{out} - V_{out\ initial})}{SF} \quad (4.9)$$

where SF is the scale factor supplied by the LVDT manufacturer.

Let  $V_{i2}$ ,  $V_{i3}$ ,  $V_{i4}$  represent the initial readings of the three LVDTs channels 2, 3 and 4; let  $V_2$ ,  $V_3$ ,  $V_4$  represent the channels 2, 3 and 4 readings. The gain of the

DAS1402 board for channels 2, 3, and 4 is  $1 (\pm 10 \text{ V})$ . The three linear relative displacements are:

$$\begin{aligned}\delta l_1 &= \frac{(V_2 - V_{i2})}{2048} \times \frac{10}{10.419} \\ &= 4.6864502 \times 10^{-4} (V_2 - V_{i2})\end{aligned}\quad (4.12)$$

$$\begin{aligned}\delta l_2 &= \frac{(V_3 - V_{i3})}{2048} \times \frac{10}{10.361} \\ &= 4.7126846 \times 10^{-4} (V_3 - V_{i3})\end{aligned}\quad (4.13)$$

$$\begin{aligned}\delta l_3 &= \frac{(V_4 - V_{i4})}{2048} \times \frac{10}{10.385} \\ &= 4.7017935 \times 10^{-4} (V_4 - V_{i4})\end{aligned}\quad (4.14)$$

The angular displacements are:

$$\delta \varphi_i = 2 \left[ \arcsin\left(\frac{l_i + \delta l_i}{2R}\right) - \arcsin\frac{l_i}{2R} \right] \quad (4.15)$$

where

$i = 1, 2, 3$

$l_i =$  LVDT initial distance between two mounting points

$R =$  radius of mounting points = 16"

The average value of the above three values  $\delta \varphi_1$ ,  $\delta \varphi_2$  and  $\delta \varphi_3$  will be used as the mean angular displacement. The use of this average value will minimize the effect of differences in the values of  $\delta \varphi$ , which are recorded in three places  $120^\circ$  apart.

CHAPTER V  
ANALYSIS OF RESULTS

Modeling the HRC Elastic Coupling

Various models may be employed to model the behavior of rubber like material (Bert, 1973). A simple one, which is the most frequently used, is the Kelvin-Voigt model. It is composed of a spring in parallel with a dashpot, as shown in Figure 5.1.

For a given mean torque,  $T_m$ , a given temperature,  $\theta$ , and a known sinusoidal displacement  $\varphi = \varphi_v \sin(\omega t)$ , the reaction torque  $T$  can be measured as shown in Figure 5.2.

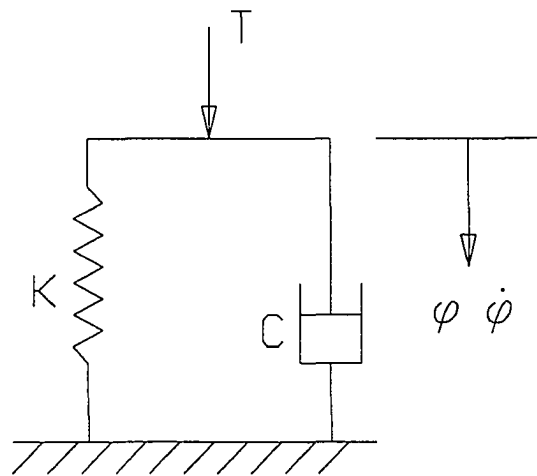


Figure 5.1 Kelvin-Voigt Model

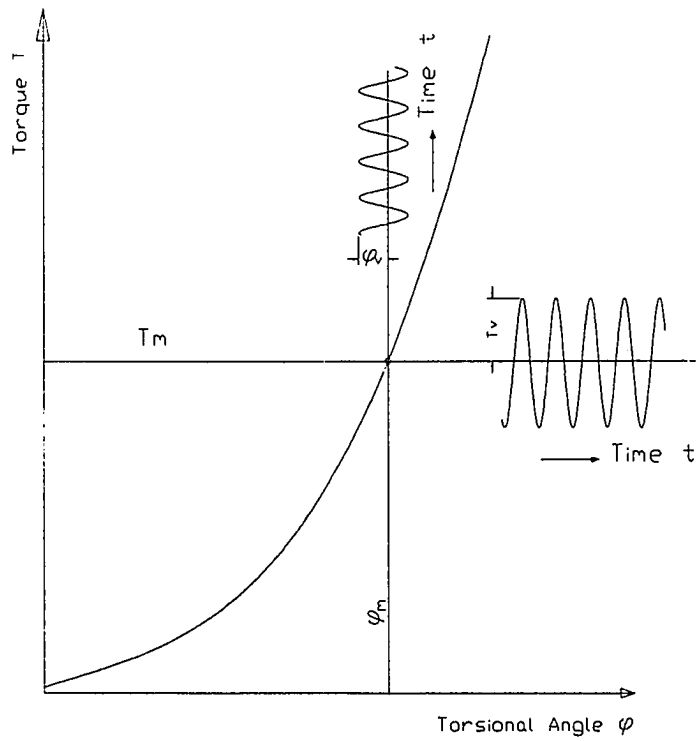


Figure 5.2 Oscillatory Torque and Angular Displacement at A Given Operating Point

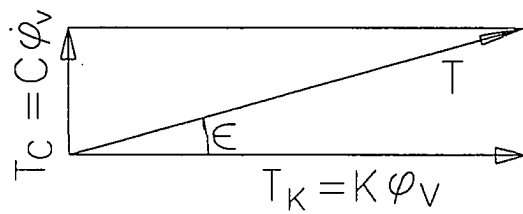


Figure 5.3 Phase Diagram of Torque



If vibration amplitude is small, the model can be assumed to be linear. The reaction torque may be expressed as

$$T = T_K(\phi) + T_C(\dot{\phi}) = T_v \sin(\omega t + \varepsilon) \quad (5.1)$$

where the angle  $\varepsilon$  is the phase angle between measured torque and input displacement, (Figure 5.3),  $T_K = K\phi = K \phi_v \sin(\omega t)$  is the spring torque, and  $T_C = C\dot{\phi} = C\omega \phi_v \cos(\omega t)$  is the damping torque. From Figure 5.3, the spring constant is

$$K = \frac{T_v \cos(\varepsilon)}{\phi_v} \quad (5.2)$$

and the equivalent viscous damping coefficient is

$$C_E = \frac{T_v \sin(\varepsilon)}{\omega \phi_v} \quad (5.3)$$

The energy dissipation by cyclic stress and strain within a rubber like material is often referred to as hysteresis damping. Hysteresis damping can be formulated in terms of complex stiffness quantities:

$$K^* = K(1 + j\eta) \quad (5.4)$$

where

$K$  = a spring constant giving the stiffness of the elastic element,

$\eta = \tan \varepsilon$  = a loss factor resulting from the deformation of the elastic element lagging the applied force during sinusoidal motion,

$$j = \sqrt{-1}.$$

The relative damping coefficient,  $\psi$ , is the ratio of the damping energy  $W_d$  produced mechanically by the coupling during a vibration cycle and converted into heat energy, to the elastic strain energy  $W_e$  with respect to the mean position.

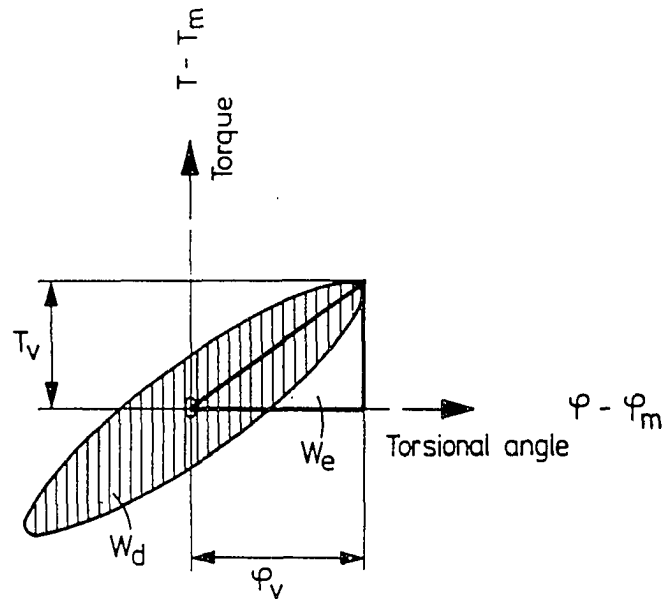


Figure 5.4 Hysteresis Loop

$$\psi = \frac{W_d}{W_e} \quad (5.5)$$

In Figure 5.4  $W_d$  is shown as an ellipse and  $W_e$  as a triangle. The relationship between loss factor  $\tan \varepsilon$  and relative damping  $\psi$  is

$$\tan \varepsilon = \frac{\psi}{2\pi} \quad (5.6)$$

The energy dissipated in one cycle for equivalent viscous damping may be expressed as

$$W_d = C_E \pi \omega \varphi^2 \quad (5.7)$$

Therefore, the equivalent viscous damping coefficient is

$$C_E = \frac{W_d}{\pi \omega \phi^2} \quad (5.8)$$

The relationship between relative damping coefficient and equivalent viscous damping coefficient is

$$C_E = \frac{K\psi}{2\pi\omega} \quad (5.9)$$

### Data Processing

For a given mean torque,  $T_m$ , temperature,  $\theta$ , vibratory frequency,  $f$ , and vibratory amplitude,  $T_v$ , the torque and displacement signals are recorded in time domain. Figure 5.5 shows one set of signals which indicates that they are not perfect sinusoidal curves because of the noise and nonlinear properties. For approximation, it is assumed that both torque and displacement are harmonic. The vibration amplitude and phase angle may be extracted by least square curve fitting. Assume the signal is sinusoidal with a frequency  $\omega$  in the following form:

$$y = a \sin \omega t + b \cos \omega t + c \quad (5.10)$$

where

$y$  = torque or displacement,

$t$  = time

$a, b, c$  are three unknown constants.

For a set of measured data  $\{t_i, y_i, i = 1, 2, 3, \dots, n\}$ , the above equation can be written in a matrix form:

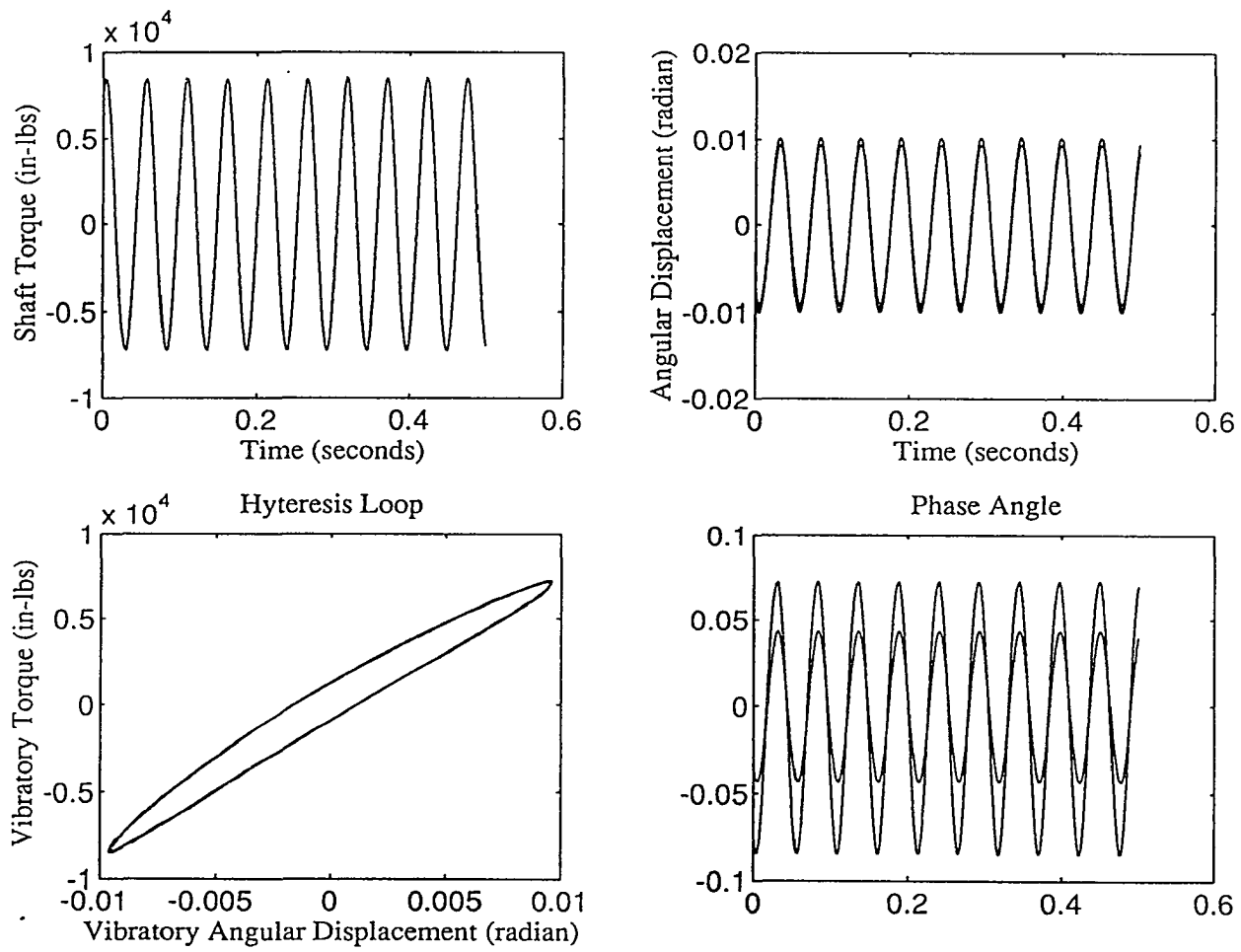


Figure 5.5 Measured Vibratory Torque and Displacement

$$\begin{bmatrix} \sin \omega t_1 & \cos \omega t_1 & 1 \\ \sin \omega t_2 & \cos \omega t_2 & 1 \\ \dots & \dots & \cdot \\ \sin \omega t_n & \cos \omega t_n & 1 \end{bmatrix} \begin{Bmatrix} a \\ b \\ c \end{Bmatrix} = \begin{Bmatrix} y_1 \\ y_2 \\ \cdot \\ y_n \end{Bmatrix} \quad (5.11)$$

or

$$A X = Y \quad (5.12)$$

where  $A \in \mathbb{R}^{n \times 3}$ ,  $X \in \mathbb{R}^{3 \times 1}$ ,  $Y \in \mathbb{R}^{n \times 1}$

It can be proved that the least square solution of above equation is:

$$X = \begin{Bmatrix} a \\ b \\ c \end{Bmatrix} = (A^T A)^{-1} A^T Y \quad (5.13)$$

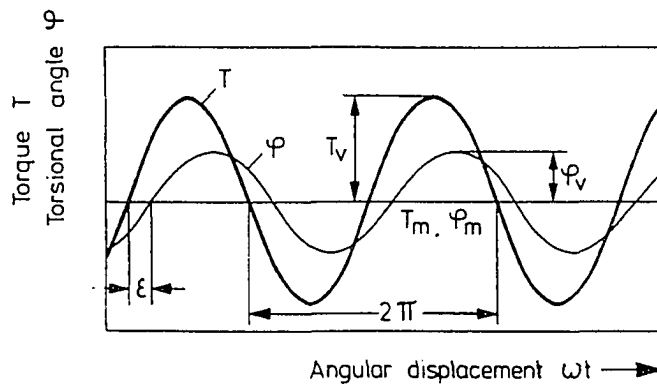


Figure 5.6 Phase Difference Between Vibratory Torque and Angle of Twist

The least square curve fitting gives the vibratory torque transmitted by the shaft,  $T_{\text{shaft}}$ , relative displacement of the coupling,  $\varphi_v$ , and the phase angle between them,  $\varepsilon$ , (Figure 5.6). The actual vibratory torque of rubber elements is  $T_v = T_{\text{shaft}} - J \omega^2$ , where  $J$  is the summation of hub and LVDT mounting device inertia. The vibration frequency is  $\omega$ .

The coupling dynamic stiffness, relative damping and equivalent viscous damping for a given mean torque, temperature, frequency, and vibratory torque amplitude are calculated by Equations (5.2), (5.6) and (5.3) respectively. A computer program, which does the least square regression and calculates the stiffness and damping, is in Appendix E.

#### Dynamic Stiffness

Figure 5.7 shows the angular displacement versus torque curve for the HRC-63K coupling for static conditions. This static curve gives the overall view of the coupling behavior, but it is not suitable for dynamic analysis because of the viscoelastic nature of the elastomer material. The static stiffness of the coupling is the slope of the curve, which shows that the stiffness is increasing when the mean torque is increased. The dynamic stiffness of the coupling at a given mean torque is not the tangent of the static torque versus displacement curve. It is always larger than the tangent of the static curve due to hysteresis damping.

For every different mean torque,  $T_m$ , frequency,  $f$ , vibratory amplitude,  $T_v$ , and temperature,  $\theta$ , the dynamic stiffness,  $K$ , is obtained. Both static and dynamic test results indicate that the dynamic stiffness is a strong function of the mean torque. The vibratory torque amplitude, vibration frequency, and temperature have the influence on the dynamic stiffness more or less. Therefore, the relationship between dynamic stiffness,  $K$ , and mean torque,  $T_m$ , vibratory torque amplitude,  $T_v$ , frequency,  $f$ , and temperature,

$\theta$ , is assumed to be in a form:

$$K = C_1 T_m^a f^b T_v^c \theta^d \quad (5.14)$$

Take the logarithm on both sides to linearized the equation:

$$\log_{10} K = \log_{10} C_1 + a \log_{10} T_m + b \log_{10} f + c \log_{10} T_v + d \log_{10} \theta \quad (5.15)$$

For a group of test results  $\{K(i), T_m(i), f(i), T_v(i), \theta(i), i=1,2,\dots,n\}$ , the above equation may be written in a matrix form

$$\begin{bmatrix} 1 & \log_{10} T_m(1) & \log_{10} f(1) & \log_{10} T_v(1) & \log_{10} \theta(1) \\ 1 & \log_{10} T_m(2) & \log_{10} f(2) & \log_{10} T_v(2) & \log_{10} \theta(2) \\ \cdot & \cdot & \cdot & \cdot & \cdot \\ 1 & \log_{10} T_m(n) & \log_{10} f(n) & \log_{10} T_v(n) & \log_{10} \theta(n) \end{bmatrix} \begin{bmatrix} e \\ a \\ b \\ c \\ d \end{bmatrix} = \begin{bmatrix} \log_{10} K(1) \\ \log_{10} K(2) \\ \cdot \\ \log_{10} K(n) \end{bmatrix} \quad (5.16)$$

where  $e = \log_{10} C_1$ .

Substituting over 500 sets of data into the above equation yields:  $C_1 = 5.5378 \times 10^4$ ,  $a = .6545$ ,  $b = -.1538$ ,  $c = -.0948$ ,  $d = -.4953$ , for HRC-63K coupling.

$$K = 5.5378 \times 10^4 T_m^{.6545} f^{-.1538} T_v^{-.0948} \theta^{-.4953} \quad (5.17)$$

where

$K$  = dynamic torsional stiffness, in-lbs/rad,

$T_m$  = mean torque, in-lbs,

$f$  = frequency, Hz,

$T_v$  = vibratory torque amplitude, in-lbs,

$\theta$  = operating temperature, °F.

The dynamic stiffness is a function of four variables. It is extremely difficult to present the measured values with calculated values in one graph to virtually check the regression because  $K$  is a function of four variables. Figure 5.8 shows the measured values (marked with "x") and values calculated by Equation (5.17) (marked with ".").

The abscissa is the mean torque; the ordinate is the dynamic stiffness. Both frequency and vibration amplitude vary while temperature is constant,  $\theta = 110^\circ\text{F}$ . This plot shows that the regression is reliable. Figure 5.9 shows the histogram of Equation (5.17), where abscissa is the relative error between the measured stiffness and the calculated stiffness:  $\text{Relative Error} = (K_{\text{measured}} - K_{\text{calculated}})/K_{\text{calculated}}$ . The ordinate is the number of occurrences. It indicates again that the regression is acceptable since 85% of the population has errors of less than  $\pm 10\%$ .

Since the vibration torque amplitude is unknown prior to the analysis, it is inconvenient to use Equation (5.17) to calculate the stiffness. As the stiffness,  $K$ , is not a strong function of vibration torque amplitude, for simplicity, an estimated vibratory torque amplitude, say 25% of mean torque, may be substituted to get the dynamic stiffness:

$$K = 6.3156 \times 10^4 T_m^{.5597} f^{-.1538} \theta^{-.4953} \quad (5.18)$$

Although Equation (5.18) is convenient for single frequency vibration analysis, it is impossible to interpret the frequency,  $f$ , for free vibration and multi-frequency vibration. Alternatively, the dynamic stiffness could be assumed to be the function of mean torque,  $T_m$ , the temperature,  $\theta$ , and vibration velocity amplitude,  $\phi_v$ , which is the product of vibration frequency and vibratory amplitude,  $\phi_v = 2\pi f \phi$ .

$$K = C_2 T_m^a (2\pi \cdot f \cdot \phi_v)^b \theta^c = C_2 T_m^a \phi_v^b \theta^c \quad (5.19)$$

Least square regression gives:  $C_2 = 1.9703 \times 10^4$ ,  $a = .6043$ ,  $b = -.1210$ ,  $c = -.4502$ . That is

$$K = 1.9703 \times 10^4 T_m^{.6043} \phi_v^{-.1210} \theta^{-.4502} \quad (5.20)$$

where

$\phi_v =$  amplitude of the angular velocity, rad/sec.



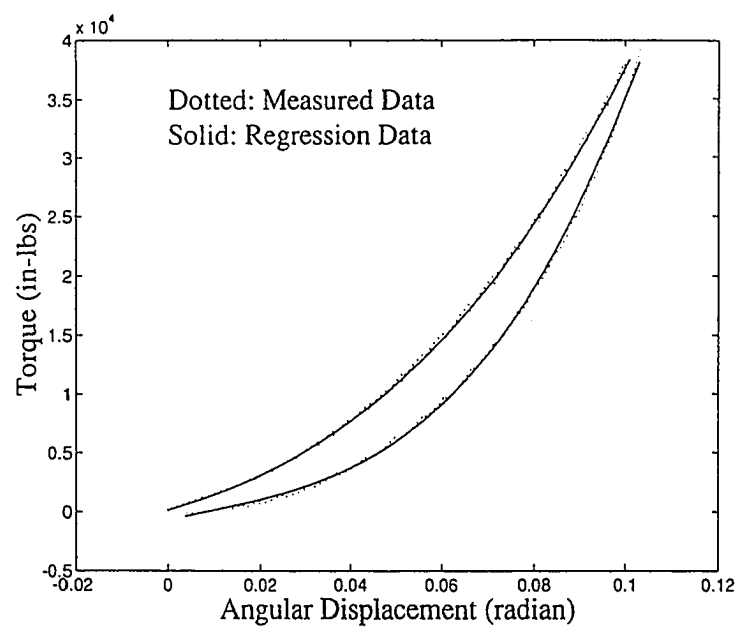


Figure 5.7 Torque Versus Displacement for Static Conditions

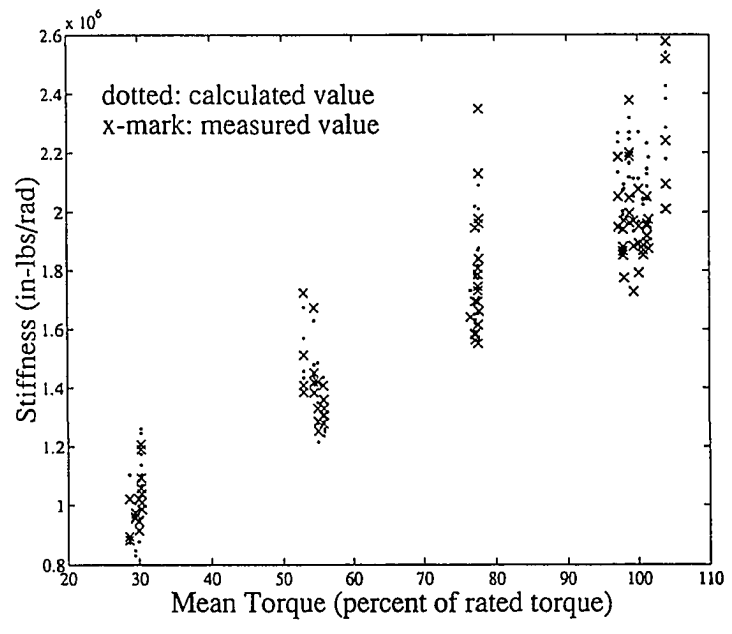


Figure 5.8 Comparison of Measured Data and Calculated Data at Temperature  $\theta = 110$  °F

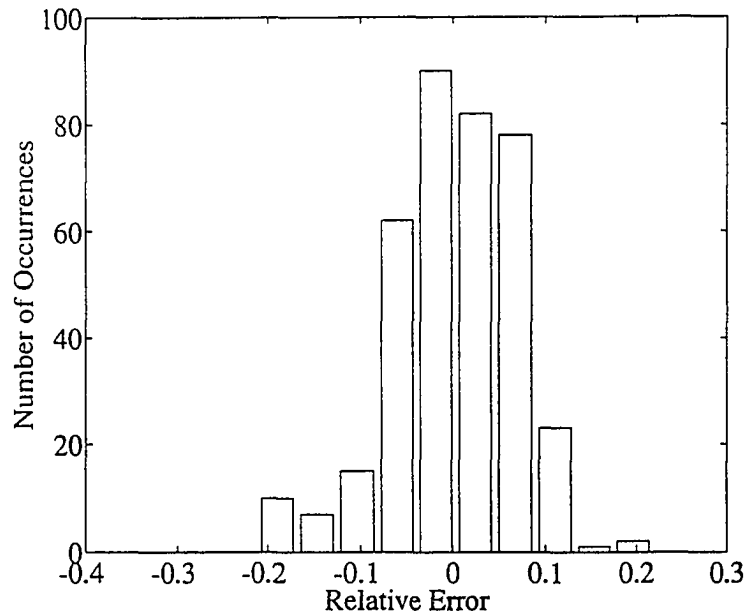


Figure 5.9 Histogram of Error of Dynamic Stiffness Between Measured Values and Values Predicted by Equation (5.17)

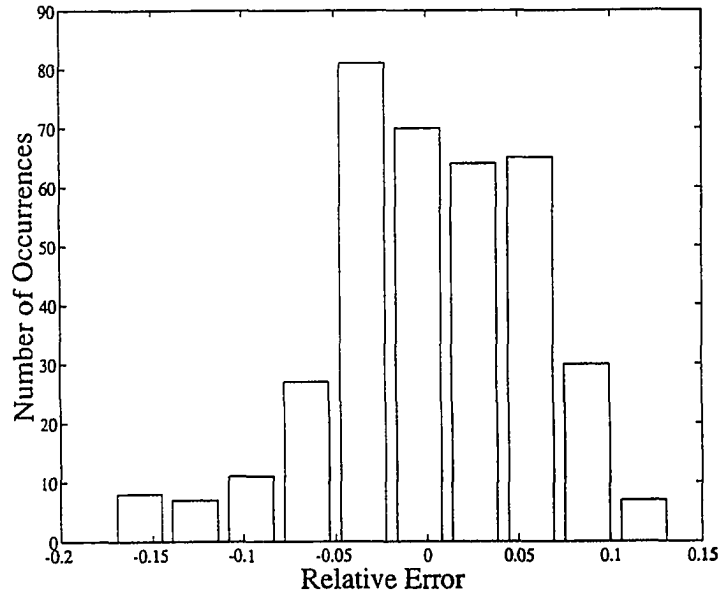


Figure 5.10 Histogram of Error of Dynamic Stiffness Between Measured Values and Values Predicted by Equation (5.20)

Figure 5.10 shows the histogram of error between measured values and values predicted by Equation (5.20). Equation (5.20) is suitable for time domain simulation. The angular velocity,  $\dot{\phi}_v$ , is available at every integration time step by feedback technique.

### Damping

For frequency domain analysis, investigators prefer to use the relative damping coefficient. But for time domain simulation, the equivalent viscous damping is more convenient. The test results presented here give damping values both ways.

In the same fashion, assume the relative damping coefficient,  $\psi$ , is a function of mean torque, vibratory torque amplitude, vibratory frequency and temperature in a form:

$$\psi = C_3 T_m^a f^b T_v^c \theta^d \quad (5.21)$$

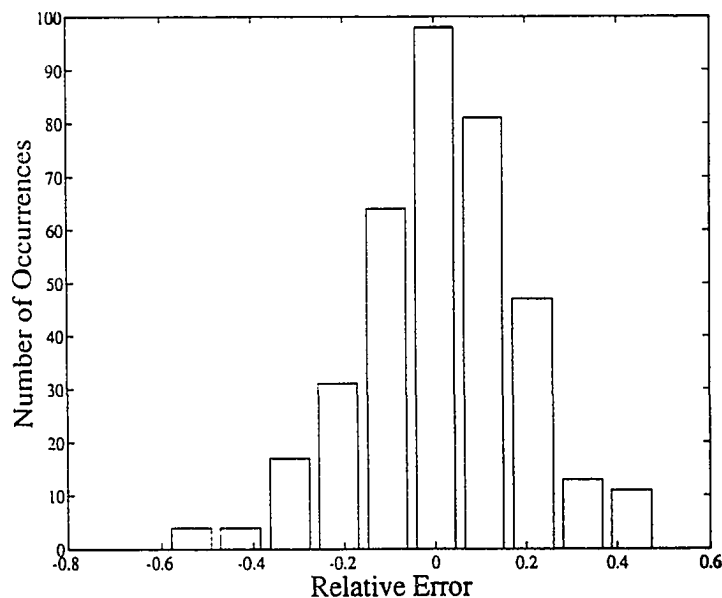


Figure 5.11 Histogram of Error of Relative Damping Between Measured Values and Values Predicted by Equation (5.21)

The constants are found to be:  $C_3 = 42.2834$ ,  $a = -.2644$ ,  $b = .2841$ ,  $c = -.0131$ ,  $d = -.3819$ . Figure 5.11 is the histogram of the relative error,  $(\psi_{\text{measured}} - \psi_{\text{calculated}})/\psi_{\text{calculated}}$ , of Equation (5.21) which shows that 80% of values fall within  $\pm 20\%$  of the equation's value.

Since the vibratory torque amplitude is unknown and since it does not influence damping very much, an estimated value,  $T_v = 25\%T_m$ , may be substituted to simplify the formula:

$$\psi = 43.0583 T_m^{-.2775} F^{.2841} \theta^{-.3819} \quad (5.22)$$

Substituting (5.21) and (5.17) into (5.9) gives the expression of equivalent viscous damping:

$$C_E = 5.9312 \times 10^4 T_m^{.3901} F^{-.8697} T_v^{-1.079} \theta^{-.8772} \quad (5.23)$$

If the vibratory torque,  $T_v$ , is assumed to be 25% of mean torque,  $T_m$ , the viscous damping coefficient is:

$$C_E = 6.8882 \times 10^4 T_m^{.2822} F^{-.8697} \theta^{-.8772} \quad (5.24)$$

For multi-frequency time domain simulation, assume the equivalent viscous damping in the form:

$$C_E = C_4 T_m^a (2\pi F \cdot \phi_v)^b \theta^c = C_4 T_m^a \phi_v^b \theta^c \quad (5.25)$$

The coefficients are:  $C_4 = 737.6065$ ,  $a = .3808$ ,  $b = -.3890$ ,  $c = -.6803$ . Figure 5.12 shows the histogram of relative error for Equation (5.25).

### Conclusions

Equations (5.17) and (5.22) indicate:

(1) The mean torque has a significant influence on the dynamic stiffness. The dynamic stiffness increases when the mean torque is increased. This nonlinear property is largely due to the nonlinear geometry of the HRC elastic coupling. The lever arm of the rubber element increases rapidly when the angular deflection increases.

(2) The relative damping decreases as the mean torque increases.

(3) The stiffness and damping vary inversely with temperature (Figures 5.13, 5.14).

(4) The stiffness is not a strong function of frequency, and the data indicates that stiffness varies inversely with frequency (Figure 5.15). This is opposite to the expected results.

(5) The damping per Figure 5.16 increases with increasing frequency.

(6) The influence of the vibratory torque amplitude on stiffness and damping is not very significant (Figure 5.17 and Figure 5.18 ). The stiffness decreases as vibratory amplitude increases. The relative damping decreases as the vibratory amplitude increased.

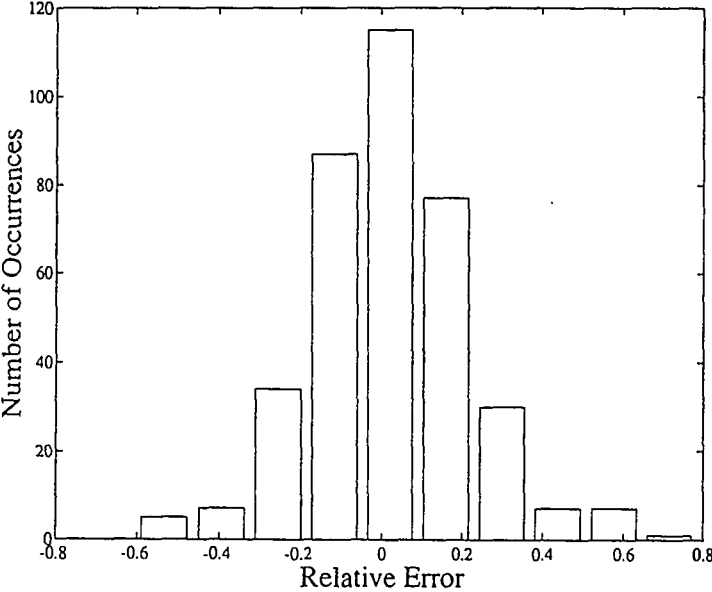


Figure 5.12 Histogram of Error of Equivalent Viscous Damping Between Measured Values and Values Predicted by Equation (5.25)

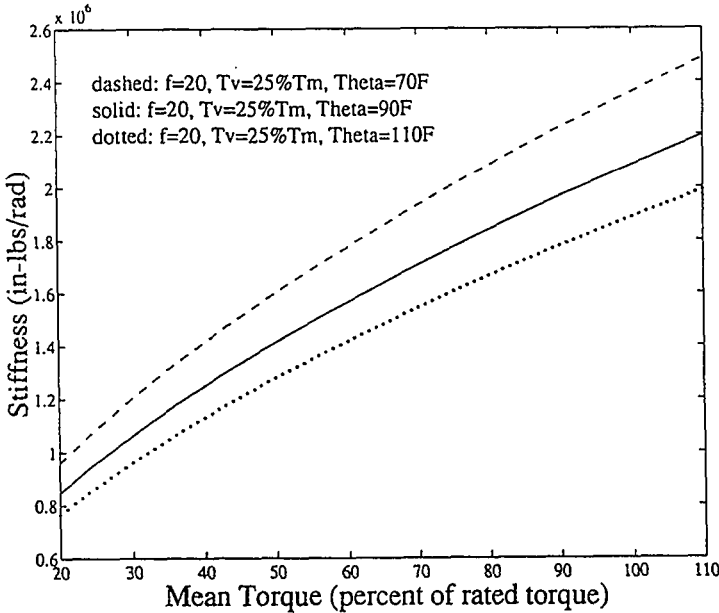


Figure 5.13 Influence of Temperature on Dynamic Stiffness

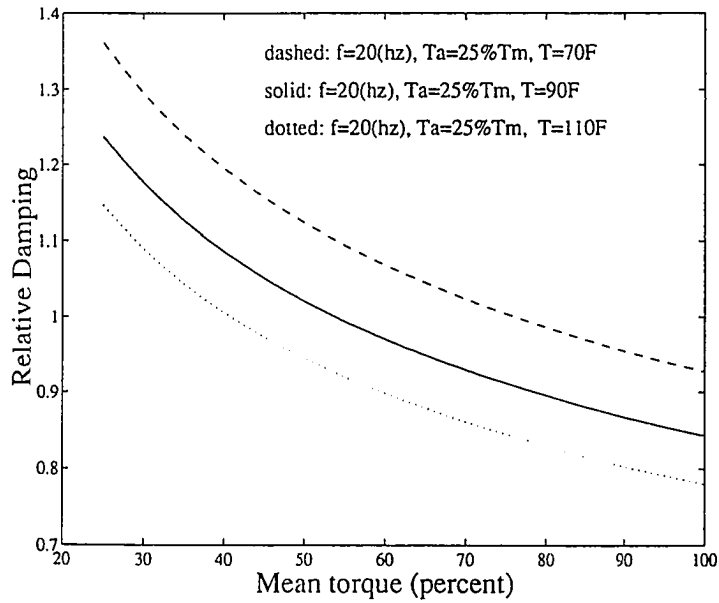


Figure 5.14 Influence of Temperature on Relative Damping

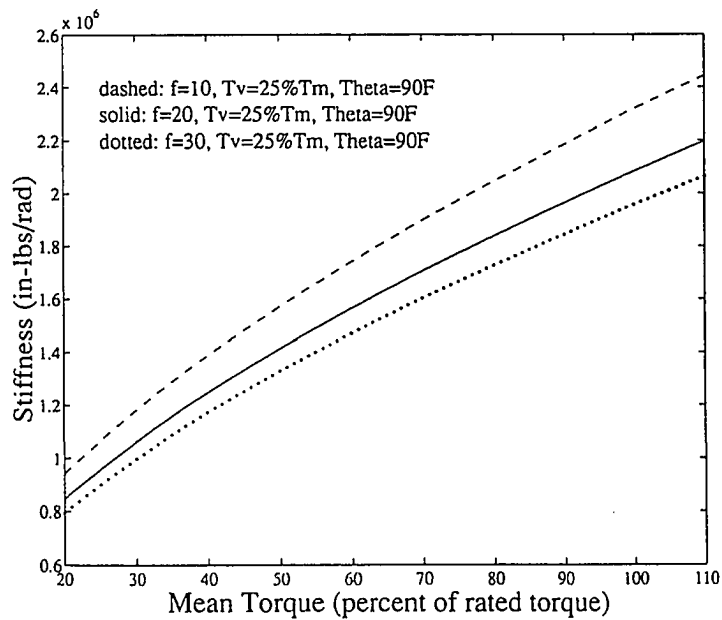


Figure 5.15 Influence of Frequency on Dynamic Stiffness

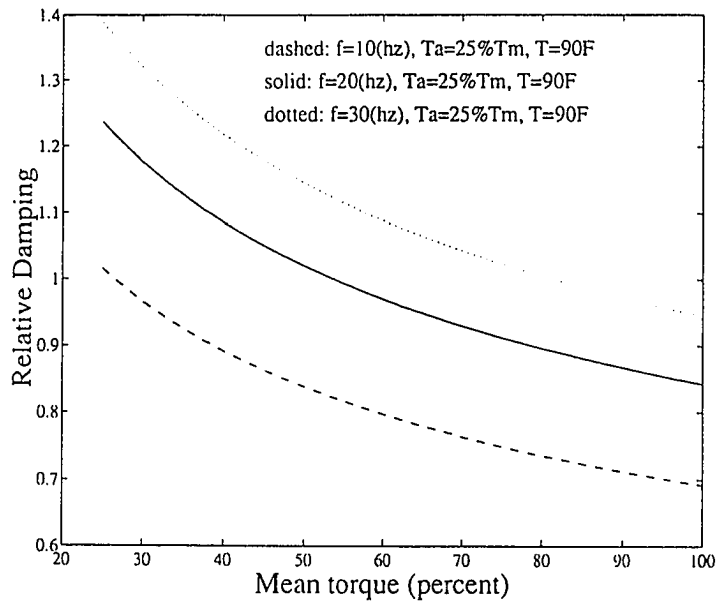


Figure 5.16 Influence of Frequency on Relative Damping

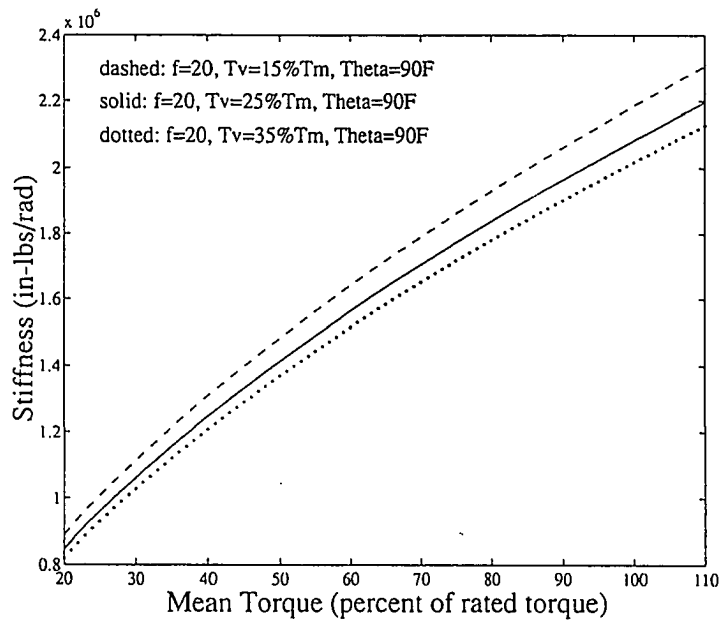


Figure 5.17 Influence of Vibration Torque Amplitude on Dynamic Stiffness



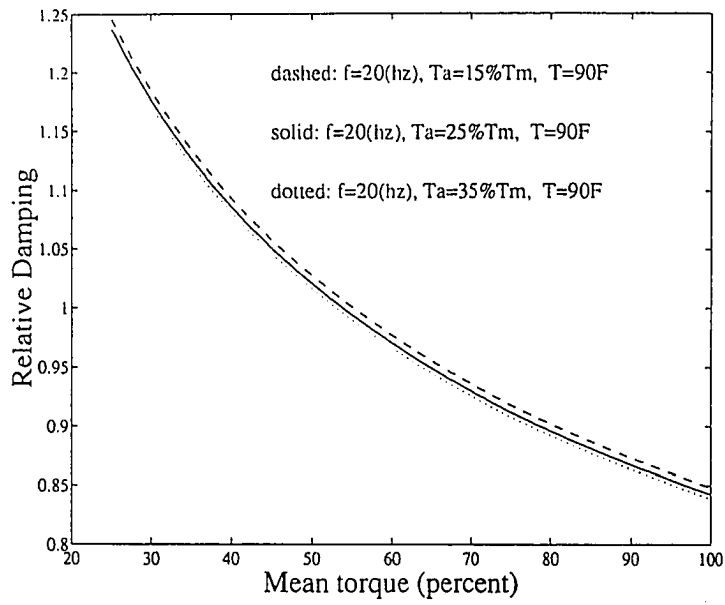


Figure 5.18 Influence of Vibration Torque Amplitude on Relative Damping

## CHAPTER VI

### SIMULATION OF THE PROPULSION SYSTEM

#### Introduction

In this chapter, a typical marine propulsion system, which is shown in Figure A.1 of Appendix A, will be used to illustrate the approach developed in Chapter II. The mass-spring model for Figure A.1 is shown in Figure A.2. Its corresponding Bond graph is illustrated in Figure A.3.

#### Simulation Program Development

For the Bond graph shown in Figure A.3, there are 19 torsional springs (bonds 1 to 19), 20 inertias (bonds 20 to 39), 20 station-to-ground dampers (bonds 40 to 59), and 19 station-to-station dampers (bonds 60 to 78). The storage field input vector is:  $\dot{x} = [f_1 f_2 \dots f_{19} e_{20} e_{21} \dots e_{39}]^T$ , where  $f$  is angular velocity,  $e$  is torque, and the subscript is the bond number. The corresponding vector  $X$  is:  $X = [q_1 q_2 \dots q_{19} p_{20} p_{21} \dots p_{39}]^T$ , where  $q$  is angular displacement,  $p$  is angular momentum. The storage field output vector is:  $Z = [e_1 e_2 \dots e_{19} f_{20} f_{21} \dots f_{39}]^T$ . The dissipation field input vector is:  $D_{in} = [f_{40} f_{41} \dots f_{59} f_{60} f_{61} \dots f_{78}]^T$ . The dissipation field output vector is:  $D_{out} = [e_{40} e_{41} \dots e_{59} e_{60} e_{61} \dots e_{78}]^T$ . The source vector is:  $U = [u_1 u_2 \dots u_{11}]^T$ .

The constitutive equation for the storage field is

$$Z = \Phi_S(X) \quad (6.1)$$

The equation (6.1) may be written in a matrix form for this case:

$$\begin{pmatrix} e_1 \\ e_2 \\ \cdot \\ \cdot \\ \cdot \\ e_{19} \\ f_{20} \\ f_{21} \\ \cdot \\ \cdot \\ \cdot \\ f_{39} \end{pmatrix} = \begin{bmatrix} k_{1,1} & 0 & \cdot & \cdot & \cdot & 0 & 0 & 0 & \cdot & \cdot & \cdot & 0 \\ 0 & k_{1,2} & \cdot & \cdot & \cdot & 0 & 0 & 0 & \cdot & \cdot & \cdot & 0 \\ \cdot & \cdot & \cdot & \cdot & \cdot & \cdot & \cdot & \cdot & \cdot & \cdot & \cdot & \cdot \\ \cdot & \cdot & \cdot & \cdot & \cdot & \cdot & \cdot & \cdot & \cdot & \cdot & \cdot & \cdot \\ \cdot & \cdot & \cdot & \cdot & \cdot & \cdot & \cdot & \cdot & \cdot & \cdot & \cdot & \cdot \\ 0 & 0 & \cdot & \cdot & \cdot & k_{4,1} & 0 & 0 & \cdot & \cdot & \cdot & 0 \\ 0 & 0 & \cdot & \cdot & \cdot & 0 & 1/j_{1,1} & 0 & \cdot & \cdot & \cdot & 0 \\ 0 & 0 & \cdot & \cdot & \cdot & 0 & 0 & 1/j_{1,2} & \cdot & \cdot & \cdot & 0 \\ \cdot & \cdot & \cdot & \cdot & \cdot & \cdot & \cdot & \cdot & \cdot & \cdot & \cdot & \cdot \\ \cdot & \cdot & \cdot & \cdot & \cdot & \cdot & \cdot & \cdot & \cdot & \cdot & \cdot & \cdot \\ \cdot & \cdot & \cdot & \cdot & \cdot & \cdot & \cdot & \cdot & \cdot & \cdot & \cdot & \cdot \\ 0 & 0 & \cdot & \cdot & \cdot & 0 & 0 & 0 & \cdot & \cdot & \cdot & 1/j_{4,1} \end{bmatrix} \begin{pmatrix} q_1 \\ q_2 \\ \cdot \\ \cdot \\ \cdot \\ q_{19} \\ p_{20} \\ p_{21} \\ \cdot \\ \cdot \\ \cdot \\ p_{39} \end{pmatrix} \quad (6.2)$$

where  $k_{1,1}$ ,  $k_{1,2}, \dots, k_{4,1}$  are torsional spring rates and  $j_{1,1}$ ,  $j_{1,2}, \dots, j_{4,1}$  are inertias. Nonconstant rates and inertias are acceptable for this analysis method since they may be functions of other parameters. Figure 6.1 is the simulation block of the storage field.

The constitutive equations for the dissipation field are

$$D_{out} = \Phi_L(D_{in}) \quad (6.3)$$

In matrix form:

$$\begin{Bmatrix} e_{40} \\ e_{41} \\ \cdot \\ \cdot \\ \cdot \\ e_{59} \\ e_{60} \\ e_{61} \\ \cdot \\ \cdot \\ \cdot \\ e_{78} \end{Bmatrix} = \begin{bmatrix} b_{1,1} & 0 & \cdot & \cdot & \cdot & 0 & 0 & 0 & \cdot & \cdot & \cdot & 0 \\ 0 & b_{1,2} & \cdot & \cdot & \cdot & 0 & 0 & 0 & \cdot & \cdot & \cdot & 0 \\ \cdot & \cdot & \cdot & \cdot & \cdot & \cdot & \cdot & \cdot & \cdot & \cdot & \cdot & \cdot \\ \cdot & \cdot & \cdot & \cdot & \cdot & \cdot & \cdot & \cdot & \cdot & \cdot & \cdot & \cdot \\ \cdot & \cdot & \cdot & \cdot & \cdot & \cdot & \cdot & \cdot & \cdot & \cdot & \cdot & \cdot \\ 0 & 0 & \cdot & \cdot & \cdot & b_{4,1} & 0 & 0 & \cdot & \cdot & \cdot & 0 \\ 0 & 0 & \cdot & \cdot & \cdot & 0 & B_{1,1} & 0 & \cdot & \cdot & \cdot & 0 \\ 0 & 0 & \cdot & \cdot & \cdot & 0 & 0 & B_{1,2} & \cdot & \cdot & \cdot & 0 \\ \cdot & \cdot & \cdot & \cdot & \cdot & \cdot & \cdot & \cdot & \cdot & \cdot & \cdot & \cdot \\ \cdot & \cdot & \cdot & \cdot & \cdot & \cdot & \cdot & \cdot & \cdot & \cdot & \cdot & \cdot \\ \cdot & \cdot & \cdot & \cdot & \cdot & \cdot & \cdot & \cdot & \cdot & \cdot & \cdot & \cdot \\ 0 & 0 & \cdot & \cdot & \cdot & 0 & 0 & 0 & \cdot & \cdot & \cdot & B_{4,1} \end{bmatrix} \begin{Bmatrix} f_{40} \\ f_{41} \\ \cdot \\ \cdot \\ \cdot \\ f_{59} \\ f_{60} \\ f_{61} \\ \cdot \\ \cdot \\ \cdot \\ f_{78} \end{Bmatrix} \quad (6.4)$$

where  $b_{1,1}$ ,  $b_{1,2}, \dots, b_{4,1}$  are station-to-ground damping factors and  $B_{1,1}$ ,  $B_{1,2}, \dots, B_{4,1}$  are station-to-station damping factors. Some of these factors are not constants due to nonlinearity. The simulation block for the dissipation field is shown in Figure 6.2.

The inputs  $U$  are external excitations, which include 20 engine cylinder excitations and 1 propeller excitation. The block diagram is shown in Figure 6.3.

The outputs  $Y$  are torques on each shaft. They are functions of state variables  $X$ . Figure 6.4 shows the block diagram.

The junction structure matrices, which define the relationship between five vectors and control the flow of vectors, depend on the structure of the original model. The junction structure equations are

$$\begin{Bmatrix} \dot{X} \\ D_{in} \end{Bmatrix} = \begin{bmatrix} J_{SS} & J_{SL} & J_{SV} \\ J_{LS} & J_{LL} & J_{LV} \end{bmatrix} \begin{Bmatrix} Z \\ D_{out} \\ U \end{Bmatrix} \quad (6.5)$$

where the matrix  $J_{LL}$  is null. Other matrices are formed by the program according to the bond graph of Figure A.3. The program is listed in Appendix B. The input for the program is the matrix  $JUNCT$ , which describes the inputs and outputs of each bond. For instance, the input to bond 1 is bond 20, and the output is bond 21. The inputs to bond 30 are bonds 10 and 69 and the outputs are bonds 11, 50 and 70.

The simulation block diagram, which is written in SIMULINK™ program, is shown in Figure 6.5. By clicking on the "Load Data" box, the input data, which includes the formation of junction structure matrices, parameters needed for constitutive equations, and excitations, are read into the program. Several algorithms are available for the integration of ordinary differential equations.

### Simulation Results

The program calculates the torque on each shaft for a given engine speed. By varying the engine speed from idle to rated speed, a group of data are obtained. Since the excitation by this engine is given in harmonic coefficients, the phase angles between the different harmonics are unknown, the reconstruction of the gas torque curve is impossible without the phase angles. In this example, the torque on each shaft for each harmonic is calculated. It is noted that the resultant torque is less than the algebraic summation the torque obtained for each harmonic due to the phase angles. The results are presented separately in Figures 6.6 to 6.11.

Figure 6.6 shows the vibratory torque in the gear box input shaft due to propeller excitation. It can be seen that there are two critical speeds for this shaft for propeller excitation. The total torque in the shaft is shown in Figure 6.7. Figures 6.8 and 6.9 show the torque in the propeller shaft due to propeller excitation. The torque in the crankshaft (shaft number 10) due to the engine's 5th order harmonic is shown in Figure 6.10 and Figure 6.11. It can be seen that for a considerable speed range (550 rpm to 1000 rpm) the actual torque is larger than the mean torque, not only at the resonance point, but also away from the resonance point. This again shows the importance of the time domain simulation. The same results at resonance points were obtained by Jones (1994) in the frequency domain, thus verifying this program.

Constitutive Law for Storage Field

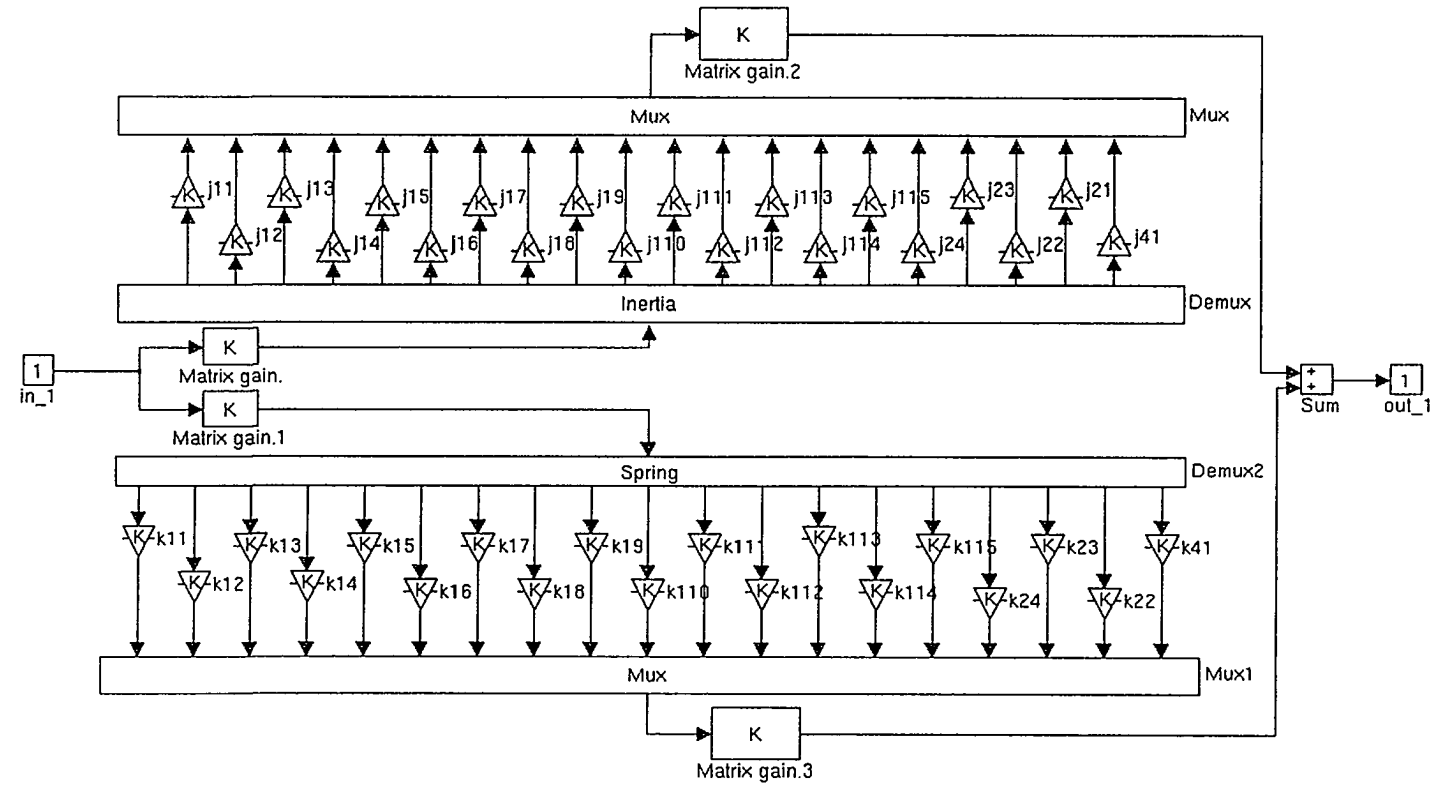


Figure 6.1 Simulation Block Diagram of the Storage Field

Constitutive Law for the Dissipation Filed

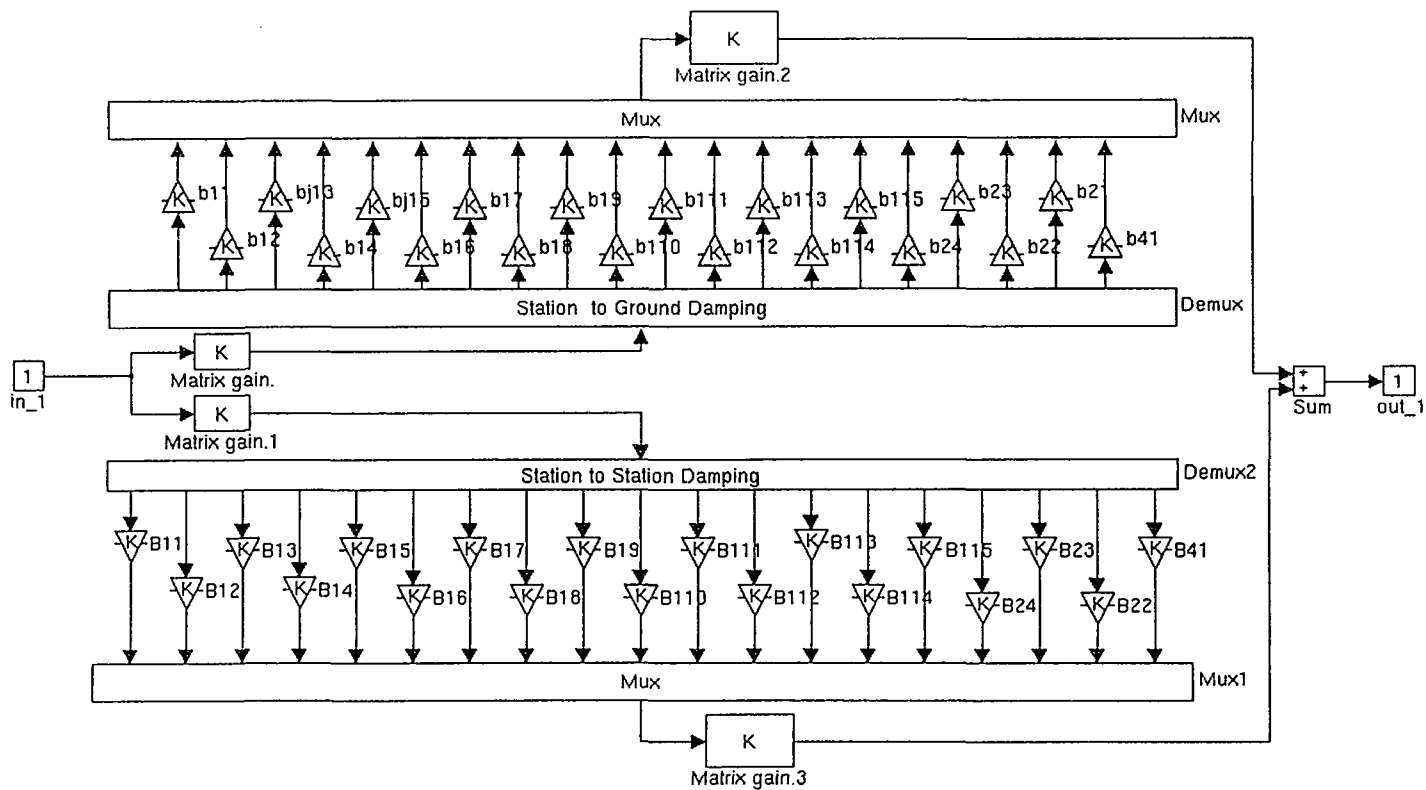


Figure 6.2 Simulation Block Diagram of the Dissipation Field

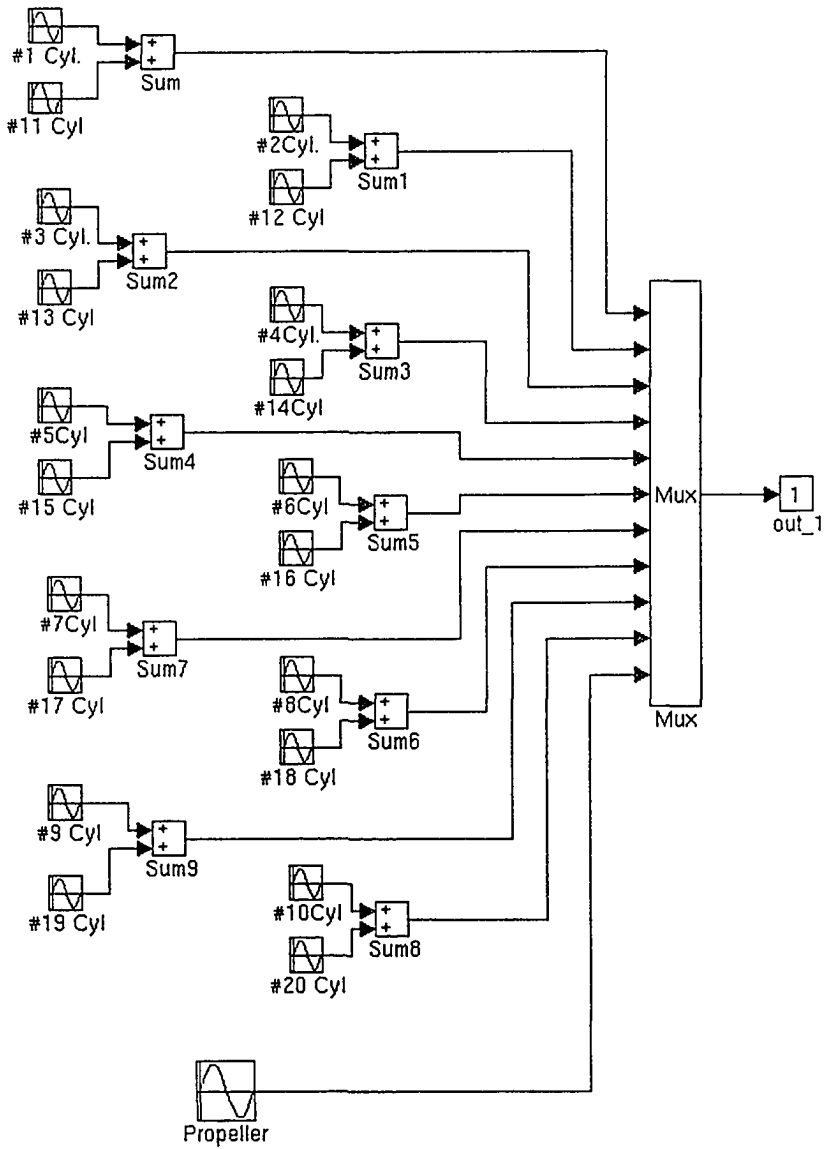


Figure 6.3 System Inputs: Excitations



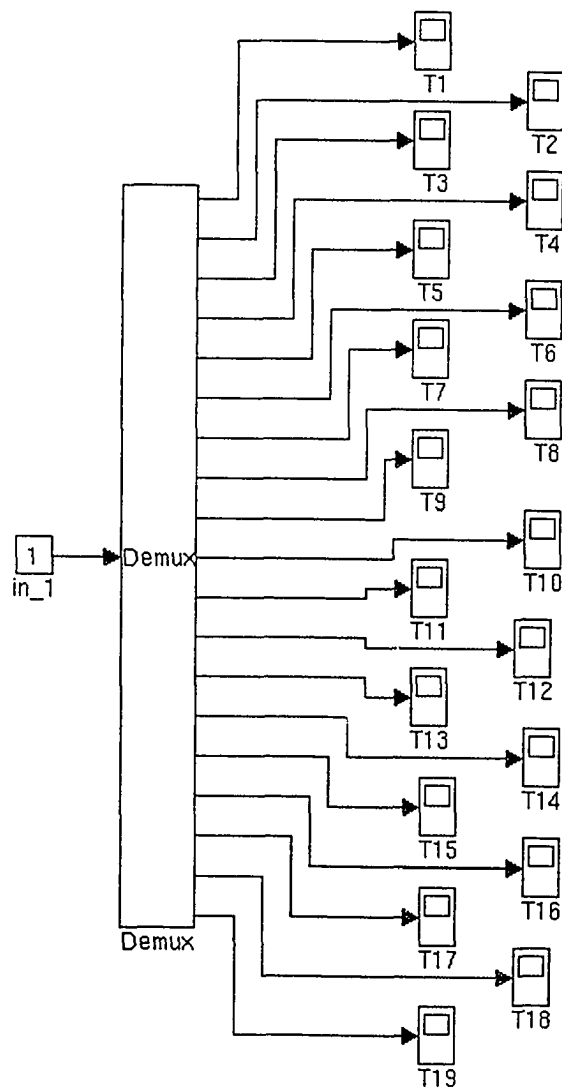


Figure 6.4 System Outputs: Torque on the Shaft

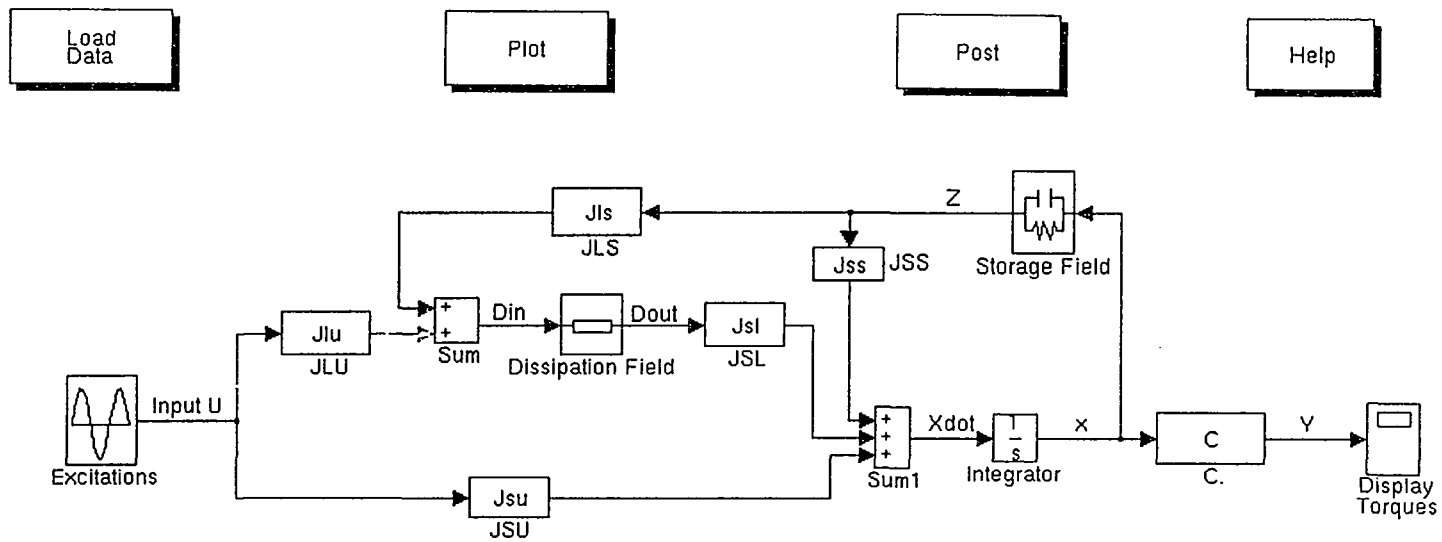


Figure 6.5 Simulation Block Diagram of A Typical Marine Propulsion System

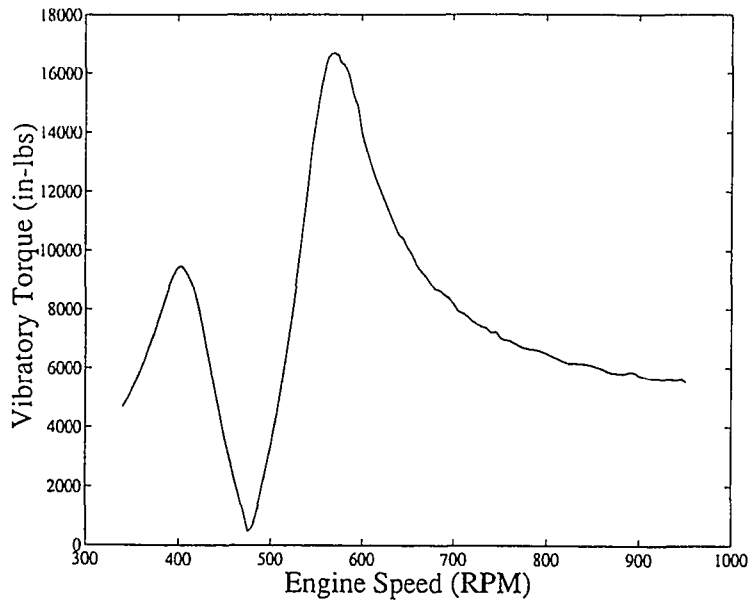


Figure 6.6 Vibratory Torque on Gear Box Input Shaft Due to Propeller Excitation

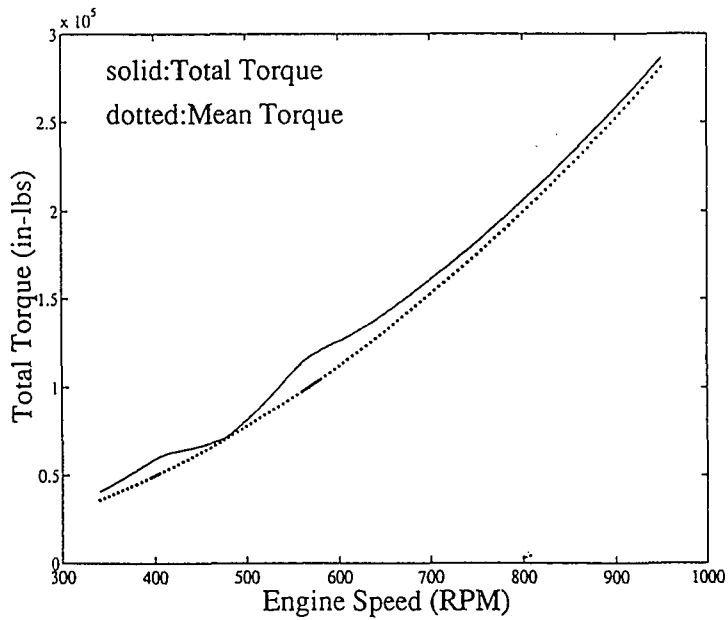


Figure 6.7 Torque on Gear Box Input Shaft Due to Propeller Excitation

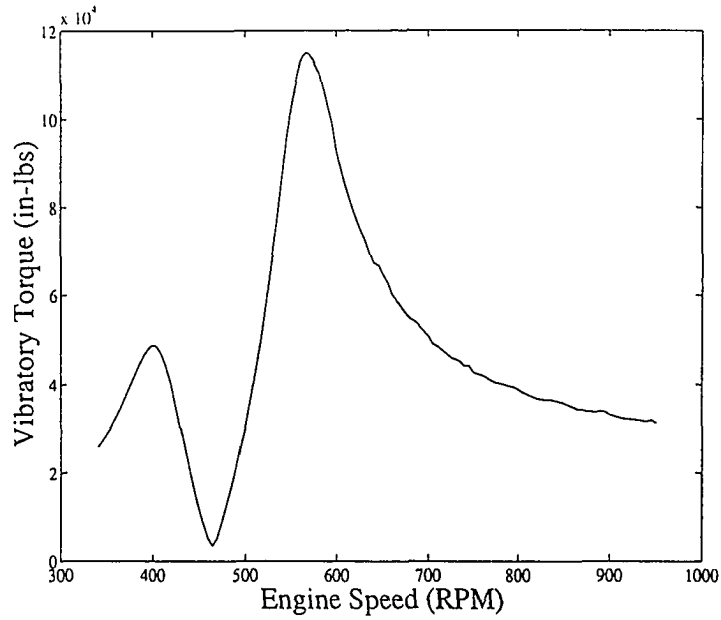


Figure 6.8 Vibratory Torque on Propeller Shaft Due to Propeller Excitation

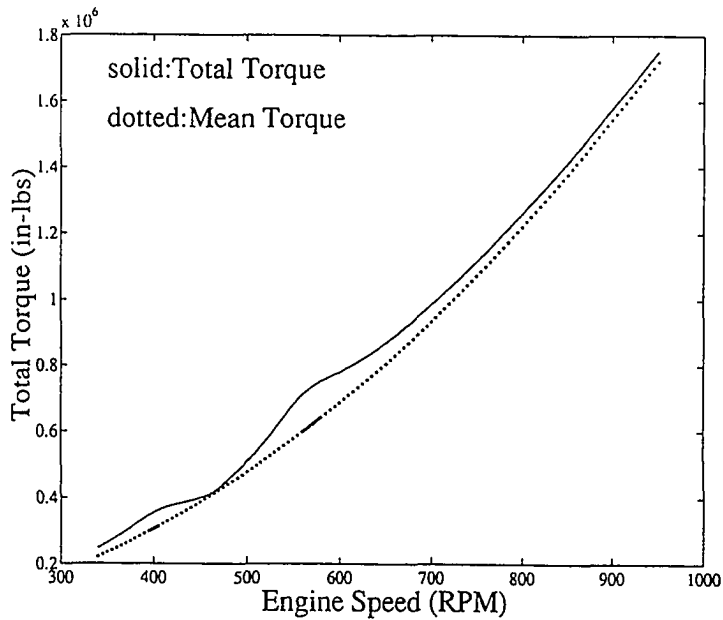


Figure 6.9 Torque on Propeller Due to Propeller Excitation

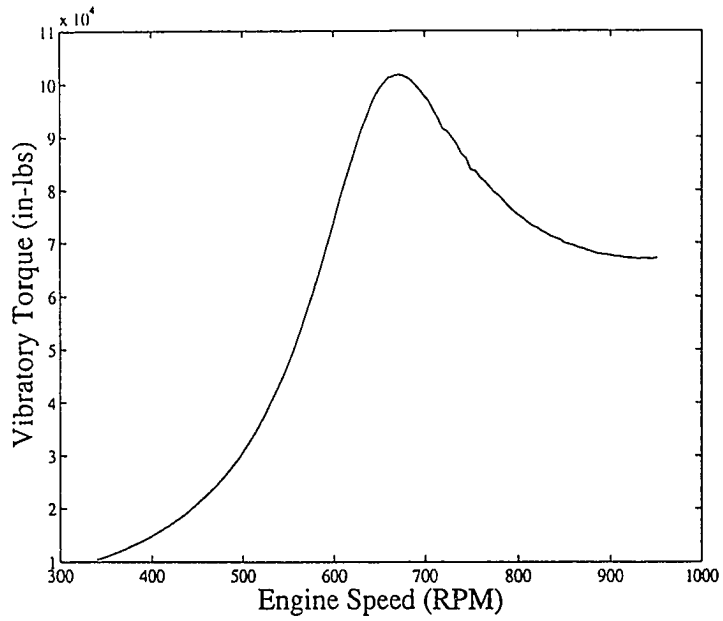


Figure 6.10 Vibratory Torque on Shaft 10 Due to Engine 5th Harmonic

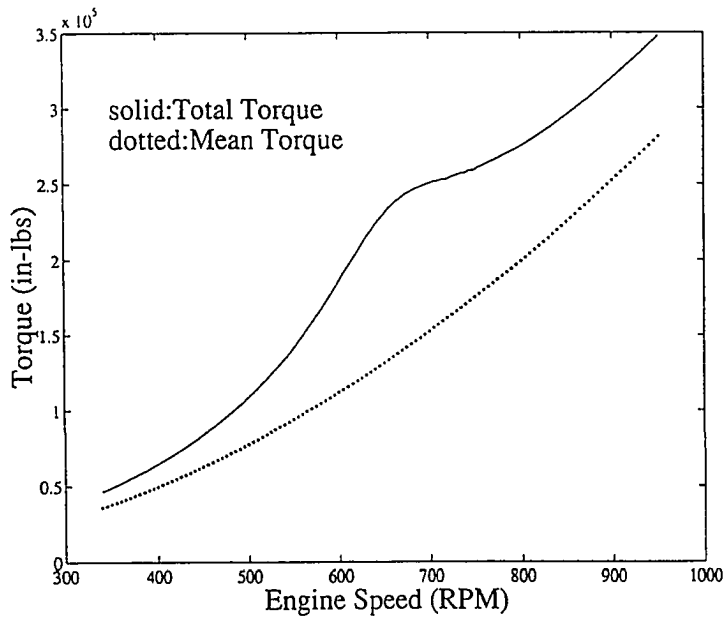


Figure 6.11 Torque on Shaft 10 Due to Engine 5th Harmonic Excitation

CHAPTER VII  
CONCLUSIONS AND RECOMMENDATIONS

Time Domain Torsional Vibrations Simulation

The advantage of time domain simulation over frequency domain analysis is obvious. It not only gives the results at resonance points for a single frequency, but also gives the results for any operating points. The method developed in this paper is suitable for both linear and nonlinear cases. For the linear case, the natural frequencies and their corresponding mode shapes may be extracted easily, thus giving the user the information which usually is obtained only by frequency domain analysis. The model is expressed in a very unique block diagram form (not program codes), which enables the user to study the sensitivity easily. For example, one can study the influence of the coupling stiffness and damping on the system by simply clicking the mouse to change the parameters.

The model may also be used to simulate abnormal working cases, such as engine misfiring, propeller hitting a log, etc. The author has successfully simulated the engine misfiring, which is very difficult to obtain by the traditional frequency domain method. The results are not presented here due to space limitations. Furthermore, the applications of the simulation model are not limited to marine propulsion systems. It can be used to simulate any lumped dynamic system, mechanical system, electrical system, hydraulic system or hybrid system.

It is noted that although the model works fine for most nonlinear systems, it may give a false or at least incomplete result for some very special cases. For instance, it is found the strong nonlinearity of the gear backlash may cause the system to have more

than one result. The results are strong functions of initial conditions. Sometimes the system may even diverge. For these special cases, a simple model may be set up first to investigate the nonlinearity. The results can be easily incorporated into the system model.

The available information for propeller and engine excitations are not complete. The engine manufacturers have not realized the advances in the torsional vibrations area. Engine harmonic coefficients are commonly supplied by engine manufacturers. The most important data, the gas pressure curve, which is the basis of the published torque harmonics, is often not available.

#### Dynamic Properties of the HRC Elastic Coupling

The dynamic test stand developed in this research has been successfully used to measure the dynamic properties of the HRC couplings. The results show that the dynamic properties of the HRC elastic coupling are nonlinear and are a function of many factors. The dynamic stiffness,  $K$ , of the HRC-63K is a function of mean torque,  $T_m$ , vibration frequency,  $f$ , vibratory torque amplitude,  $T_v$ , and temperature,  $\theta$ :

$$K = 5.5378 \times 10^4 T_m^{.6545} f^{-.1538} T_v^{-.0948} \theta^{-.4953} \quad (7.1)$$

For free and multi-frequency vibration, the above equation may be written in another form:

$$K = 1.9703 \times 10^4 T_m^{.6043} \phi_v^{-.1210} \theta^{-.4502} \quad (7.2)$$

where  $\phi_v$  is the amplitude of the angular velocity.

The relative damping,  $\psi$ , of the HRC-63K is determined as:

$$\psi = 42.2834 T_m^{-.2644} f^{.2841} T_v^{-.0131} \theta^{-.3819} \quad (7.3)$$

The viscous damping factor,  $C_E$ , are presented in two different forms:

$$C_E = 5.9312 \times 10^4 T_m^{.3901} f^{-.8697} T_v^{-.1079} \theta^{-.8772} \quad (7.4)$$

$$C_E = 737.6065 T_m^{.3808} \dot{\phi}_v^{-.3890} \theta^{-.6803} \quad (7.5)$$

It seems that there is a relationship between static and dynamic stiffness of the HRC coupling. Although the relationship is obvious, its mathematic expression is difficult to obtain. Further research to define this relationship is necessary.

The dynamic properties of the HRC coupling depend mainly on the rubber elements and coupling geometry. Determining the relationship between the properties of a single rubber element and a whole coupling may provide a useful design process which will simplify the design of new couplings.



APPENDIX A  
DESCRIPTION OF A TYPICAL MARINE  
PROPULSION SYSTEM

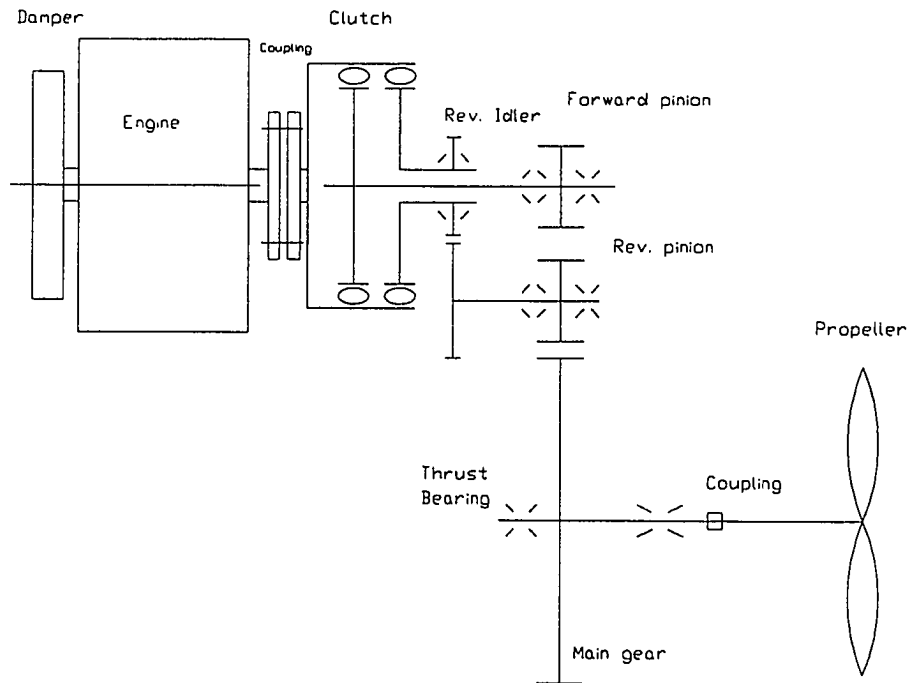


Figure A.1 A Typical Marine Propulsion System

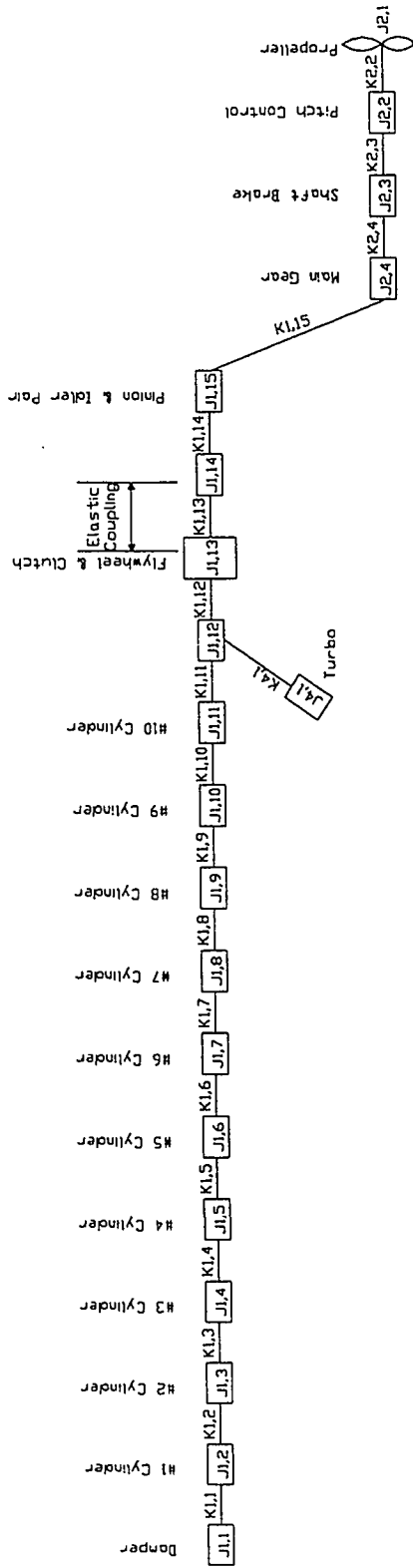


Figure A.2 Mass-spring Model of the Marine Propulsion System

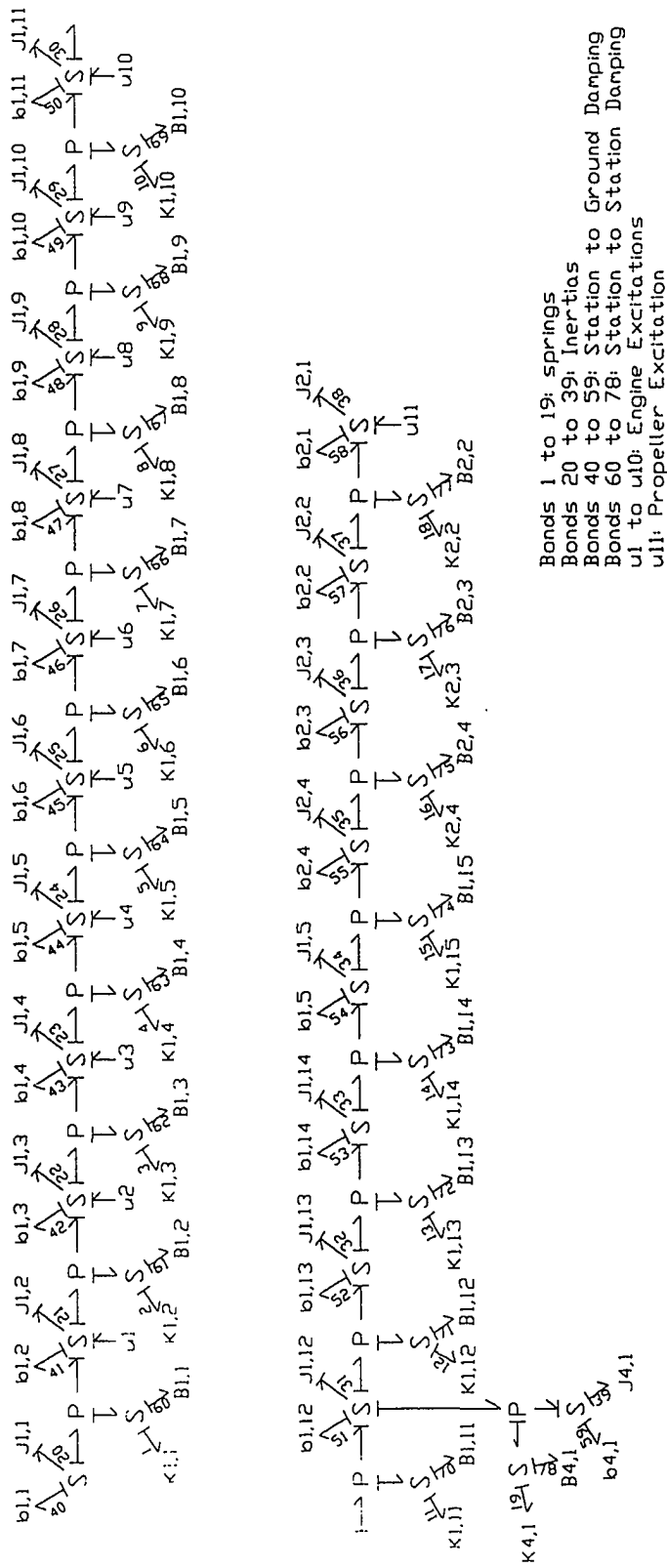


Figure A.3 Bond Graph Representation of the Marine Propulsion System

APPENDIX B  
PROGRAM FOR FORMATION OF JUNCTION STRUCTURE  
MATRICES FOR BOND GRAPH SHOWN IN FIGURE A.3

```

%
%This subroutine is used to form junction matrix
%
JUNCT=[1  20 -21  0  0  0  0  0  0
 2  21 -22  0  0  0  0  0  0
 3  22 -23  0  0  0  0  0  0
 4  23 -24  0  0  0  0  0  0
 5  24 -25  0  0  0  0  0  0
 6  25 -26  0  0  0  0  0  0
 7  26 -27  0  0  0  0  0  0
 8  27 -28  0  0  0  0  0  0
 9  28 -29  0  0  0  0  0  0
10  29 -30  0  0  0  0  0  0
11  30 -31  0  0  0  0  0  0
12  31 -32  0  0  0  0  0  0
13  32 -33  0  0  0  0  0  0
14  33 -34  0  0  0  0  0  0
15  34 -35  0  0  0  0  0  0
16  35 -36  0  0  0  0  0  0
17  36 -37  0  0  0  0  0  0
18  37 -38  0  0  0  0  0  0
19  31 -39  0  0  0  0  0  0
20  0  0  40  -1 -60  0  0
21  1  60  41  -2 -61  0  0
22  2  61  42  -3 -62  0  0
23  3  62  43  -4 -63  0  0
24  4  63  44  -5 -64  0  0
25  5  64  45  -6 -65  0  0
26  6  65  46  -7 -66  0  0
27  7  66  47  -8 -67  0  0
28  8  67  48  -9 -68  0  0
29  9  68  49  -10 -69  0  0
30  10 69  50  -11 -70  0  0
31  11 70  51  -12 -71 -19 -78
32  12 71  52  -13 -72  0  0
33  13 72  53  -14 -73  0  0
34  14 73  54  -15 -74  0  0
35  15 74  55  -16 -75  0  0
36  16 75  56  -17 -76  0  0
37  17 76  57  -18 -77  0  0
38  18 77  58  0  0  0  0
39  19 78  59  0  0  0  0
40  20 0  0  0  0  0  0
41  21 0  0  0  0  0  0
42  22 0  0  0  0  0  0
43  23 0  0  0  0  0  0
44  24 0  0  0  0  0  0
45  25 0  0  0  0  0  0
46  26 0  0  0  0  0  0
47  27 0  0  0  0  0  0

```

```

48 28 0 0 0 0 0 0
49 29 0 0 0 0 0 0
50 30 0 0 0 0 0 0
51 31 0 0 0 0 0 0
52 32 0 0 0 0 0 0
53 33 0 0 0 0 0 0
54 34 0 0 0 0 0 0
55 35 0 0 0 0 0 0
56 36 0 0 0 0 0 0
57 37 0 0 0 0 0 0
58 38 0 0 0 0 0 0
59 39 0 0 0 0 0 0
60 20-21 0 0 0 0 0 0
61 21-22 0 0 0 0 0 0
62 22-23 0 0 0 0 0 0
63 23-24 0 0 0 0 0 0
64 24-25 0 0 0 0 0 0
65 25-26 0 0 0 0 0 0
66 26-27 0 0 0 0 0 0
67 27-28 0 0 0 0 0 0
68 28-29 0 0 0 0 0 0
69 29-30 0 0 0 0 0 0
70 30-31 0 0 0 0 0 0
71 31-32 0 0 0 0 0 0
72 32-33 0 0 0 0 0 0
73 33-34 0 0 0 0 0 0
74 34-35 0 0 0 0 0 0
75 31-36 0 0 0 0 0 0
76 36-37 0 0 0 0 0 0
77 37-38 0 0 0 0 0 0
78 31-39 0 0 0 0 0 0);

```

```

[m,n]=size(JUNCT);
J=zeros(m,m);
for i=1:m;
    for j=2:n;
        if JUNCT(i,j) ~= 0
            k=abs(JUNCT(i,j));
            J(i,k) = k/JUNCT(i,j);
        end
    end
end
end
% | Jss Jsl Jsu |
% J= |           |
% | Jls Jll Jlu |
% Jss(39:39)

Jss=J(1:39, 1:39);
Jsl=J(1:39, 40:78);
Jls=J(40:78, 1:39);

```

```
Jl = J(40:78, 40:78);  
%Now we need Jsu (39x11) and Jlu (39x11)  
Jsu = zeros(39,11);  
Jsu(21,1) = 1; Jsu(22,2) = 1; Jsu(23,3) = 1;  
Jsu(24,4) = 1; Jsu(25,5) = 1; Jsu(26,6) = 1;  
Jsu(27,7) = 1; Jsu(28,8) = 1; Jsu(29,9) = 1;  
Jsu(30,10) = 1; Jsu(38,11) = 1;  
  
Jlu = zeros(39,11);  
  
%above program finishing the junction matrix forming
```



APPENDIX C  
PROGRAM FOR TEST STAND DYNAMIC ANALYSIS

```

%
%Natural Frequencies, Mode Shapes and Forced Vibration Analysis
%of Elastic Coupling Test Stand
%
%Filename: HRC.m
% Analysis suitable for HRC63, HRC105, and HRC 390
%July 23th, 94
%Revised Jan 8, 1995
%The beam is connected to inner hub of the right side coupling
%
%(1)Model Diagram
%      K1      K2
%      J1—J2—J3
%      Kr||Cr  Kr||Cr
%      -      -
%
clear;

fre=input('Vibration Frequency (HZ):');
id=1; %id= 1 for HRC63, 2 for HRC105, 3 for HRC390

Jhub=[1.86 5 41.6]; %inertia of hub
Krub=[2*5.714e5 9.69375e5 4.76375e6]; %coupling stiffness
%1/2 elements for HRC 63, 1/4 elements for other
Trate=[63000 105000 390000]; %rated torque

em=input('Estimated Eccentric mass (lb):');
m=(15+em)/386; %mass of excitation device + eccentric weight
%15 is an estimated number

J1=Jhub(id)+2.5; %inertia of coupling inner hub + LVDT holding
J2=Jhub(id)+13.26; %inertia of coupling inner hub + part of beam
J3=9.8+m*30^2; %Equivalent inertia of mass m + part of beam
J=diag(J1 J2 J3); %inertia matrix

K1=5.13e6; %stiffness of the shaft
K2=3.83e7; %torsional stiffness of beam
Kr1=Krub(id); %stiffness of the rubber
Kr2=Krub(id);

K=[K1+Kr1 -K1 0; %stiffness matrix
-K1 K1+K2+Kr2 -K2;
0 -K2 K2];

A=[zeros(3,3) eye(3);
-inv(J)*K zeros(3,3)]; %state space matrix (exclude damping)

%Natural Frequencies and Mode Shapes

```

```

[v,d]=eig(A);
w(1)=abs(d(1,1));
shape(:,1)=sign(real(v(1:3,1)))*abs(v(1:3,1));
w(2)=abs(d(3,3));
shape(:,2)=sign(real(v(1:3,3)))*abs(v(1:3,3));
w(3)=abs(d(5,5));
shape(:,3)=sign(real(v(1:3,5)))*abs(v(1:3,5));

disp('Frequencies:');
disp(w/2/pi)
disp('Mode Shapes:');
disp(shape)

%Frequency response

Cr1=Kr1*1.1/(4*pi^2*fre);           %damping of elastic coupling
Cr2=Kr2*1.1/(4*pi^2*fre);
C=[Cr1 0 0;                        %damping matrix
  0 Cr2 0;
  0 0 0];

factor=input('Factor:');
%
T0=[0;0;0.25*0.25*Trate(d)*factor]; %Excitations

if id==1
    T0(3)=T0(3)*2;                 %for HRC 63, half elements
end

omega=2*pi*fre;
i=sqrt(-1);
theta=inv(K-omega^2*J+i*omega*C)*T0;
disp('Frequency Response:');
disp(theta)
disp(abs(theta))

TT=K1*(theta(1)-theta(2));         %torque on the shaft
eps=8*abs(TT)/(11.5e6*pi^2.5^3);   %strain on the shaft
stroke=abs(theta(1))*16;          %vibration stroke, 16" is the length
Tr1=Kr1*abs(theta(1));            %vibatory torque on coupling
percent=Tr1*4*4/Trate(d);

if id==1
    percent = percent /2;
end

disp('Excitation torque:');
disp(T0(3))

```

```

disp('Torque on the shaft:')
disp(abs(TT))
disp('Strain on the shaft:')
disp(eps);
disp('Vibration Stroke:')
disp(stroke)
disp('Vibratory torque on coupling:')
disp(Tr1)
disp(percent)
%
%output format
%f TO FO Trubber % Tshaft Strain Stroke WR W R

out=[ire TO(3) TO(3)/30 Tr1 percent*100 abs(TT) eps*1e6 stroke 9.7876*TO(3)/ire^2 em 9.7876*TO(3)/ire^2
em];
fprintf(1,'%5d %8.2f %6.2f %6.2f %6.2f %8.2f %6.2f %8.4f %6.2f %6.2f %6.2f\n',out)

```

**APPENDIX D**  
**PROGRAM FOR DATA ACQUISITION SYSTEM**



```

DERR = DAS1600DEVOPEN%(SSEGADD(a$), NumOfBoards)
IF DERR <> 0 THEN BEEP: PRINT "ERROR "; HEX$(DERR); " OCCURED DURING '..DEVOPEN'": STOP

'-----
' STEP 4: This step establishes communication with the driver through the
' Device Handle.
'
DERR = DAS1600GETDEVHANDLE%(0, DAS1600)
IF (DERR <> 0) THEN BEEP: PRINT "ERROR "; HEX$(DERR); " OCCURED DURING '..GETDEVHANDLE'": STOP

'-----
' PLACE
' YOUR PROGRAM CODE
' HERE
300 CLS

INPUT " Filter(5,10,100,200...)", filter

1000 v0 = 0: v1 = 0: v2 = 0: v3 = 0: v4 = 0
FOR I = 1 TO filter
DERR = KADRead%(DAS1600, 0, 3, ADValue)
IF DERR <> 0 THEN BEEP: PRINT "ERROR "; HEX$(DERR); "DURING"
    "KADRead ": STOP
v0 = v0 + ADValue

DERR = KADRead%(DAS1600, 1, 3, ADValue)
IF DERR <> 0 THEN BEEP: PRINT "ERROR "; HEX$(DERR); "DURING"
    "KADRead ": STOP
v1 = v1 + ADValue
DERR = KADRead%(DAS1600, 2, 0, ADValue)
IF DERR <> 0 THEN BEEP: PRINT "ERROR "; HEX$(DERR); "DURING"
    "KADRead ": STOP
v2 = v2 + ADValue
DERR = KADRead%(DAS1600, 3, 0, ADValue)
IF DERR <> 0 THEN BEEP: PRINT "ERROR "; HEX$(DERR); "DURING"
    "KADRead ": STOP
v3 = v3 + ADValue
DERR = KADRead%(DAS1600, 4, 0, ADValue)
IF DERR <> 0 THEN BEEP: PRINT "ERROR "; HEX$(DERR); "DURING"
    "KADRead ": STOP
v4 = v4 + ADValue

NEXT I

v0 = v0 / filter: v1 = v1 / filter: v2 = v2 / filter
v3 = v3 / filter: v4 = v4 / filter
v0 = ((v0 / 16) AND &HFFF) - 2048
v1 = ((v1 / 16) AND &HFFF) - 2048
v2 = ((v2 / 16) AND &HFFF) - 2048
v3 = ((v3 / 16) AND &HFFF) - 2048
v4 = ((v4 / 16) AND &HFFF) - 2048

```

```

rv0 = v0 / 2048! * FACTOR(4)
rv1 = v1 / 2048! * FACTOR(4)
rv2 = v2 / 2048! * FACTOR(1)
rv3 = v3 / 2048! * FACTOR(1)
rv4 = v4 / 2048! * FACTOR(1)

torque = 104.28162# * (ABS(v0) + ABS(v1)) / 10.883
force = torque / 18!
percent = torque * 2 / 63000 * 100
PRINT USING p1$; v0, v1, v2, v3, v4
PRINT
REM PRINT #1, USING p1$; v0, v1, v2, v3, v4
PRINT USING p2$; force, torque, percent
PRINT

a$ = INKEY$: IF a$ = "" THEN 1000

5 a$ = INKEY$: IF a$ = "" THEN 5

REM CLOSE #1
END

'Program DYNAMIC.BAS reads five channels (0-4) simultaneously with
'different gain: ch 0-1: (strain gages) gain = 0 (+-1.25v)
'ch 2-4: (3 LVDTs) gain = 3 (+-10v)
'January 17, 1995

' This file includes all function DECLARATION supported by the driver.
' $INCLUDE: 'Q4IFACE.B'

DIM BufA(20000) AS INTEGER ' A/D data buffer
DIM CHANGAINARRAY(50) AS INTEGER ' Chan/Gain array

DIM NumOfBoards AS INTEGER
DIM DERR AS INTEGER ' Error flag
DIM DEVHANDLE AS LONG ' Device Handle
DIM ADHANDLE AS LONG ' A/D Frame Handle

'DEFINE USER USED VARIABLES HERE

DIM I%, J AS INTEGER
DIM RATE AS INTEGER
DIM NumOfData AS INTEGER
DIM TotalData AS INTEGER
DIM FileName$, a$, p$
DIM DT, Time AS DOUBLE

p$ = "### #####"
RATE = 5000 'total sample rate (HZ)
DT = 5 / RATE 'time (second) interval between sampling

```



```

RATE = 1000000 / RATE
NumOfData = 500 'for one channel
TotalData = 5 * NumOfData 'for five channels
FileName$ = "f15_31.dyn"
INPUT "File name (ying?.dyn)", FileName$
'
' STEP 1: This step is mandatory; it initializes the internal data tables
' according to the information contained in the configuration file
'DAS1600.CFG.
'
a$ = "DAS1600.CFG" + CHR$(0)
DERR = DAS1600DEVOPEN%(SSEGADD(a$), NumOfBoards)
IF DERR <> 0 THEN BEEP: PRINT "ERROR "; HEX$(DERR); " OCCURED DURING '.DEVOPEN'": STOP
'
' STEP 2: This step is mandatory; it establishes communication with the driver
' through the Device Handle.
'
DERR = DAS1600GETDEVHANDLE%(0, DEVHANDLE)
IF (DERR <> 0) THEN BEEP: PRINT "ERROR "; HEX$(DERR); " OCCURED DURING '.GETDEVHANDLE'": STOP
'
' STEP 3: To perform any A/D operations, you must first get a Handle to an
' A/D Frame (the data tables inside the driver pertaining to A/D operations).
'
DERR = KGetADFrame%(DEVHANDLE, ADHANDLE)
IF (DERR <> 0) THEN BEEP: PRINT "ERROR "; HEX$(DERR); " OCCURED DURING 'KGETADFRAME'": STOP
'
' STEP 4: Assign the data array declared above to the Frame Handle
'
DERR = KSetBuf%(ADHANDLE, BufA(0), TotalData)
IF DAS1600ERR <> 0 THEN BEEP: PRINT "ERROR "; HEX$(DAS1600ERR); " OCCURED DURING 'KSetBuf'": STOP
'
' STEP 5: Create the array of channel/gain pairs
'
CHANGAINARRAY(0) = 5 ' # of chan/gain pairs
CHANGAINARRAY(1) = 0: CHANGAINARRAY(2) = 3 ' Chan 0, Gain 8
CHANGAINARRAY(3) = 1: CHANGAINARRAY(4) = 3 ' Chan 1, Gain 8
CHANGAINARRAY(5) = 2: CHANGAINARRAY(6) = 0 ' Chan 2, Gain 1
CHANGAINARRAY(7) = 3: CHANGAINARRAY(8) = 0 ' Chan 3, Gain 1
CHANGAINARRAY(9) = 4: CHANGAINARRAY(10) = 0 ' Chan 3, Gain 1
'
' STEP 6: Reformat the channel/gain array so that it is readable by the
' DAS-1600 driver. Note that, after this step, this array is no longer
' readable from QuickBASIC; use KRestoreChanGAr% to restore it to the values
' as assigned above.
'
DERR = KFormatChanGAr%(CHANGAINARRAY(0))

```

```

IF DERR <> 0 THEN BEEP: PRINT "ERROR "; HEX$(DERR); " OCCURED DURING 'KFormatChnGAry': STOP

'-----
' STEP 7: Assign the reformatted Channel/Gain array to the A/D Frame.
'
DERR = KSetChnGAry%(ADHANDLE, CHANGAINARRAY(0))
IF DERR <> 0 THEN BEEP: PRINT "ERROR "; HEX$(DERR); " OCCURED DURING 'KSetChnGAry': STOP

'-----
' STEP 8: This example program uses the internal (default) conversion clock
' source; the following call specifies the divider to the Clock Source
' (1MHz or 10MHz)
'
DERR = KSetClkRate%(ADHANDLE, RATE) ' ADJUST THIS NUMBER LATER
IF DERR <> 0 THEN BEEP: PRINT "ERROR "; HEX$(DERR); " OCCURED DURING 'KSetClkRate': STOP

CLS
LOCATE 22, 1: PRINT "Press a key to start Synchronous Acq..."
DO
LOOP WHILE INKEY$ = ""
LOCATE 22, 1: PRINT "Synchronous Acq, now active...Wait  "

'-----
' STEP 9: Begin Synchronous data aquisition.
'
DERR = KSyncStart%(ADHANDLE)
IF DERR <> 0 THEN BEEP: PRINT "ERROR "; HEX$(DERR); " OCCURED DURING 'KSyncStart': STOP

PRINT "Acquisition is done. . A/D Data is BUFFA() array."

'-----
' STEP 10: Display and write the results to a file
'
OPEN FileName$ FOR OUTPUT AS #1

Time = 0!
FOR J = 0 TO NumOfData - 1
PRINT USING p$; Time;
PRINT #1, USING p$; Time;
FOR I% = 0 TO CHANGAINARRAY(0) - 1
PRINT ((BuffA(I% + 5 * J) / 16) AND &HFFF) - 2048;
PRINT #1, ((BuffA(I% + 5 * J) / 16) AND &HFFF) - 2048;
NEXT I%
PRINT #1,
PRINT
Time = Time + DT
NEXT J
CLOSE #1
END

```

APPENDIX E  
PROGRAM FOR TEST DATA POST PROCESSING

```

%Postprocessing Dynamic Test Data
%File name: post.m          (Jan. 28, 95, Feb. 8, Feb 12)

%Note: Amplifier gain is 100

clear
v0=-676;
v1=676;
v2=-235;
v3=-242;
v4=807;
Vin=10.867;
l1=3.5;
l2=3.375;
l3=3.125;
lhub=1.86+2.5;

load f14_7.dyn          %load the test data
common=f14_7;          %store to common
clear f14_7;
%above parameters need to be changed every time
t=common(:,1);        %first column is time
Tmean=104.28162*(abs(v0)+abs(v1))/Vin;
%mean torque is calculated according to the initial readings

DT1=208.56324*(common(:,2)-v0)/Vin; %vibratory torque with filter
DT2=208.56324*(common(:,3)-v1)/Vin; %vibratory torque without filter
[ft1, At1, phi1, at1, bt1, ct1, T1_new] = least0(t,DT1);
disp('Torque T1');
%call least square curfit to get frequency, amplitude, phase, offset
%check the curve to decide to call least1 or least2 or least0
pause;
[ft2, At2, phi2, at2, bt2, ct2, T2_new] = least0(t,DT2);
disp('Torque T2');
pause;

d1=4.6864502e-4*(common(:,4)-v2);          %relative dis. for S/N 8176
d2=4.7126846e-4*(common(:,5)-v3);          %relative dis. for S/N 8171
d3=4.7017935e-4*(common(:,6)-v4);          %relative dis. for S/N 8178

phi1=2*(asin((d1+l1)/32)-asin(l1/32));      %relative angular dis. S/N 8176
phi2=2*(asin((d2+l2)/32)-asin(l2/32));      %S/N 8171
phi3=2*(asin((d3+l3)/32)-asin(l3/32));      %S/N 8178

plot(t,phi1,t,phi2,t,phi3),grid,title('Three Phi'),pause;
%phi=(phi1+phi2+phi3)/3;                    %average angular displacement

[phi1, Aphi1, phi1p1, aphi1, bphi1, cphi1, phi_new1] = least0(t,phi1); %curvefit
disp('Displacement');

```

```

pause

(fphi2, Aphi2, phi2, bphi2, cphi2, phi_new2) = least0(t,phi2); %curvefit
disp('Displacement');
pause

(fphi3, Aphi3, phi3, bphi3, cphi3, phi_new3) = least0(t,phi3); %curvefit
disp('Displacement');
pause

disp('Aphi1:'); disp(Aphi1);
disp('Aphi2:'); disp(Aphi2);
disp('Aphi3:'); disp(Aphi3);
disp('phi1:'); disp(phi1);
disp('phi2:'); disp(phi2);
disp('phi3:'); disp(phi3);
disp('phi1:'); disp(phi1);
disp('phi2:'); disp(phi2);
disp('phi3:'); disp(phi3);
disp('phi1:'); disp(phi1);
disp('phi2:'); disp(phi2);
disp('phi3:'); disp(phi3);

%*****
f = (f12 + fphi1 + fphi2 + fphi3)/4;          %vibration frequency
%f = (f12 + fphi1 + fphi3)/3;

Aphi = (Aphi1 + Aphi2 + Aphi3)/3;
%Aphi = (Aphi1 + Aphi3)/2;

phi1 = (phi11 + phi12 + phi13)/3;
%phi1 = (phi11 + phi13)/2;

cphi = (cphi1 + cphi2 + cphi3)/3;
%cphi = (cphi1 + cphi3)/2;
%*****

scale1 = (At1*(2*pi*f)^2*Aphi*hub)/At1;      %scale vibratory torque down
scale2 = (At2*(2*pi*f)^2*Aphi*hub)/At2;

Trubber1 = T1_new*scale1;                    %scale vibratory down due to hub inertia
Trubber2 = T2_new*scale2;
Ar1 = At1*scale1;
Ar2 = At2*scale2;

plott(T1_new,'y',t, Trubber1,'r'),grid,title('T1_new, Trubber2');
pause;
plott(T2_new,'y',t, Trubber2, 'r'), grid,title('T2_new, Trubber2');
pause

t0=0;          %just choose one cycle
te=1/t;
dt=(te-t0)/200;
t_short=t0:dt:te;

```

```

phi_short=Aphi*sin(2*pi*f*t_short+phi0)+cphi;
plot(t_short, phi_short),grid
pause
T2short=At2*sin(2*pi*f*t_short+phi2)+ct2;
Trubber=T2short*scale2;
plot(t_short, Trubber),grid
pause
plot(phi_short, Trubber),grid
pause

%subplot(2,2,1),plot(phi_short, Trubber),grid %put three figures in one page
%xlabel('Angular Displacement (rad)');
%ylabel('Vibratory Torque (lb-in)');
%title('Hysteresis Loop');

%subplot(2,2,2),plot(t_short, Trubber),grid
%xlabel('time (seconds)');
%ylabel('Vibratory Torque (lb-in)');
%title('Vibratory Torque vs. time');

%subplot(2,2,3),plot(phi_short,t_short),grid
%ylabel('time (seconds)');
%xlabel('Angular displacement (rad)');
%title('Time vs. angular displacement');
%print -dps loop

%pause
%subplot(1,1,1)

deltaphi=abs(phi2-phi0); %phase difference between force and dis.
%C=At2*scale2*sin(deltaphi)/2*pi*f*Aphi; %damping C
%K=2*(At2*scale2*cos(deltaphi))/Aphi; %stiffness K
%K1=K*scale2;
%Wd=C*(2*pi*f)*Aphi^2; %area
%sai=2*Wd/(Aphi*At2*scale2); %relative damping

K=2*Ar2/Aphi;
K1=2*At2/Aphi;
sai=2*pi*tan(deltaphi);

fid = fopen('HRC63.OUT', 'a');
out1=[Tmean Tmean*2/63000*100 f Ar2 At2 Ar2/Tmean*100 Aphi];
out2=[K K1 sai deltaphi*180/pi];
out=[out1 out2];
fprintf(' TMean Tmean/rated f e Trubber Tshaft Trubber/Tmean Aphi \n');
fprintf(1, '%10.2f %6.2f %6.2f %10.2f %10.2f %6.2f %6.4f\n', out1);
disp(' ');
fprintf(' K K1 sai phi\n');
fprintf(1, '%10.2f %10.2f %6.4f %6.4f\n', out2);
disp(' ');

```

```

fprintf(fid, 'f14_7 %10.2f %6.2f %6.2f %10.2f %10.2f %6.2f %6.4f %10.2f %10.2f %6.4f %6.4f\n', out);
fclose(fid);

```

```

function [f, Amp, phi, a, b, c, y_new] = least0 (ty1)
%Post Processing for time domain signal
%t = time
%y = amplitude (could be displacement or torque)

%program to find the average frequency f

y=y1-mean(y1);

index1=[];
for i=1:length(y)-1;
    if y(i)>=0 & y(i+1)<=0
        index1=[index1;i];
    end
end

dt1=[];
for j=1:length(index1)-1
    dt1=[dt1 t(index1(j+1))-t(index1(j))];
end

index2=[];
for i=1:length(y)-1;
    if y(i)<=0 & y(i+1)>=0
        index2=[index2;i];
    end
end

dt2=[];
for j=1:length(index2)-1
    dt2=[dt2 t(index2(j+1))-t(index2(j))];
end

f1=1/mean(dt1);
f2=1/mean(dt2);
f=(f1+f2)/2;

%least square program

omega = 2*pi*f;

A=[sin(omega*t) cos(omega*t) ones(length(t),1)]; %form matrix A
B=A\y1; %find coefficient B

y_new=A*B;

```

```
plot(ty1, Y.t, y_new, 'r', grid);  
  
a=B(1); b=B(2); c=B(3);           %y=a.sin(omega t) + b cos(omega t) + c  
Amp=sqrt(a^2+b^2);  
phi=atan(b/a);
```



## BIBLIOGRAPHY

- Amara, Maher, "A Procedure to Match Bond Graph and Scattering Formalism", J. of the Franklin Institute, Vol.328 No.5/6, 91.
- American Bureau of Shipping, Rules for Building and Classing Steel Vessels, Part 4 Machinery Equipment and Systems, New York, N.Y. 1992.
- Aspragathos, N A, "Program for torsional dynamic modeling of drive systems and fatigue life predication", CAD, Vol.20 No.9,(1988).
- Auslander, D.M., Tsai, N.T., "Bond Graph Models for Torsional Energy Transmission", J. of Dynamic Systems, Measurement, and Control, March 1975.
- Bert, C.W., "Material Damping: An Introductory Review of Mathematical Models, Measures and Experimental Techniques", J. of Sound and Vibration (1973) 29(2), 129-153.
- Choy, F.K., Tu, Y.K., Savage, M., "Vibration Signature and Modal Analysis of Multi-stage Gear Transmission", J. of the Franklin Institute, Vol.328, No.2/3, 1991.
- Cho, D., and Hedrick, J.K., "Automotive Power Train Modeling for Control", J. of Dynamic Systems, Measurement, and Control, Vol.111, Dec 1989.
- Den Hartog, J.P., Mechanical Vibrations, McGraw-Hill, 4th edition, 1956.
- Eshleman, R.L., "Torsional Response of Internal Combustion Engines", J. of Engineering for Industry, May 1974.
- Elahi, Mehran, "Measurement of Static and Dynamic Characteristics of Elastomer Couplings Using Computerized Data Acquisition System", Master Thesis, Mississippi State University, 1985.
- Firestone, F.A., "A New Analogy Between Mechanical and Electrical Systems", J. of the Acoustical Society, Jan. 1933.
- Furrow, R.W., Mabie, H.H., "The Measurement of Static Deflection in Spur Gear Teeth", J. of Mechanisms, Vol.5, pp147-166, 1970.
- Harris, C.M., Shock and Vibration Handbook, Third Edition, McGraw Hill, 1988.
- Hillberry, B.M. et al, The Measurement of the Dynamic Properties of Elastomers and Elastomeric Mounts, SAE International Automotive Engineering Congress, Detroit, Michigan, Jan 8-12, 1973.

Hsiao, M.H., Haug, E.J. and Arora, J.S., "A State Space Method for Optimal Design of Vibration Isolators", *J. of Mechanical Design*, Vol.101, April, 1979.

Harrington, Roy L., Marine Engineering, SNAME, New York, N.Y., 1971.

Hrovat, D., Margolis, D.L., and Hubbard, M., "An Approach Toward the Optimal Semi-Active Suspension:", *J. of Dynamic Systems, Measurement, and Control*, Vol.110, Sep. 1988.

Inman, D.J., Vibration with Control, Measurement, and Stability, Prentice-Hall, Inc., 1989.

Jones, E.W., "Torsional Vibration Analysis for LEEVAC Shipyards", 1990.

Jones, E.W., Shen, A., and Brown, R.E., "Fatigue Analysis of Shafts for Marine Gearboxes", AGMA Technical Paper, October, 1994.

Jones, E.W., Shen, A., and Li, F., "Torsional Vibrations and the Design of Marine Gear Systems", 2nd Seminar for Gear Users and Manufactures, Queretaro, Mexico, 1993.

Jones, E.W., Peng, C.H., Pan, C.T.A., "Torsional Vibration in Work Boat Power Trains from the Designer's Point of View", New Orleans, LA, 1982.

James, M.L., Smith, G.M., Wolford, J.C. and Whaley, P.W., Vibration of Mechanical and Structural Systems, Harper and Row, Publisher, New York, 1989.

Kahraman, A., "Effect of Axial Vibration on the Dynamics of a Helical Gear Pair", *J. of Vibration and Acoustics*, Jan. 1993.

Kahraman, A., "Non-linear Dynamics of a Spur Gear Pair", *J. of Sound and Vibration* (1990) 142(1), 49-75.

Karnopp, Dean C. et al, System Dynamics--A Unified Approach, 2nd ed, 1990.

Karnopp, D., Crosby, M.J., and Harwood, R.A., "Vibration Control Using Semi-Active Force Generators", *J. of Engineering for Industry*, May 1974.

Karnopp, D., "Design Principles for Vibration Control Systems Using Semi-Active Dampers", *J. of Dynamic Systems, Measurement, and Control*, Vol.112, Sept. 1990.

Lancaster, P., 1966, Lambda Matrices and Vibrating Systems, Elmsford, N.Y.: Pergamon Press.

Lloyd's Register, Rules and Regulations for the Classification of Ships, Part 5 Main and Auxiliary Machinery, 1989.

Mowers, G.P., "Diesel Reduction Gear Design and System Considerations from a Torsional Vibration Viewpoint", *Marine Technology*, Vol.20, No.2, April 1983.

- Meirovitch, L., Introduction to Dynamics and Control, John Wiley & Sons, Inc., 1985.
- Nessler, G.L., Brown, D.L., Stouffer, D.C., and Maddox, K.C., "Design of a Viscoelastic Dynamic Absorber for Machine Tool Applications", J. of Engineering for Industry, Aug. 1977.
- Nestorides, E.J., A Handbook on Torsional Vibration, B.I.C.E.R.A. Research Laboratory, 1958.
- Obert, E.F., Internal Combustion Engines, 3rd edition, 1968.
- Ozguven, H.N., "Mathematical Models Used in Gear Dynamics-- A Review", J. of Sound and Vibration, (1988) 121(3), 383-411.
- Peng, Chien-Hua Howard, "Sensitivity Studies in the Design of Ship Drive for Torsional Vibration", MS Thesis, Mississippi State University, Aug. 1981.
- Porter, F.P., "The Range and Severity of Torsional Vibration in Diesel Engines", ASME Transactions, 1927-1928, Vol.49-50.
- Porter, F.P., "Harmonic Coefficients of Engine Torque Curves", J. of Applied Mechanics, Mar. 1943.
- Paynter, Henry M., "Wave-scattering Approaches to Conservation and Causality", J. of the Franklin Institute, Vol.325, No.3, 1988.
- Rosenberg, R.C., "A definition of the Bond Graph Language", J. of Dynamic Systems, Measurement, and Control, Sept 1972.
- Seireg, A., "Evaluation of Dynamic Factors for Spur and Helical Gears", J. of Engineering for Industry, May 1970.
- Singh, R., Xie, H. and Comparin, R.T., "Analysis of Automotive Neutral Gear Rattle", J. of Sound and Vibration (1989) 131(2), 177-196.
- Shearer, J.Lowen, Dynamic Modeling and Control of Engineering Systems.
- Strang, G., Linear Algebra and Its Applications, Academic Press, Inc., 1980.
- Soom, A. and Lee, M., "Optimal Design of Linear and Nonlinear Vibration Absorbers for Damped Systems", J. of Vibration, Acoustics, Stress, and Reliability in Design, Vol.105, Jan. 1983.
- Thoma, J.U., Simulation by Bondgraphs, Springer-Verlag Berlin Heidelberg, 1990.
- Timoshenko, S. and Baud, R.V., "Strength of Gear Teeth is Greatly Affected by Fillet Radius", Automat, Ind.55, 13-142 (1926).
- Trent, Horace M., "Isomorphisms between Oriented Linear Graphs and Lumped Physical Systems", The J. of Acoustical Society of America, Vol.27, No.3, May 1955.

Wang, S.M., "Analysis of Nonlinear Transient Motion of a Geared Torsional", J. of Eng. for Industry, Feb., 1974.

Wang, S.M., "Torsional Response of a Gear Train System", J. of Engineering for Industry, May 1972.

Wang, Qi, Torsional Vibration of the Diesel Engine, National Defense Industry Press, Beijing Xinhua Book House, 1985.(in Chinese).

Wilson, W. Ker, Practical Solution of Torsional Vibration Problems, Volume Four: Third Edition, Devices for Controlling Vibration, Chapman and Hall, 1968.

Yae, K.H. and Inman, D.J., "Response Bounds for Linear Underdamped Systems", J. of Applied Mechanics, Vol.54, June 1987.